Design and Testing of Antenna Deployment System for Aalto-1 Satellite

Mikko Lankinen

School of Electrical Engineering

Thesis submitted for examination for the degree of Master of Science in Technology.

Espoo 18.11.2015

Thesis supervisor:

Prof. Esa Kallio

Thesis advisor:

Assistant Prof. Jaan Praks

Aalto University
School of Electrical Engineering

AALTO UNIVERSITY
SCHOOL OF ELECTRICAL ENGINEERING

ABSTRACT OF THE
MASTER'S THESIS

Author: Mikko Lankinen

Title: Design and Testing of Antenna Deployment System for Aalto-1 Satellite

Date: 18.11.2015 Language: English Number of pages: 9+89

Department of Radio Science and Engineering

Professorship: Space Technology Code: S-92

Supervisor: Prof. Esa Kallio

Advisor: Assistant Prof. Jaan Praks

Aalto-1 is a nanosatellite based on CubeSat standard which will be launched in 2016. For command link and telemetry, Aalto-1 uses a UHF radio system operating at a 437.22 MHz frequency. For transmitting data to Earth, the UHF radio system requires antennas as well as an antenna deployment system (ADS), which would enable the antennas to be opened in operational confguration after the launch. The ADS compactly stores antennas into a small space before launch and then deploys them once the satellite is in orbit.

This thesis designs, constructs and tests an ADS for the Aalto-1 satellite. The thesis focuses on three areas of the ADS design: mechanical design, electrical design and radio frequency (RF) design. The mechanical design includes selection of antenna stowage confguration, ADS location on the satellite and an antenna release mechanism. Electrical design includes a trade-off between various solutions for implementing the required ADS timer, design of the circuit schematic for the ADS timer, design of the Printed Circuit Board (PCB) for the ADS timer, and electronic component selection. RF design includes modelling the satellite structure, ADS and antennas using 3D electromagnetic simulation software. Antenna performance was optimized to meet mission requirements. To verify the simulation results, antennas were measured in an anechoic chamber. Moreover, ADS was subjected to a series of tests: vibration testing, thermal cycling testing and communication range testing. Thorough testing has not only ensured that ADS can withstand launch conditions and the space environment but will also work according to specifcations.

Keywords: CubeSat, nanosatellite, antennas, ADS, UHF, RF

AALTO-YLIOPISTO
SÄHKÖTEKNIIKAN KORKEAKOULU

DIPLOMITYÖN
TIIVISTELMÄ

Tekijä: Mikko Lankinen

Työn nimi: Antennien avautumisjärjestelmän suunnittelu ja testaus Aalto-1 satelliitille

Päivämäärä: 18.11.2015 Kieli: Englanti Sivumäärä: 9+89

Radiotieteen ja -tekniikan laitos

Professuuri: Avaruustekniikka Koodi: S-92

Työn valvoja: Prof. Esa Kallio

Työn ohjaaja: Apulaisprof. Jaan Praks

Aalto-1 on CubeSat-standardin mukainen nanosatelliitti, joka suunnitellaan laukaistavaksi vuonna 2016. Telemetria- ja komentolinkkiä varten Aalto-1 käyttää UHF radiojärjestelmää, joka toimii 437,22 MHz taajuudella. Datan siirtämiseksi Maahan UHF radiojärjestelmää tarvitsee antennit sekä antennien avautumisjärjestelmän (Antenna Deployment System, ADS), joka avaa antennit toiminta-asentoon laukaisun jälkeen. ADS pakka antennit pieneen tilaan ennen laukaisua ja avata ne, kun satelliitti on kiertoradalla.

Tässä diplomityössä suunnitellaan, rakennetaan ja testataan Aalto-1 satelliitin ADS:ää. Diplomiytyössä keskitytään kolmeen erilliseen suunnittelualueeseen: mekaaninen suunnittelu, sähköinen suunnittelu ja radiotekninen suunnittelu. Mekaaninen suunnittelu sisältää erilaisten antennien pakkaustapojen selvittämisen, ADS:n sijoituspaikan valinnan satelliitissa ja ADS:n antennien avautumismekanismin valinnan. Sähköinen suunnittelu sisältää selvityksen ajastimen toteutuksen vaihtoehtoista, ajastimen piirikaavion suunnittelun, ajastimen piirilevyn suunnittelun ja elektronisten komponenttien valinnan. Radiotekninen suunnittelu sisältää satelliitin, ADS järjestelmän ja antennien mallintamisen sähkömagnetiikan 3D simulointiohjelmalla. Antennien toiminta oli optimoitu mission vaatimusten mukaisesti. Optimoidut antennit mitattiin kaiuttomassa huoneessa varmistakseen simulaatiotulokset. Valmiin ADS järjestelmän toiminta varmistettiin tärinä- lämpösyklaus- ja kantamatesteillä. Perinpohjainen testaus varmistaa, että ADS kestää laukaisuolosuhteet ja avaruusympäristön sekä tulee toimimaan sunnitelmien mukaisesti.

Avainsanat: CubeSat, nanosatelliitti, antennit, ADS, UHF, radiotekniikka

Preface

I wish to thank my parents for their continuous support throughout this thesis. I also want to express my gratitude to my thesis instructor Jaan Praks and whole Aalto-1 team.

Otaniemi, 18.11.2015

Mikko Lankinen

Contents

Symbols and abbreviations

Symbols

$\mathbf{D}$	electric flux density [C/m]
$\mathbf{B}$	magnetic flux density [T]
$\mathbf{E}$	electric field intensity [V/m]
$\mathbf{H}$	magnetic field intensity [A/m]
$\mathbf{J}$	current density [A/m^2]
ρ	electric charge density [C/m^3]
k	wave number $\frac{2\pi}{\lambda}$ [1/m]
k_B	Boltzmann's constant 1.38×10^{-23} [J/K]

Operators

$\frac{\partial}{\partial t}$	partial derivative with respect to variable t
$\mathbf{A} \cdot \mathbf{B}$	dot product of vectors $\mathbf{A}$ and $\mathbf{B}$
$\mathbf{A} \times \mathbf{B}$	cross product of vectors $\mathbf{A}$ and $\mathbf{B}$
$\int_a^b$	defined integral from a to b

Abbreviations

AaSI	Aalto-1 Spectral Imager
ADCS	Attitude Determination and Control System
ADI	Antenna Deployment Indicator
ADS	Antenna Deployment System
BST	Berlin Space Technologies
BW	Bandwidth
CDS	CubeSat Design Specification
COTS	Commercial Off The Shelf
CubeSat	Standard for nanosatellites
CVCM	Collected Volatile Condensable Materials
EM	Engineering Model
EPS	Electrical Power System
EPB	Electrostatic Plasma Brake
EQM	Engineering Qualification Model
FM	Flight Model
FMI	Finnish Meteorological Institute
FPGA	Field-Programmable Gate Array
FSPL	Free-Space Path Loss
GS	Ground Station
IARU	International Amateur Radio Union
IEEE	Institute of Electrical and Electronics Engineers
ISIS	Innovative Solutions in Space
ITAR	International Traffic in Arms Regulations
ITU	International Telecommunication Union
LNA	Low Noise Amplifier
LV	Launch Vehicle
MDS	Minimum Discernable Signal
OBC	On-Board Computer
PCB	Printed Circuit Board
P-POD	Poly Picosatellite Orbital Deployer
POM	Polyoxymethylene
RADMON	Radiation Monitor, Aalto-1 payload
RBF	Remove Before Flight
RF	Radio Frequency
RL	return Loss
SEL	Single Event Latchup
SEU	Single Event Upset
SOIC	Small Outline Integrated Circuit
TEC	Total Electron Content
TML	Total Mass Loss
TVAC	Thermal Vacuum
UHF	Ultra High Frequency
VHF	Very High Frequency
VTT	Technical Research Center of Finland
WVR	Water Vapour Release

1 Introduction

The space age began in October 4th 1957 when Soviet Union launched Sputnik 1 satellite into Earth's orbit [1]. Since then, thousands of satellites have been launched. The size and mass of satellites have increased and typical satellite today has mass from tens of kilograms up to few tons [2]. The satellites play important role in modern society, providing services such as communications, navigation and weather forecast. Since the launch of Sputnik 1, the space industry has grown considerably, over 7000 satellites have been launched and today there are over 1000 active satellites [3][4].

The commercial aspects of satellites were quickly discovered and soon after the first satellite in the 60's the first commercial satellites have been launched. It is predicted that over the next decade (2013 – 2022) on average 115 satellites will be launched each year. Revenues from the manufacture and launch of these 1150 satellites are expected to be worth $236 billion [5].

Building and launching of satellites is expensive and the cost is directly related to the mass of the satellite. The high cost of launch has restricted satellite business mainly to big governmental institutions such as national space agencies. However, satellite building didn't stayed for long as a prerogative of governments or big companies. Just four years after the first satellite the first amateur satellite, OSCAR-1, was launched in 1961 in the United States [6]. Over the next four decades, the number of amateur satellites sent into orbit grew steadily. However, compared to commercial or government satellites the total number remained low, about 50 [7]. This trend has changed dramatically in the beginning of 2000 with the development of CubeSat standard. During the past decade more CubeSat standard amateur satellites have been launched than in all previous decades together [8].

The first amateur satellites were build by radio amateurs. Satellites were the natural expansion of radio amateurs continuous experiments in designing new antennas and radio systems. Today, most of the amateur satellites still use radio amateur frequencies in VHF and UHF bands for communication due to existing inexpensive hardware and benefit from radio amateur ground stations located around the world for telemetry reception. Also, amateur radio frequency bands are open for public and application process for reserving frequency for amateur satellite is easier. International Amateur Radio Union coordinates the use of radio amateur frequencies and assigns them to amateur satellites [8][9].

This thesis presents the design, testing and construction of Antenna Deployment System (ADS) for Aalto-1, a student built satellite. The Aalto-1 ADS is a double redundant system consisting of two v-shaped dipole antennas and an antenna release mechanism integrated with a timer circuit. Thesis chapters are organized as follows: chapters 2 and 3 introduces nanosatellites and theoretical background about antennas and radiowave propagation. Chapter 4 describes steps of designing antenna deployment system for Aalto-1. The workflow is divided into three parts: mechanical design, radio frequency (RF) design and electrical design. In chapter 5 the constructed prototype of Aalto-1 ADS is subjected to a series of tests to verify its performance. The final chapter 6 summarizes the achieved results.

2 Nanosatellite Communication and Antennas

This chapter introduces the CubeSat concept. Aalto-1, a CubeSat standard nanosatellite, its mission, structure and payloads are described. Also nanosatellite communications, antennas and antenna deployment systems are described in details.

2.1 Nanosatellites

Sputnik 1 had a mass of 83 kg [1]. The development of more powerful launch vehicles has allowed launching more bigger and heavier satellites. However, the continuous miniaturization of electronics and sensors in the past decades has changed the trend towards smaller satellites. The small satellites today can perform missions that previously required a big satellite.

As miniaturization of electronics continues, even smaller classes of satellites have been developed. The smallest satellites today have mass less than 100 g. Table 1 summarizes classification of satellites according to their wet mass [10].

Table 1: Small satellite classification.

Satellite Class	**Wet Mass**
Mini Satellite	100 – 500 kg
Micro Satellite	10 – 100 kg
Nano Satellite	1 – 10 kg
Pico Satellite	0.1 – 1 kg
Femto Satellite	10 – 100 g

2.2 CubeSat Design Specification

The CubeSat project was started in 1999 by California Polytechnic State University and Stanford University. The project developed a standard which defines the basic mechanical requirements for a 10 x 10 x 10 cm cube shaped satellite [11]. The 10 cm cube is known as 1U (one unit) and can be stacked on top each other making the design easily scalable. This standardized design has reduced costs and development time and helped to expand the market for nanosatellites. Especially universities have embraced this standard, which is the reason why the most of the CubeSats launched so far are by educational institutions [12].

CubeSat Design Specification (CDS) [11], first published in 2000 and still maintained by California Polytechnic State University, defines a list of requirements that all CubeSat standard nanosatellites have to follow to be compatible with a standardized deployment pod, Poly Picosatellite Orbital Deployer (P-POD) [13]. The P-POD, shown in Figure 1, is a square box with a door and a spring mechanism inside. The satellite is placed inside the P-POD which in turn is placed on the launch vehicle. Once in orbit, the spring pushes the CubeSat out of the P-POD. The relatively low launch cost of around $30000/kg [14], has allowed universities to launch their own satellites. Because of active development, the CubeSat has become a de facto standard in nanosatellite design.

Figure 1: P-POD deployment pod and 1U CubeSat [15].

The purpose of CDS is to ensure that all CubeSats are designed in such way that they don't pose threat to other CubeSats or to the launch vehicle (LV) and its primary payload. The most important requirements are listed below [11].

- The maximum mass of 1U CubeSat shall be 1.33 kg
- The maximum mass of 3U CubeSat shall be 4 kg
- All parts shall remain attached to the CubeSat during launch, ejection and operation
- No pyrotechnics shall be permitted
- CubeSat materials shall have a Total Mass Loss (TML) $\leq$ 1.0 %
- All deployables such as booms, antennas and solar panels shall wait to deploy a minimum of 30 minutes after deployment from P-POD

The CDS do not define the internal structure, allowing developers a freedom to choose a suitable design. Usually, CubeSat teams use stacked design for internal structure e.g. Aalto-1 design shown in Figure 2. The stacked design was introduced by Pumpkin company in their commercial satellite building kit CubeSat Kit [16]. Printed circuit boards (PCBs) in the stack are loosely based on PC/104 standard which is widely used in embedded computer systems. The PC/104 defines the form factor of the PCB board and the bus connector. The form factor of PCB is very close to CubeSat standard defined 10 x 10 cm size [17]. Boards can be stacked on top each other thus making the system easily scalable from 1U to 3U CubeSats.

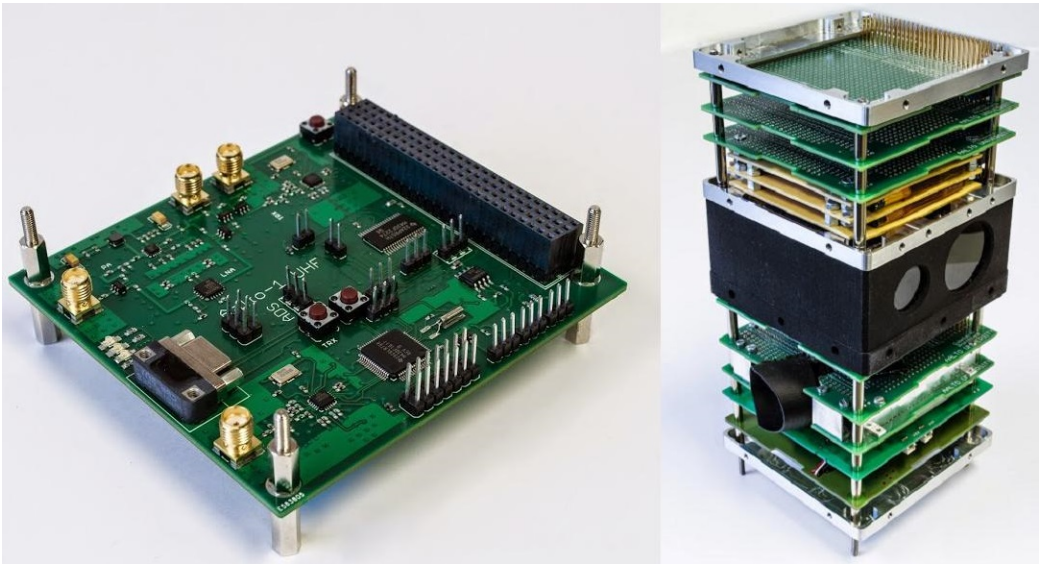

Figure 2: CubeSat Kit style board and stack of boards used in Aalto-1 (Picture by Tuomas Tikka).

Electronics in satellites are usually made using special space grade components. These components are made using special space qualified materials with higher level quality process when compared to components for normal commercial use. Space qualified components also are subjected to comprehensive testing to verify tolerance to vibrations, radiation and extreme temperatures. Small manufacturing numbers and comprehensive testing makes space qualified components very expensive. In addition, majority of space qualified components are US origin and thus subject to US government International Traffic in Arms Regulations (ITAR) restrictions. The ITAR controls what US made components can be exported to foreign countries [18]. Getting export license can be difficult. All this makes acquiring space qualified components a difficult task.

Electronics in CubeSats are typically made using cheap non-space graded components. While these components haven not been designed for space use, some CubeSats have remained functioning for several years [9]. CubeSats are usually launched to low Earth orbits (200 – 3000 km) [19]. At these altitudes, radiation levels are not high because of the Earth's protective magnetosphere.

2.3 Aalto-1 Nanosatellite

The Aalto-1 nanosatellite project began in winter 2010. The satellite is based on CubeSat 3U design and has external dimensions of 34 x 10 x 10 cm and mass of 4 kg. The satellite is planned to be launched into 400 – 750 km sun-synchronous polar orbit in 2016 and to have operational mission time of 2 years [20]. The goal of the project is to give students an experience in carrying out a real space project as well as building a real space hardware.

The satellite is designed and build mainly by students of Aalto University in co-operation with Technical Research Center of Finland (VTT), Finnish Meteorological Institute (FMI), University of Turku, University of Helsinki, Turku University of Applied Sciences, Berlin Space Technologies (BST) and Clyde Space. The following satellite systems are designed and built in Aalto University: satellite structure, UHF antennas deployment system (ADS), UHF radio, On-Board Computer (OBC) system, S-band radio, S-band antenna, sun sensors and solar panels. Electrical Power System (EPS) is purchased from Clyde Space. Attitude Determination and Control System (ADCS) is provided by BST.

The satellite has three scientific payloads. The main payload is AaSI or Aalto-1 Spectral Imager. It is a spectral camera based on the novel miniaturized Fabry-Pérot interferometer, developed by VTT. AaSI will be used to take images of a selected target, e.g. forest or water for studying [21].

The second payload is RADMON or Radiation Monitor developed by University of Turku and University of Helsinki. The sensor unit of RADMON consists of two detectors that will measure the flux densities of charged particles. The RADMON uses novel front-end electronics. Instead of conventional approach using analog detector electronics for signal processing, the signal from the sensor is digitized first and the processed with FPGA logic [22].

The third payload is an Electrostatic Plasma Brake (EPB). EPB is a spin-off of an Electric Solar Wind Sail (E-Sail) concept, developed by Pekka Janhunen at FMI [23]. While E-Sail is designed to propel spacecraft without fuel, EPB is designed for deceleration. The EPB consists of a 100 m long tether that will be deployed after the end of the Aalto-1 mission. EPB will demonstrate the possibility to bring satellites down faster when their mission is over.

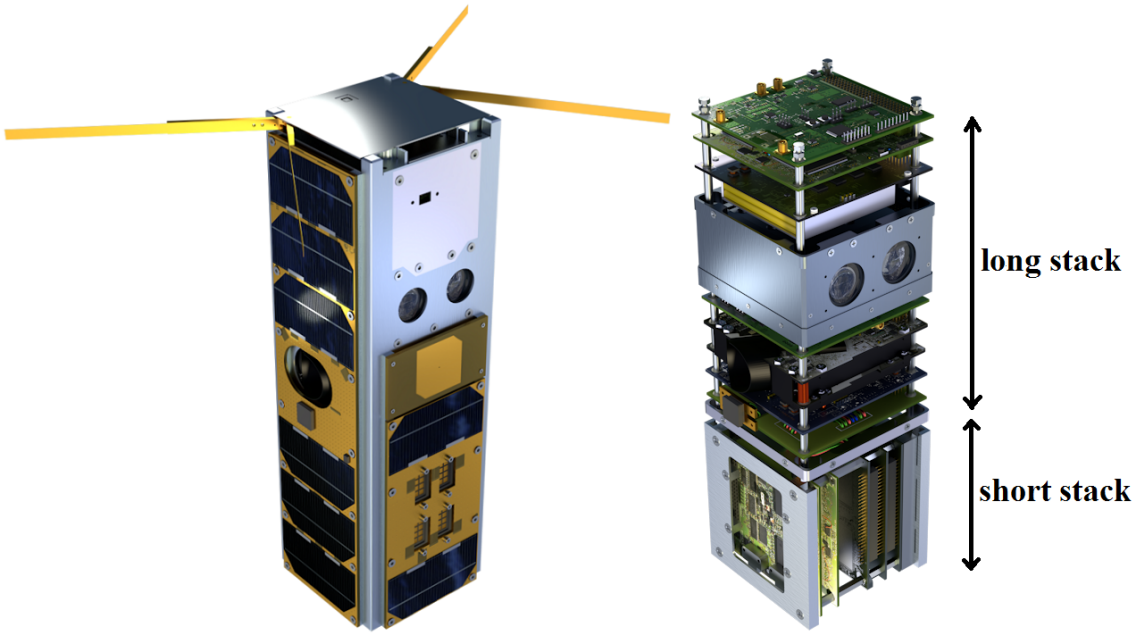

Figure 3: Aalto-1 satellite and its internal structure (Picture by Pekka Laurila).

The outer structure of Aalto-1 is made from two aluminium blocks milled into U-shape. The gap between them is covered by additional two aluminium panels. The outer structure is covered with solar panels which are PCB boards to which solar cells are glued. Like many other CubeSats, Aalto-1 internal structure, shown in Figure 3, is based on Pumpkin's CubeSat Kit stack design. There are two stacks, the long stack and the short stack. On top is Antenna Deployment System (ADS). ADS forms part of the outer structure and covers the top of the satellite. ADS contain two UHF antennas, a timer circuit for deployment mechanism and a sun sensor for ADCS.

The long stack assembly contains UHF radio board that provides communication link with the ground station and a beacon signal. The On-Board Computer (OBC) controls the satellite subsystems and payloads. The battery board provides power for subsystems and payloads when power output from solar panels is not enough. The S-band radio board provides a higher downlink data rate than UHF radio and is used to transmit images obtained by AaSI. The ADCS controls satellite orientation in orbit and EPS board distributes power generated by solar panels to subsystems, payloads and charges batteries. At the end of the long stack is the short stack. The short stack is positioned perpendicularly to the long stack. The reason for that is requirement by EPB. The short stack contains the other two payloads RADMON and EPB.

2.4 Nanosatellite Communications

In order to deliver the measurements and receive commands, a satellite need a communication system. The communication system has to overcome several challenges. The long distance between the orbiting satellite and the ground station, Earth's atmosphere and ionosphere, all this creates a challenging path for transmitted radio signal. An additional layer of constrains are international treaties regarding what frequencies can be used for satellite communications.

Designing communication system for a nanosatellite is even more challenging as nanosatellites have very limited power generation capability. Additional constrain is the small size of the nanosatellite which makes complex antenna structures not feasible.

Nanosatellites utilize mostly radio amateur frequencies for communications. Globally, International Telecommunication Union (ITU) coordinates the use of radio spectrum from 3 kHz to 300 GHz and has set aside frequency bands reserved for radio amateur transmissions [24]. The radio amateur transmissions are specified as radio transmissions intended for private recreation, wireless experimentation and non-commercial purpose. International Amateur Radio Union (IARU) coordinates the use of radio amateur frequencies and represents radio amateurs in ITU [25].

To apply for frequencies to be used in nanosatellite communications, a frequency coordination request has to be sent to IARU and to national telecommunication authority. IARU allocates a freely available frequency in the requested frequency band. National authority checks whether allocated frequency can be used in the host country and provides a call sign for the satellite.

Most nanosatellite missions don't require a high data throughput and communication links typically use frequencies below 1 GHz. Usually, nanosatellites use two frequency bands, VHF (144 – 146 MHz) and UHF (435 – 438 MHz) [9]. Higher frequencies are used in some satellites usually as an experiment to test high frequency communication link or they have payloads that generate large amount of data such as spectral imager in the case of Aalto-1. The complete list of nanosatellites launched since 2003, their communication frequencies and antenna types is listed in Appendix A [26].

2.5 Nanosatellite Antennas

Satellite communication system needs antennas to function. The most common nanosatellite antennas can be categorized into two groups: a wire antenna and a microstrip patch antenna. Wire antennas are typically monopole, dipole or turnstile antennas that use a conductive wire as a radiating element [27]. These antennas are typically used in VHF and UHF frequency bands. They are the most popular antenna type in CubeSat nanosatellites because the limited space and mass restrictions prevents the use of more complex antenna geometries. The radiating element is usually made from flexible metal strip, similar to one used in the measuring tape. This flexible metal strip offers the best properties for a CubeSat antenna: it is cheap, flexible and allows antenna to be rolled in a small space without permanent deformation.

Another type of antenna used nanosatellites is patch antenna. As the name implies this antenna uses a conductive patch as a radiating element. Patch antenna requires an electrical ground to function properly. In nanosatellites the function of ground plays the body of the satellite to which patch antenna is attached. Because patch antenna size depends on the operating frequency they are typically used at frequencies above 1 GHz. Only then antenna becomes small enough to be fitted on the side of the satellite.

Since the launch of the first amateur nanosatellite, they have become more sophisticated and their sensor payloads generate more data. Transferring the data to Earth has become a bottleneck using current antenna designs. Lately, more complex designs have started to appear on nanosatellites, allowing higher data throughput to Earth. Examples of these antennas are: deployable helical antennas [28][29], deployable mesh dish antennas [30][31] and an inflatable dish antenna [32].

2.6 Antenna Deployment Systems for CubeSats

The CubeSat standard satellites are deployed from the P-POD or a similar system. The Poly Picosatellite Orbital Deployer is standardized CubeSat deployment system. It is capable of carrying three standard 1U CubeSats and serves as the interface between the CubeSats and the launch vehicle. The P-POD is a rectangular box made from anodized aluminum with a door and a spring mechanism (see Figure 4). CubeSats slide along rails positioned in the corners of the P-POD during ejection into orbit.

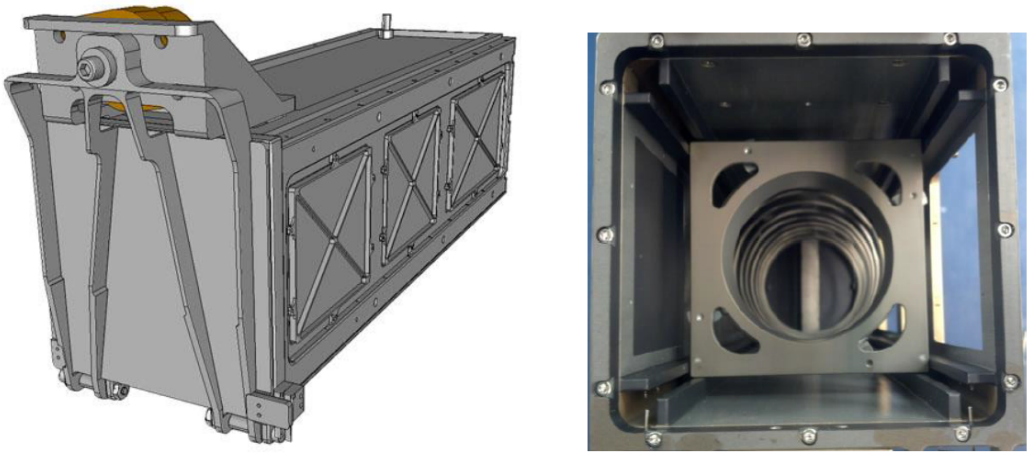

Figure 4: Poly-Picosatellite Orbital Deployer (P-POD) [11].

Wire antennas typically used in CubeSats are relatively long in comparison to satellite size because of the frequencies used in communications. These antennas cannot be sent into space already deployed. The Antenna Deployment System (ADS) allows them to be stowed during the journey and deployed once the satellite is in orbit.

The antenna deployment systems can be roughly divided into two categories: the "wrap-around" and "roll-up" designs. In wrap-around design, antennas are simply wrapped around the body of the satellite or around a support structure attached to the side of the satellite. In a roll-up design, the antennas are rolled into a coil, like a measuring tape, and stored inside the ADS. In both designs a release mechanism keeps antennas in stowed position. Once satellite is deployed from the P-POD, the satellite has to wait 30 minutes before opening antennas and additional 15 minutes before any transmissions from the satellite are allowed. This is a requirement specified by the CDS [11].

2.6.1 Commercial Antenna Deployment Systems

Since the 2000, the active development of CubeSat based nanosatellites has led to CubeSat becoming a de facto standard in nanosatellite design. This has led to growth of a number of companies providing standardized CubeSat parts like, structure, batteries, solar panels, power systems, etc. [16][34][35]. Some companies, like ISIS (Innovative Solutions In Space) and GomSpace, started as spin-off companies from university CubeSat projects.

There are few commercially available antenna deployment systems for CubeSat standard satellites. One of them is provided by ISIS [33]. The ISIS ADS uses "roll-up" design. It has four antennas and a RF phasing circuitry which allows configuration into monopole, dipole or turnstile configuration (see Figure 5). In stowed position the antennas are rolled inside ADS like in measuring tape. Release mechanism of this ADS is a heating-element-and-retention-string design which is widely used in CubeSats.

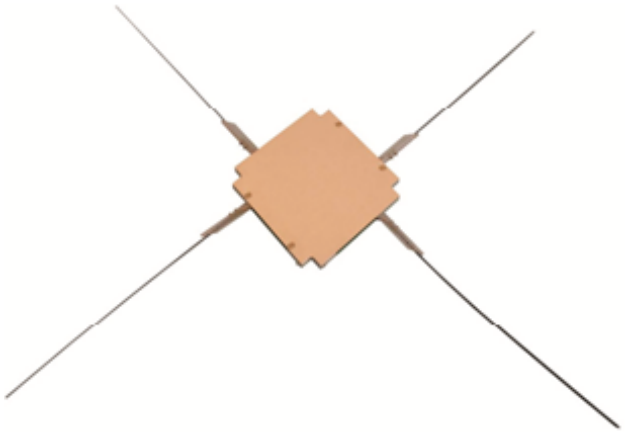

Figure 5: ISIS Antenna Deployment System [34].

Another commercial ADS is from GomSpace [35]. Unlike ISIS, GomSpace offers only one antenna configuration, turnstile. The four antennas looks to be a wrap-around design but antennas are rigid not flexible (see Figure 6). There is a hinge at the base of the antenna that allows antenna to be rotated parallel to the side of the satellite. According to GomSpace, rigid antennas eliminates the risk of antenna deformation while stowed. On the other hand, if this type of ADS is used in 1U CubeSat antennas have to be shortened to fit 1U size. This will degrade antenna performance. The release mechanism is the standard heating-element-and-retention-string design.

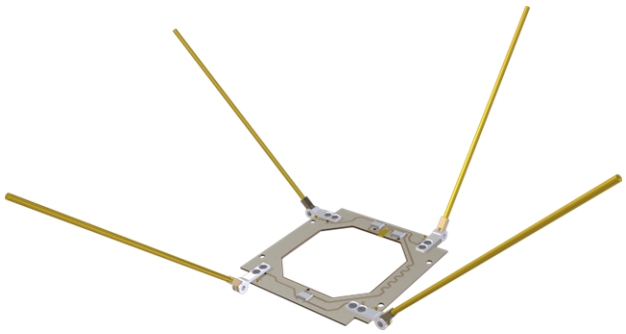

Figure 6: GomSpace Antenna Deployment System [35].

2.6.2 Other Designs

Most of the CubeSats by today are designed by educational institutions [12]. Typically, the main goal of the project is educational, to give students an opportunity to participate in a real space project and design and build an actual space hardware. The CubeSat standard allows a great flexibility to choose whether you use commercially available subsystems or design your own. In many CubeSats ADS is often an indigenous design which is specifically tailored for mission requirements.

Depending on the antenna type and number of antennas, CubeSat size and space available, there are numerous creative ADS designs. ADS can be very simple such as monopole attached on one side and wrapped around satellite structure (see Figure 7). Some ADS designs, e.g. Univeristy of Tokyo's XI-V satellite, use a support structure on the surface of the satellite to wrap antennas around (see Figure 7).

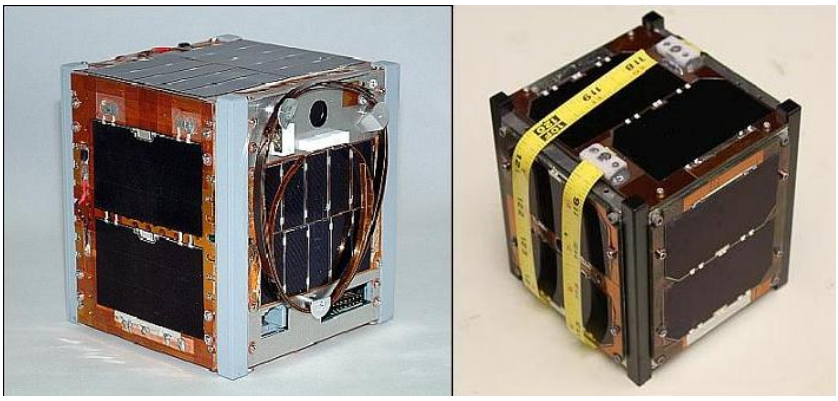

Figure 7: Wrap-around dipole and monopole antennas on XI-V and M-Cubed satellites [36][37].

Some Cubesats, like Dutch Delfi-C^3 and Norwegian nCube, use roll-up design where the antennas are rolled into a coil and stored in a special antenna housing. In Delfi-C^3, antenna housings are placed onto a printed circuit board which is part of the internal stack structure (see Figure 8). The board is located at the top of the stack so that once deployed antennas stick ouside the satellite structure [38].

In the nCube satellite, instead of separate board, antenna housings are intergrated into the side wall of the satellite structure. Antenna deployment happens when housing swings open like a door allowing antenna stored in the housing to unroll (see Figure 8) [39].

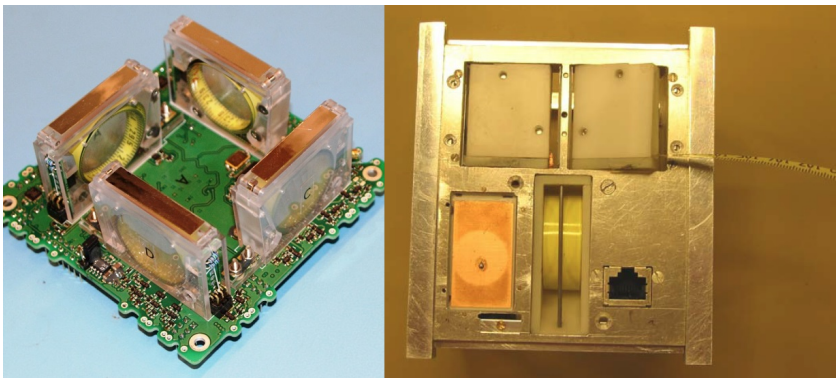

Figure 8: Antennas inside Delfi-C^3 antenna housings and nCube with antenna deployed from the antenna housing [38][39].

3 Antenna Theory

This chapter gives theoretical background of antenna design and antennas. Different types of antennas are briefly described with emphasis on wire antennas. Also, central concepts of RF engineering are explained such as reflection coefficient, gain, antenna impedance and bandwidth. In addition, concepts related to radiowave propagation and specific aspects related to satellite-to-Earth communications are explained.

3.1 Electromagnetic Radiation

Electromagnetic radiation is a phenomenon of electromagnetism - one of the fundamental interactions in nature. The radiation propagates through space as oscillating electromagnetic wave. As the name implies, it has both electric and magnetic components. Electric and magnetic fields oscillate orthogonally and transversely to direction of propagation (see Figure 9).

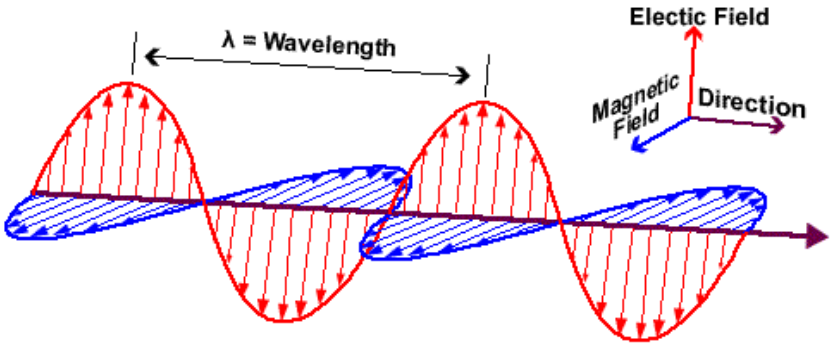

Figure 9: Electromagnetic wave [40].

Electricity and magnetism were for a long time considered to be a separate phenomena until James Clerk Maxwell published his theory on electromagnetics in 1873 [41]. The equations in his theory described how electric and magnetic fields can propagate and how these fields are altered by each other and by electric charges. These equations became to be known as Maxwell's equations:

$$\nabla \cdot D = \rho, \tag{1}$$

$$\nabla \cdot B = 0, \tag{2}$$

$$\nabla \times E = -\frac{\partial B}{\partial t}, \tag{3}$$

$$\nabla \times H = J + \frac{\partial D}{\partial t}, \tag{4}$$

where D is the electric displacement field, ρ is the electric charge density, B is magnetic flux, E is electric field, H is magnetic field and J is current density.

The Maxwell's equations predicted existence of radio waves which were empirically confirmed 20 years later by Heinrich Hertz [41]. The International Telecommunications Union (ITU), which coordinates the use of radio spectrum, has defined radio waves as electromagnetic radiation covering the lower part of electromagnetic spectrum starting from 3 kHz to 300 GHz. This spectrum has been devided into several frequency bands with specific names (see Table 2) [24]. The frequency above 1 GHz has additional division into more narrower bands which are named using letters L, S, C, X, Ku, K, Ka, V and W [42].

Table 2: ITU radio bands [24].

Abbreviation	**Designation**	**Frequency Range**
VLF	Very Low Frequency	3 to 30 kHz
LF	Low Frequency	30 to 300 kHz
MF	Medium Frequency	300 to 3000 kHz
HF	High Frequency	3 to 30 MHz
VHF	Very High Frequency	30 to 300 MHz
UHF	Ultra High Frequency	300 to 3000 MHz
SHF	Super High Frequency	3 to 30 GHz
EHF	Extremely High Frequency	30 to 300 GHz

3.2 Antennas

According to IEEE definition antenna is a "transmitting or receiving system that is designed to radiate or receive electromagnetic waves" [43]. In other words antenna is a transducer, a device that converts electrical signals to propagating electromagnetic waves. A transmission line equivalent of an antenna can be represented by impedance Z_A, (see Figure 10) where resistance R_L reprecents dielectric losses and conduction losses caused by antenna structure and radiation resistance R_r represents the radiation of antenna. The power that is dissipated in R_r is the power that is radiated by the antenna. The radiation resistance is determined by geometry of the antenna, while loss resistance is primarily determined by the materials of which it is made. Reactance X_A is an imaginary part of antenna impedance. It represents the energy stored in the near-field of the antenna.

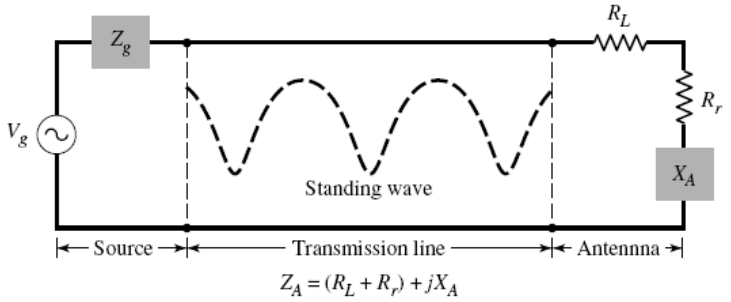

Figure 10: Transmission line equivalent of antenna [27].

In the early days of radio communications, wire antennas such as dipole and monopole were the most common antenna types. In the 1930's, interest in higher frequencies and maturation of antenna theory led the development towards other antenna types like horn, slot and reflector antennas. The 1960's introduced numerical methods (Moment Method, Finite-Difference Method) that allowed complex antenna structures to be analyzed. Microstrip antennas were developed in the 1970's and have become widely used in many communication devices today. Advances in computer technology and numerical electromagnetic analysis softwares in the 1980's allowed even more complex antenna structures to be developed [44]. Today, the latest developments in the field of antenna engineering are utilization of new materials such as metamaterials and articifial magnetic conductors to improve antenna performance. The advancement in computing capabilities has led the development of smart antennas that can dynamically reconfigure their parameters such as frequency, radiation pattern or polarization.

3.3 Wire Antennas

The first antennas were made in 1886 by Heinrich Hertz in his experiment to prove electromagnetic wave theory proposed by James Clerk Maxwell. Hertz himself didn't thought there would be any practical use of this experiment. It was Italian Guglielmo Marconi who saw the potential in Hertz's experiment and led the pionering work in long-distance radio communications.

Prior to World War II, the radiating elements of antennas were mostly wires in different configurations e.g. dipoles, monopoles, helices, rhombuses, etc. Wire antennas were the only practical mean to transmit signals over long distances in the early days of radio communications up until mid-thirties. At that time the need for compact communication equipment made utilization of highter frequencies attractive. Nevertheless, wire antennas being one of the most simple antenna types have remained in use until these days [45]. Because of their simplicity, wire antennas are the most common antenna type used in CubeSats. Another reason is allowed radio amateur bands for satellite communications are in VHF and UHF range. At these frequencies other antenna types such as patch or dish become impracticly large to be used in CubeSats.

3.3.1 Infinitesimal Dipole

Infinitesimal dipole (also known as Hertzian Dipole) is not an actual antenna but a mathematical approximation that is used as a building block for calculating current distributions and fields of other practical wire antennas. Infinitesimal dipole (see Figure 11) is infinitesimally short ($l \ll \lambda$) and infinitesimally thin ($a \ll \lambda$) and thus has a uniform current distribution. Because of linearity of Maxwell's equations, any arbitrary current distribution in a wire antenna can be represented as a series of infinitesimal dipole current distributions. Thus, a field produced by arbitrary current distribution of a wire antenna of a finite length can be calculated by summing the contributions of all infinitesimal dipoles [46].

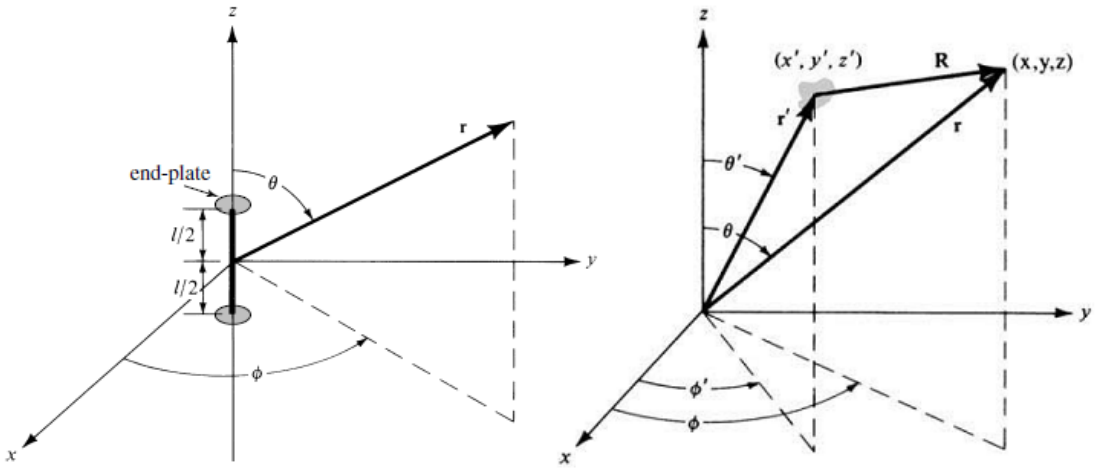

Figure 11: Infinitesimal dipole and coordinate system for computing fields [27].

Electric and magnetic fields are usually calculated from a magnetic vector potential A. The magnetic vector potential is a vector field that satisfies criteria $B = \nabla \times A$. For line current e.g. in a wire antenna the magnetic vector potential has the following equation:

$$A(x, y, z) = \frac{\mu}{4\pi} \int I(x', y', z') \frac{e^{-jkR}}{R} dl', \tag{5}$$

where μ is permeability, I is the current distribution along the wire, j is the imaginary unit, k is the wave number, (x, y, z) are coordinates of the observation point, (x', y', z') are coordinates of the source and R represents the distance between these two points. For infinitesimal dipole $x' = y' = z' = 0$, current distrinbution simplifies to:

$$I(x', y', z') = \mathbf{a}_z I_0, \tag{6}$$

and

$$dl' = dz', \tag{7}$$

where I is the current distribution along the wire, I_0 is current with constant amplitude and $\mathbf{a}_z$ is a unit vector along the z-axis. Distance R simplifies to:

$$R = \sqrt{(x - x')^2 + (y - y')^2 + (z - z')^2} = \sqrt{x^2 + y^2 + z^2} = r, \tag{8}$$

where r is constant [27]. Substituting (6), (7) and (8) into (5) the magnetic vector potential for infinitesimal dipole is thus:

$$A(x, y, z) = \mathbf{a}_z \frac{\mu I_0}{4\pi r} e^{-jkr} \int_{-l/2}^{+l/2} dz' = \mathbf{a}_z \frac{\mu I_0 l}{4\pi r} e^{-jkr}, \tag{9}$$

where $\mathbf{a}_z$ is a unit vector along the z-axis, I_0 is current with constant amplitude and l is length of the dipole.

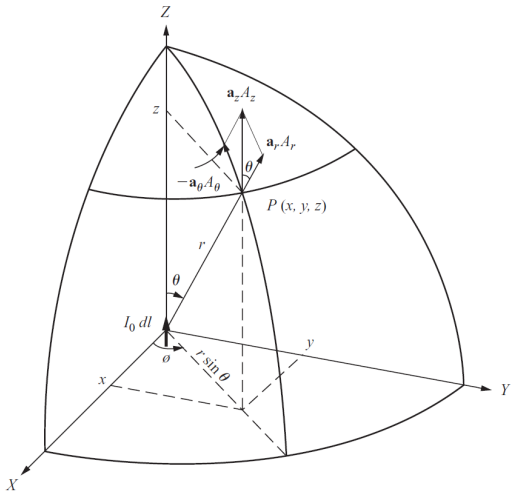

Figure 12: Components of the vector potential on the surface of a sphere [46].

The magnetic vector potential is shown in Cartesian coordinates but fields are more suitable to be represented in spherical coordinates because of the e^{-jkr} term which indicates an outgoing spherical wave. From Figure 12 componets of A in spherical coordinates are:

$$A_r = A_z cos\theta, \tag{10}$$

$$A_\theta = -A_z sin\theta, \tag{11}$$

$$A_\phi = 0. \tag{12}$$

The corresponding magnetic and electric fields are obtained from magnetic vector potential using relationships in Equations (13) and (14):

$$H = \frac{1}{\mu}\nabla \times A, \tag{13}$$

$$E = \frac{1}{j\omega\epsilon}\nabla \times H, \tag{14}$$

where ω is angular frequency and ϵ is permittivity. Using Equations (13) and (14) magnetic and electric fields of infinitesimal dipole are:

$$H_\phi = j\frac{kI_0 l sin\theta}{4\pi r}\left[1 + \frac{1}{jkr}\right]e^{-jkr}, \tag{15}$$

$$E_r = \eta\frac{I_0 l cos\theta}{2\pi r^2}\left[1 + \frac{1}{jkr}\right]e^{-jkr}, \tag{16}$$

$$E_\theta = j\eta\frac{kI_0 l sin\theta}{4\pi r}\left[1 + \frac{1}{jkr} - \frac{1}{(kr)^2}\right]e^{-jkr}, \tag{17}$$

where η is is the wave impedance of the medium. Equations (15), (16), (17) are the starting point from which electric and magnetic fields of any wire antenna can be calculated.

3.3.2 Dipole and Monopole Antennas

Two of the most common wire antennas are dipole antenna and monopole antenna. As the name implies the dipole antenna consists of two radiating wires that are fed in the center. The antenna becomes resonant and radiates well when its length is an odd multiple of a half-wavelength e.g. 0.5λ or 1.5λ. The radiation properties of the dipole depends on the current distribution along the wire which in turn depends on the length of the dipole. For the half-wavelength dipole antenna, which is the most common of all dipole antennas, radiation pattern is symmetrical along the azimuthal ϕ coordinate as can be seen in Figure 13b.

The monopole antenna is formed by replacing the other half of the dipole antenna with a conductive ground plane shown in Figure 13d. Using image theory, the conductive ground plane can be replaced with the missing half of the dipole. In case of infinite ground plane, the radiation pattern of a monopole above the ground plane is similar to the dipole pattern and zero below the ground plane. The directivity of monopole on the infinite ground plane is twice that of the similar dipole antenna. In reality the ground plane is not infinite and could be very small as in the case of the satellite. As a rule of thumb, directivity, the total radiated power and the radiation resistance are half of a dipole antenna, resulting in overall lower effciency compared to dipole antenna.

The wire antennas are inherently resonant and thus they have a narrow bandwidth centered around antenna's resonant frequency. Due to the narrow bandwidth and omnidirectional radiation properties, wire antennas are typically used in spacecrafts for low data rate applications such as telemetry transmissions for CubeSats.

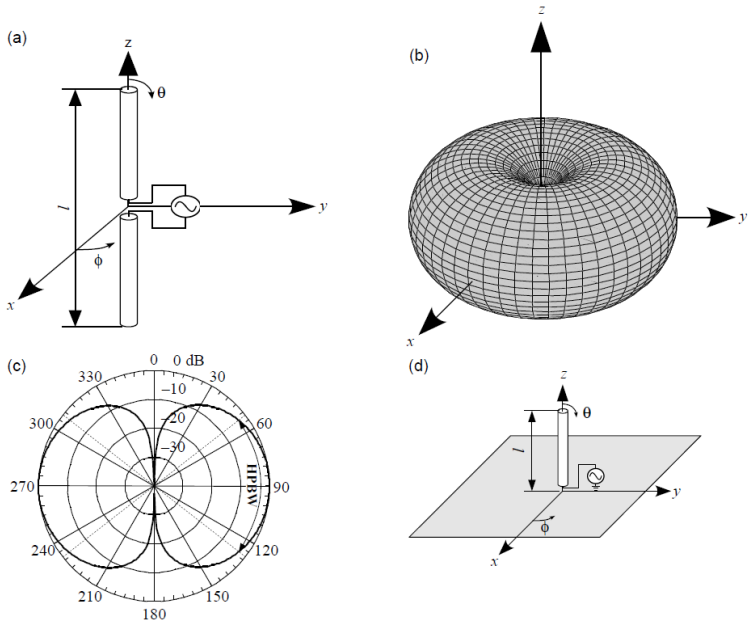

Figure 13: Dipole and monopole antennas: (a) dipole antenna geometry; (b) 3D radiation pattern; (c) elevation plane radiation pattern; (d) monopole antenna geometry [47].

3.4 Antenna Performance Parameters

In this chapter performance parameters of antenna are described. Performance of antenna is characterized by parameters such as gain, impedance, resonant frequency, etc. In addition, the fundamental property of all antennas is reciprocity which means that antenna characteristics such as impedance, gain, resonant frequency, etc. are same whether antenna is transmitting or receiving.

3.4.1 Radiation Pattern

Antennas radiate electromagnetic waves in the surrounding environment. This radiation is not uniformly distributed in space and strongly depends on the antenna geometry. The non-uniform spatial distribution of radiated energy as a function of the observer's position is called radiation pattern. It is typically represented in spherical coordinates $[\theta, \phi]$ as a three-dimensional diagram using logarithmic scale (see Figure 13b). Often a more useful representation is a planar cut along E- or H-plane of the antenna which shows radiation pattern in elevation plane (see Figure 13c) or azimuthal plane. Usually, the radiation pattern is not uniform. Some regions have stronger radiation and some have weaker. Regions of stronger radiation are called lobes (see Figure 14). The region of strongest radiation is called the main lobe. The other lobes are called side lobes. Associated with lobes is parameter Half-Power Beamwidth (HPBW) which indicates how wide is the lobe between two directions in which the radiation intensity is one-half value of the beam.

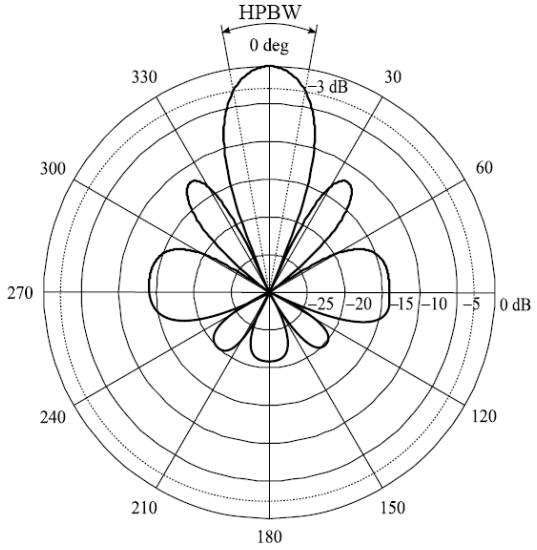

Figure 14: Lobes in radiation pattern [47].

Antennas that have a strong main lobe are called directional antennas. If antenna has uniform radiation pattern along ϕ coordinate it is called omnidirectional antenna. Isotropic antenna is an ideal antenna that radiates uniformly in all directions. Such antennas are physically impossible but isotropic antenna is often used as a reference for gain of other antennas.

3.4.2 Directivity

Directivity D shows how much energy antenna radiates in certain direction compared to the radiation of an isotropic antenna. In physics, the directional energy flux density of an electromagnetic field is represented by the Poynting vector S. Isotropic antenna radiates uniformly in all directions, thus the average Pointing vector over a sphere is:

$$S(\theta, \phi)_{ave} = \frac{1}{4\pi} \int_0^{2\pi} \int_0^{\pi} S(\theta, \phi) d\Omega, \tag{18}$$

where $d\Omega$ is element of solid angle shown in Figure 15.

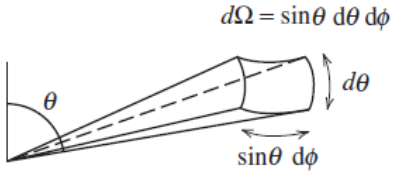

Figure 15: Element of solid angle [45].

Directivity is thus can be expressed as:

$$D(\theta, \phi) = \frac{S(\theta, \phi)_{max}}{S_{ave}}. \tag{19}$$

Substituting (18) into (19) we get:

$$D = \frac{1}{\frac{1}{4\pi} \int_0^{2\pi} \int_0^{\pi} \frac{S(\theta,\phi)}{S(\theta,\phi)_{max}} d\Omega} = \frac{4\pi}{\Omega_A}, \tag{20}$$

where Ω_A is a beam solid angle [41]. From the Equation (19) we can see that the narrower the angle the more directive antenna is. Conversely, omnidirectional antennas have low directivity.

3.4.3 Antenna Efficiency

An ideal lossless antenna would radiate all power that it accepts. In reality that is not the case. The losses assosiated with antenna can be defined by a number of efficiency factors. Radiation efficiency e_r is defined as the ratio of power that antenna radiates away to the net power accepted by the antenna:

$$e_r = \frac{P_{rad}}{P_{in}}, \tag{21}$$

where P_{rad} is radiated power and P_{in} is power accepted by the antenna [45]. Reflection mismatch efficiency e_ρ is the ratio of power accepted by the antenna to the power delivered to the antenna by transmission line:

$$e_\rho = 1 - |\Gamma|^2, \tag{22}$$

where Γ is a voltage reflection coefficient at the antenna input [27].

3.4.4 Gain

One of the most important antenna performance parameters is gain. Gain is closely related to directivity but, while directivity is determined by the radiation pattern of the antenna, gain also takes into account radiation efficiency e_r.

$$G = e_r D \tag{23}$$

According to IEEE standards, the definition of antenna gain does not include impedance mismatch loss e_ρ nor mismatch from polarization e_{PLF} [43]. The realized gain $G_{realized}$ takes into account these losses.

$$G_{realized} = e_r e_\rho e_{PLF} D \tag{24}$$

3.4.5 Bandwidth

In chapter 3.2 transmission line equivalent of antenna is represented by input impedance Z_A. Input impedance is the ratio of voltage V and current I at the antenna feedpoint. At radio frequencies voltage and current are not practical quantities and input impedance is usually defined using antenna reflection coefficient Γ and characteristic impedance Z_0 of transmission line which is connected to antenna feedpoint [47].

$$Z_A = \frac{V}{I} = Z_0 \frac{1+\Gamma}{1-\Gamma} \tag{25}$$

Antenna impedance usually changes as a function of frequency and thus impedance mismatch is also depending on frequency. Usually, impedance mishmatch is represented in decibels and known as return loss (RL) (see Figure 16). The bandwidth of an antenna is defined as the range of frequencies within which the performance of the antenna, with respect to some characteristic, conforms to a specified standard [27]. Typically, a sertain level e.g. -10 dB or -15 dB of RL defines the bandwidth.

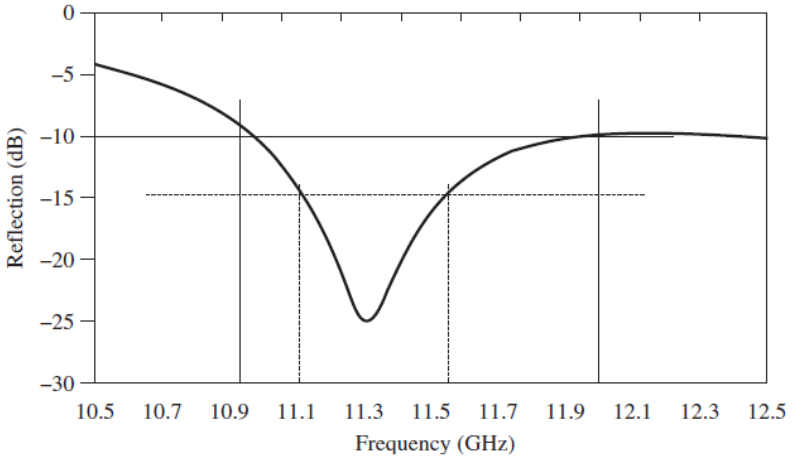

Figure 16: Bandwidth defined by return loss as a function of frequency [44].

3.4.6 Polarization

Polarization of an antenna refers to polarization of electromagnetic wave radiated by the antenna. Polarization is a property of electromagnetic wave describing a time-varying direction and relative magnitude of electric field vector. Specifically it is a figure traced as a function of time by vector at a fixed location in space [27]. Polarization is classified into linear, circular or elleptical (see Figure 17). Linear polarization can be divided into vertical and horizontal polarizations with respect to the observer. Circular and elliptical polarizations can be left-handed or right-handed.

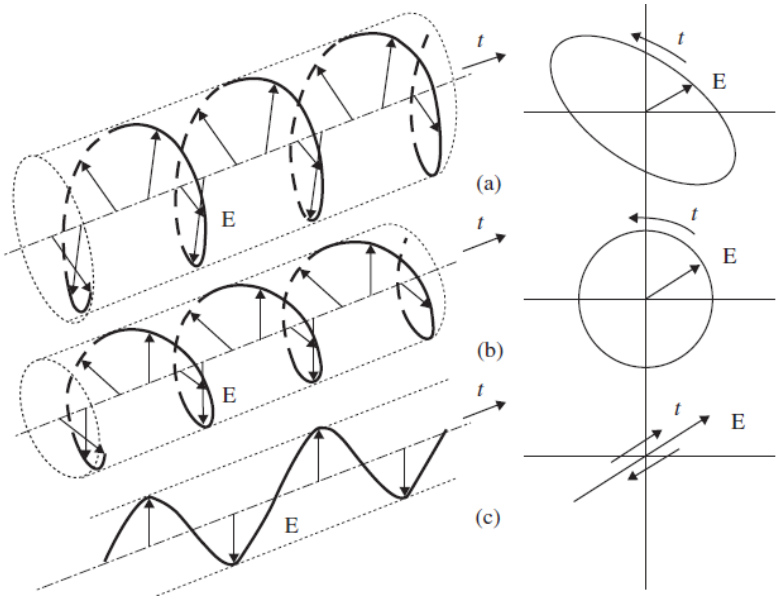

Figure 17: Polarization states. (a) Elliptical polarization. (b) Circular polarization. (c) Linear polarization [44].

Axial ratio AR is a term assosiated with circularly polarized antennas. In Figure 18, AR is the ratio of two orthogonal components of electric field vector and describes how circular the polarization is. Linearly polarized wave has $AR = \infty$ and ideal circularly polarized wave has $AR = 1$. Usually AR is expressed in dB.

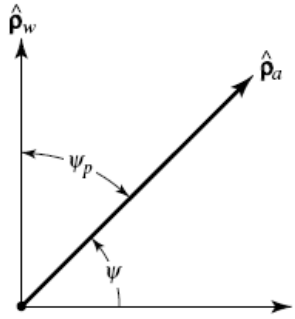

Figure 18: Polarization vectors of incident wave (p_w) and antenna (p_a) [27].

Typically, polarization of transmitting antenna is not the same as the polarization of receiving antenna. The result of this is a polarization mismatch which means that not all energy radiated by transmitting antenna will be accepted by receiving antenna. Figure 18 shows that when vectors are aligned the polarization mismatch loss is zero and when vectors are orthogonal the loss is maximum. Polarization loss factor can be defined as:

$$e_{PLF} = |p_w \cdot p_a|^2 = |cos\psi_p|^2, \tag{26}$$

where p_w and p_a are polarization vectors of incident wave and receiving antenna [27].

3.5 Radiowave Propagation

In Earth-satellite transmissions there are always losses due to various sources. Daily changes in water wapor in troposphere increases attenuation. Sun's activity affects the ionization of upper atmosphere which in turn affects polarization of transmitted signal. All these losses have to be taken into account when calculating communication link budget between the ground station and the satellite. Figure 19 summarizes the major losses in satellite communications.

<table>
<tr><td rowspan="11">TRANSMISSION LOSSES</td><td rowspan="9">PROPAGATION LOSSES</td><td colspan="3">FREE SPACE LOSSES</td></tr>
<tr><td rowspan="8">ATMOSPHERIC LOSSES</td><td>Ionospheric effects</td><td>Faraday rotation
Scintillation effects</td></tr>
<tr><td rowspan="6">Tropospheric effects</td><td>Attenuation</td></tr>
<tr><td>Rain attenuation</td></tr>
<tr><td>Gas absorption</td></tr>
<tr><td>Depolarization</td></tr>
<tr><td>Sky noise</td></tr>
<tr><td colspan="2">Local effects</td></tr>
<tr><td colspan="3">POINTING LOSSES</td></tr>
<tr><td rowspan="3">LOCAL LOSSES</td><td rowspan="2">EQUIPMENT LOSSES</td><td>Feeder losses</td></tr>
<tr><td>RF switch losses</td></tr>
<tr><td colspan="2">ENVIRONMENT LOSSES</td></tr>
</table>

Figure 19: Major losses in satellite communications [48].

3.5.1 Free Space Loss

As electromagnetic wave propagates through space it attenuates as the power density of the wave decreases. The free-space path loss (FSPL) describes the attenuation of the wave as a function of distance [46]. The wavelength λ relates to the frequency f as $\lambda = \frac{c}{f}$. Thus, the free-space path loss increases as the frequency increases.

$$FSPL = 10 \cdot log_{10} \frac{(4\pi r)^2}{\lambda^2} \tag{27}$$

3.5.2 Atmospheric Losses

Earth's atmosphere creates additional losses for signal travelling to the ground station. The main contributing factors are ionospheric effects and tropospheric effects. Ionospheric effects include Faraday rotation and Scintillation effects.

Faraday rotation is a progressive change of polarization sense of radio wave as it propagates through Earth's ionosphere. The rotation is caused by the interaction of radio wave with electrons in the ionosphere in the presence of the Earth's magnetic field.[49] The effect varies depending on the total electron content (TEC) in ionosphere which in turn depends on the Sun activity (see Figure 20). To mitigate this effect space communication systems use usually circularly polarized antennas for transmission and reception.

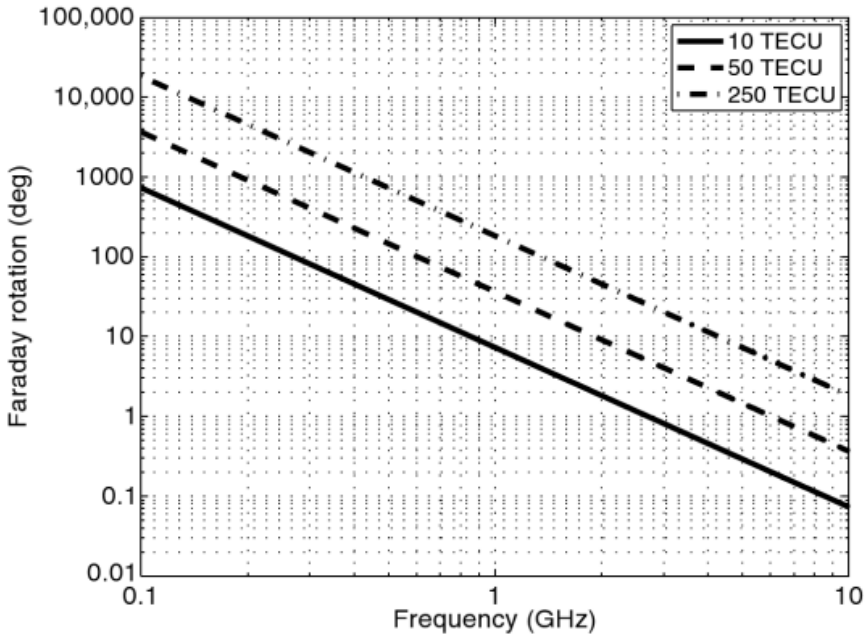

Figure 20: Faraday rotation as a function of frequency and TEC units [50].

Turbulent atmosphere results fluctations in air density which leads to a time dependent refractive index. Differences in atmospheric refractive index create scintillation effect which causes signal scattering and multipath effects. Scintillation affects signals below 3 GHz and is more pronounced near the horizon when signal has to pass trhroung thicker layer of atmosphere.

Tropospheric effects include different attenuations caused by rain, clouds and atmospheric gasses. Tropospheric effects are usually neglected at frequencies below 10 GHz. Table 3 summarizes attenuation levels caused by ionospheric and tropospheric effects.

Table 3: Atmospheric losses [51].

Source	**Level (dB)**
Gasses	0.05 – 0.25
Clouds and fog	0.006 – 0.035
Rain	0.007 – 0.035
Scintillations	0.04 – 0.35
Total	0.09 – 0.6

3.5.3 Pointing Losses

Pointing losses refers to misalignment of receiving and transmitting antennas. Realistically it is very difficult to acheve perfect alignment between ground station antenna and a fast moving satellite. In case of Aalto-1, communication link misalignment affects only ground station antenna which is directive unlike satellite antenna wich is omnidirectional. De-pointing loss can be defined using the following equation:

$$L = 12(\theta/\theta_{3dB})^2, \tag{28}$$

where θ is misalignment angle and θ_{3dB} is the 3 dB angular beam width of the antenna [52].

3.5.4 Equipment Losses

Equipment losses typically refer to various feeder and switch losses. Antenna is usually not directly connected to transmitter or receiver. In between there are usually cables, filters, couplers, waveguides and switches which all add a small ammount of attenuation to the signal.

4 Aalto-1 Antenna Deployment System

A UHF transceiver operating at 437.22 MHz is used to receive commands for the Aalto-1 satellite and transmit telemetry to Earth. This transceiver will be also used to transmit a radio beacon. To transmit large amounts of data requires a directive antenna and thus for separate radio operating in the S-band (2402 MHz) a patch antenna was selected. Telemetry and commands don't require large bandwidth thus wire antennas, a common solution in CubeSats, were selected. Wire antennas require ADS. Instead of commercial ADS a custom build design was chosen for Aalto-1.

4.1 Operation Environment

The design of the ADS has to take into account the environment in which ADS will operate. The vibration and shocks during the launch and vacuum and temperature changes once satellite is in orbit. The aspects which have to be taken into account are presented in the following sections.

4.1.1 Launch

The launch event, albeit short in duration, is the most critical time in the satellite's life from mechanical point of view. Operation of launch vehicle's main engines and aerodynamic buffeting creates severe acoustic and structural random vibrations. In Figure 21 is an example of Falcon 1 random vibration spectrum shown as acceleration vs frequency. As can be seen the frequency of these vibrations can be from tens of hertzs to few kilohertz. These vibrations are transmitted to ADS through launch vehicle's (LV) structural components. Vibrations cause tension and bending loads that can be many times higher than normal loads. Vibrations are especially problematic to bolted joints that tend to get loose unless special considerations are taken to prevent bolts and nuts from unscrewing.

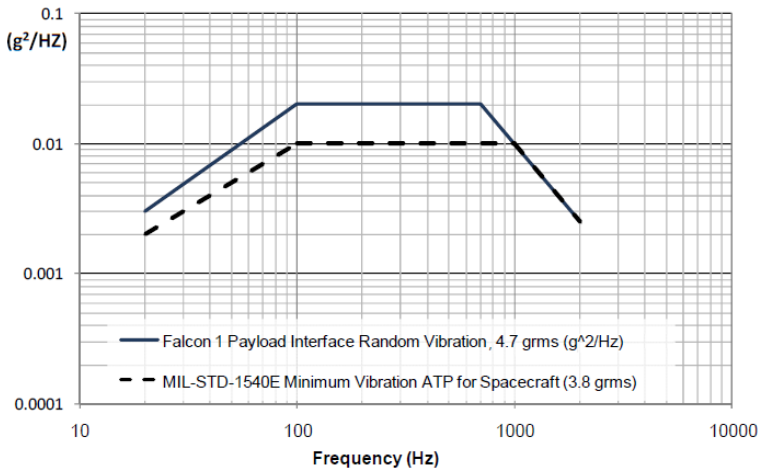

Figure 21: Random vibration spectrum of Falcon 1. Acceleration as a function of frequency [53].

Additional structural load is caused by steady acceleration of LV as it must achieve a speed increase of 9.5 km/s to reach the orbit [54]. This steady acceleration is interrupted by mechanical shocks caused by LV's pyrotechnical devices and ignition of rocket motor stages (see Figure 22). The launch acceleration profile depends on the LV. Smaller LVs generally exhibit higher peak accelerations than larger LVs.

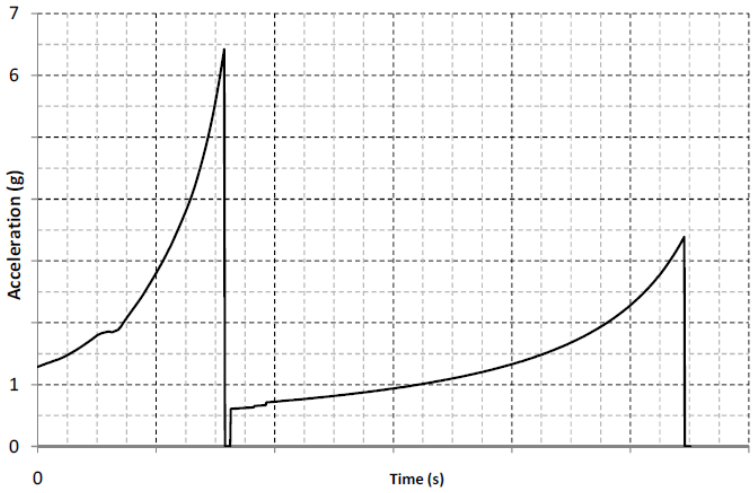

Figure 22: Falcon 1 static acceleration profile [53].

During flight LV is also subjected to varying acoustic environment which is due to LV's main engines, and also the aerodynamic buffeting caused by the LV accent through Earth's atmosphere (Figure 23). For the light and flexible components on the satellite such as solar panels, acoustically induced vibrations could be more severe than mechanically induced ones [54].

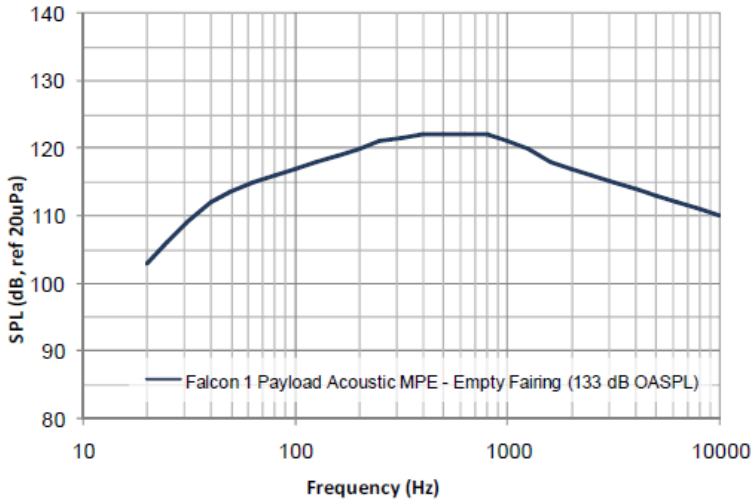

Figure 23: Sound pressure level (SPL) spectra for Falcon 1 [53].

4.1.2 Radiation

The main source of radiation in the Earth's orbit is the Sun. Sun emits constantly a plasma flow commonly known as solar wind. Sun activity oscillates with a period of 11 years [54]. This directly affects the speed and density of solar wind which in turn affects the radiation environment in the Earth's orbit (see Figure 24). Additional radiation hazard comes in the form of solar flares. They may last for periods of minutes to several hours. During solar flare event radiation level rise significantly and even traditional big satellites with space grade components may malfunction.

The effects of radiation on the mechanical parts of the ADS are negligble considering the planned two year mission time. However, electronic components can be quite sensitive. Especially commercial of-the-shelf (COTS) components which are not designed for space use are susceptible to malfunction. Accumulated dose from radiation can cause Single Event Upsets (SEU). Heavy charged particles such as protons and neutrons can dislocate atoms from component crystal lattice and cause Single Event Latchups (SEL) which permanently damages the component [54].

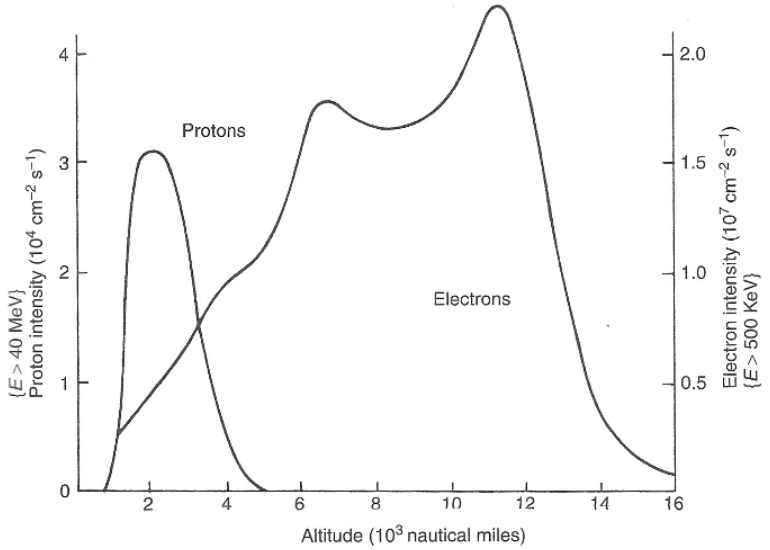

Figure 24: The structure of the Van Allen belts [54].

4.1.3 Vacuum

Vacuum presents a difficult environment for certain materials. At very low ambient pressures materials like plastics, adhesives and lubricants start to outgas. Outgassing is a process where surface atoms of the material vaporize. Over time this changes material properties. In worst case the material can completely evaporate. Outgassing can cause a problem to spacecraft since outgassing products can condence onto sensitive instruments e.g. optics. Materials most succeptible to outgassing are plastics, adhesives and lubricants (Table 4). If they have to be used in spacecraft construction, then designers have to carefully choose such materials that have low outgassing properties.

Metals are not that succeptible to outgassing but they have another problem – cold welding. If two surfaces of similar metals are in contact in vacuum for a long period of time they could fuse together. Cold welding can severly affect the performance of spacecraft. Parts that are designed to be moved could get stuck such as the case of Galileo probe. Cold welding prevented the deployment of antenna significantly limiting performance of the spacecraft [55].

Table 4: Outgassing properties (abbreviations are defined on page ix) [56].

Material	**TML %**	**CVCM %**	**WVR %**
Aluminium	0.12 – 0.04	0.0	0.0
Steel	0.02 – 0.0	0.01 – 0.0	0.0
POM plastic	0.78 – 0.28	0.1 – 0.0	0.24 – 0.07
Teflon	1.48 – 0.00	0.57 – 0.0	0.15 – 0.00
FR-4	0.42 – 0.0	0.02 – 0.0	0.25 – 0.03
Polyethylene	2.46 – 0.02	1.34 – 0.01	0.41 – 0.0
Lubricants	22.93 – 0.02	11.91 – 0.0	2.77 – 0.0

4.1.4 Temperature

Once in orbit the spacecraft will experience a periodic temperature changes as it passes from Earth shadow to the sun side. The surface temperature of spacecraft can change from −30 to +20 degrees (Figure 25) [57]. This thermal cycling put stress on mechanical components as they experience periodic expansion and contraction which eventually could lead to breaking of the component. In addition to mechanical stress, increase of temperature also increases the outgassing of the material.

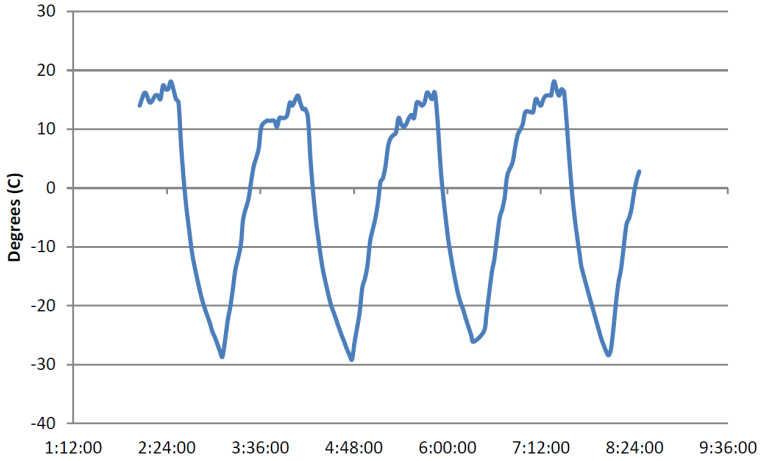

Figure 25: Temperature telemetry from CP3 satellite [57].

Electronic components also suffer from thermal cycling. Especially COTS electronics which are not designed for such temperature changes can experience fast degradation and eventual failure.

4.2 Requirements Specification

For Aalto-1, it was desided to build a custom ADS instead of buying a ready system. Building a custom ADS is risky. Unlike commercially available systems that already have a flight history, custom desing is untested and unproven. Aalto-1 Product Assurance Plan is used as a guideline in designing the ADS [58]. Upper level requirements are derived from mission objectives. For ADS the primary requirement is ability to communicate with the ground station. Other requirements arise from the primary requirement and form a hierarchical structure which is devided into RF, electrical and mechanical requirements shown in Figure 26.

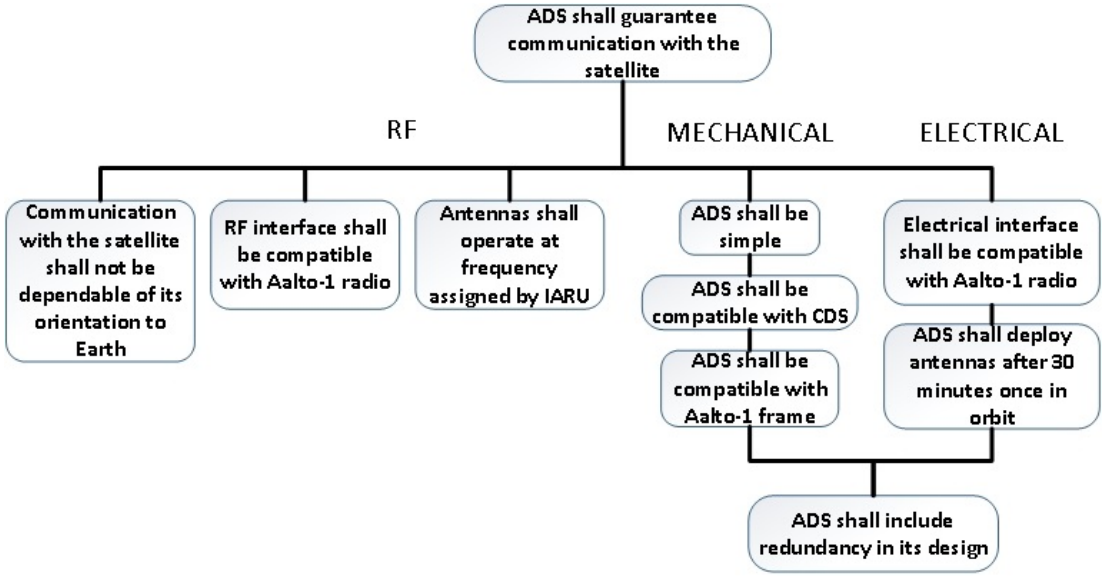

Figure 26: Requirement specifications for Aalto-1 ADS.

4.3 ADS Models

In space engineering, design of a system is usually divided into numerous phases during which several models of the system are built. This is known as "model philosophy". The Aalto-1 ADS development was divided into three main design phases: mechanical design, RF design and electrical design. During the mechanical design phase, several mock-up models (MM) of ADS were constructed. ADS MMs were externally similar to each other. They had similar dimensions and similar mechanical interface allowing them to be integrated into satellite mock-up. Internally, different MMs had different internal structure to test different antenna stowage configurations. ADS MMs had no functionality i.e. they could not be used for antenna deployment testing or antenna measurements.

Engineering model (EM) is mechanically identical to the final flight model and is fully functional. However, EM typically don't use flight-grade components. In ADS design, the final MM was upgraded to EM level and was used for antenna measurements as well as initial functional, vibration and shock testing.

Engineering Qualification Model (EQM) is fully functional copy of the flight model and uses the same components as the flight model. However, EQM is used for qualification testing which stresses the model beyond the normal operating conditions. As a result, for reliabillity reasons tested components can't be reused for the flight model. In ADS design, EQM incorporated minor modifications from EM and was used for qualification testing.

Flight model (FM) is the final version of the system that will be flown into space. In ADS design, FM is practically a copy of EQM and was subjected only to acceptance level testing.

4.4 Mechanical Design

Mechanical design started with study of different placement positions for ADS as well as trying different antenna stowage configurations that would meet the requirements defined for Aalto-1 ADS.

4.4.1 ADS Position Trade-off

The CubeSat standard doesn't define placement of the antennas. However, commercial ADS form factor dictates the placement on top (+Z) or bottom (−Z) side of the satellite. Since Aalto-1 has a custom ADS, it allows more freedom in placement of ADS. There are basically three options for ADS placement: top/bottom, sides and inside the satellite (see Figure 28). Placing ADS inside the satellite will take the space away from payloads and other satellite subsystems. Also testing such system is problematic since it is located inside. If something goes wrong, the whole satellite would have to be dismantled to access the ADS. A more practical choice is to place ADS on the surface of the satellite. The P-POD deployer has an extra space around the satellite (see Figure 27) and CDS specifies that components should not exceed 6.5 mm from the surface of the CubeSat. Thus, a 6.5 mm of height is available on the surface of the CubeSat that can be utilised.

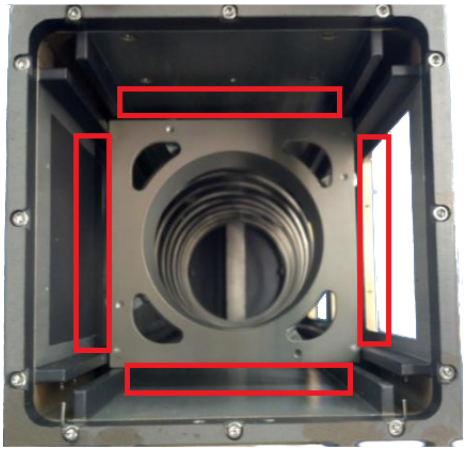

Figure 27: Additional space available in the P-POD around the satellite [11].

The disadvantage of placing ADS outside is reduction of the surface area that could have been used for solar panels. Because of the limited surface area, power generation on CubeSats is always a critical issue and in Aalto-1 AaSI and EPB payloads will require significant ammount of power during operation. During preliminary design phase, the optimal orientation of Aalto-1 was chosen so that it will be orbiting with the long side pointed to the Sun. This will maximize power generation. The short sides of the satellite (+Z and −Z) will not be illuminated by the Sun as intensively as the long side and thus those areas can be used for the ADS. Also during the preliminary design phase of the satellite structure, the −Z side was reserved for RADMON and plasma brake. Thus, the +Z side became the choice for ADS.

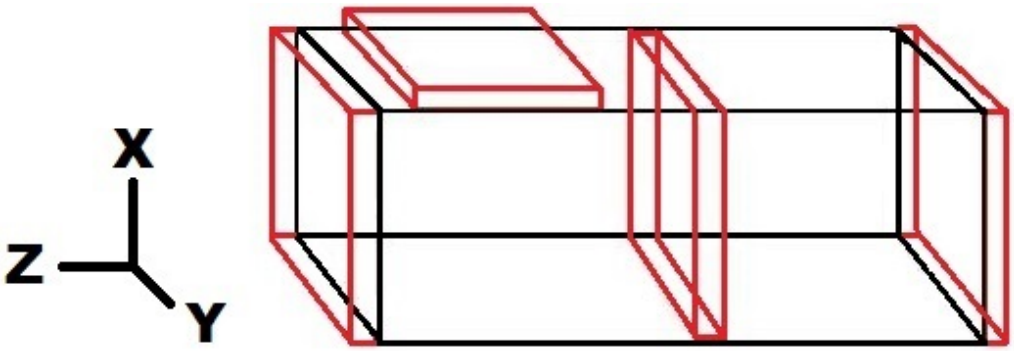

Figure 28: Possible ADS placement positions (red) on 3U CubeSat.

4.4.2 Stowage Configuration Trade-off

Another step in mechanical design is to decide how antennas are going to be stowed. In case of Aalto-1, the space allocated for ADS is +Z side of the satellite. The chosen place dictates the form factor of ADS which is a 10 x 10 cm square. Several CAD models of stowage configurations were made to visualize the general layout. The most promising ones were further developed into mock-up models. Deployed antennas in all configurations formed two v-shaped dipoles on the opposing ends of ADS. According to antenna simulations v-dipole provides the most omnidirectional radiation pattern.

The first idea for stowage configuration was to use a wrap-around design. The wrap-around stowage configuration is the most widely used configuration in custom ADS designs because of its simplisity. The design chosen would be similar to one used in GomSpace ADS only instead of rigid tubes, antennas would be made from flexible metal tape (see Figure 29). This design would copy the existing RAX-2 CubeSat ADS. RAX-2 was launched in 2011 and operated for two years, thus this desing could have been considered to be flight proven [59]. However, during preliminary desing phase, a consern arose whether stowing antennas against the fragile solar cells would damage them as flexible antennas would rub against the cells during launch vibrations. Because of these concerns, this design was rejected.

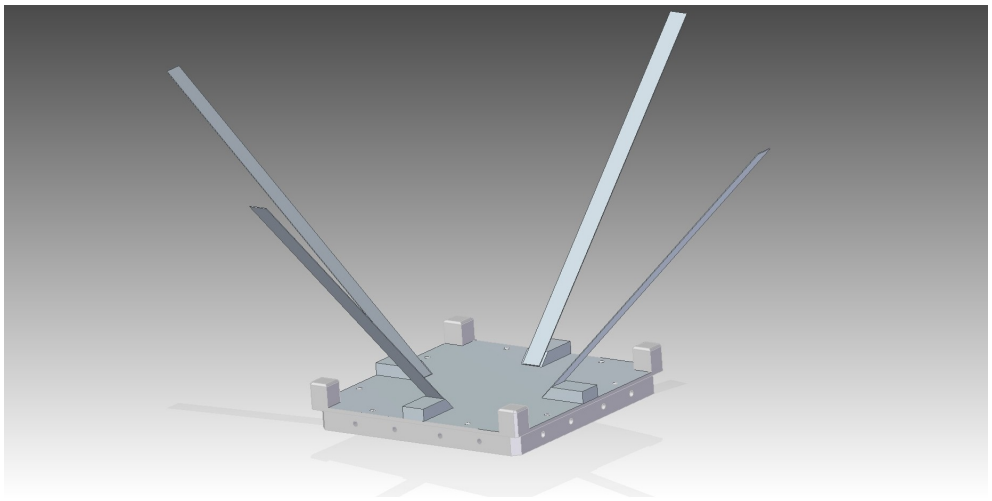

Figure 29: Wrap around ADS design.

The second prototype, shown in Figure 30, kept the wrap-around design but instead of wrapping antennas around the satellite body, antennas were wrapped around support structures in the corners of the ADS. A retention string attached to outermost antenna and connected to a release mechanism would kept antennas pressed against the support structures and inside the ADS. The second prototype removed problems associated with stowing antennas agains the solar cells. Like the first prototype was very simple. Besides antennas, there were no other moving parts which made this prototype very promising from reliability point of view. However, during Preliminary Design Review several structural shortcomings were pointed out and subsequently this design was rejected.

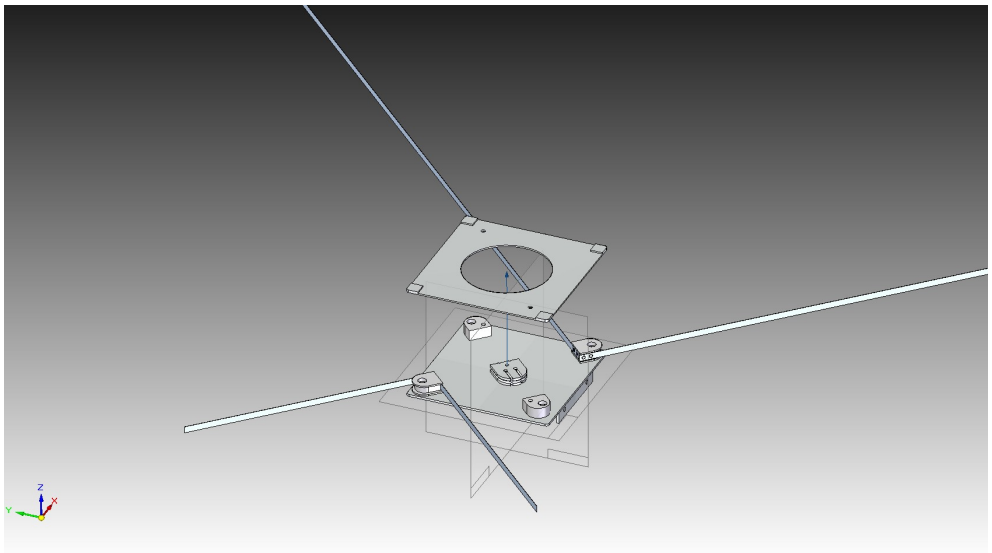

Figure 30: Alternative wrap around ADS design.

The third prototype abandoned the wrap-around design and used roll-up design similar to ISIS ADS. However, while studying ISIS ADS internal structure (see Figure 31), it looked to be quite complex. It has four antennas housed in four separate antenna housings. Each antenna is attached to an antenna door which keep antennas rolled inside the housings during the launch. Four doors also means that there are four release mechanisms. All this creates a complex design. Since one of the guiding principles in designing Aalto-1 ADS was to keep design as simple as possible, this design was modified to make it simpler.

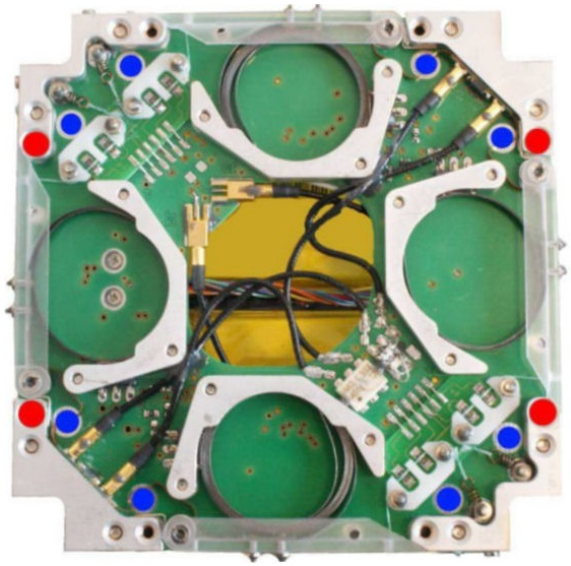

Figure 31: ISIS ADS internal structure [60].

The simplified design, shown in Figure 32, combined antenna housings so that there is one housing for two antennas. This also reduced the number of required doors to two. Arranging antenna housings to be on the opposite side of ADS allowed to have only one release mechanism for two doors. All this simplified the design but on the down side created problem for attaching antennas. In the ISIS ADS design, each of the four antennas are attached to an antenna door. Now, with two door design this was no longer possible. A solution to this problem was to move antenna attachment point from doors to inside the ADS. However, this created a problem from radio engineering point of view. Since Aalto-1 ADS forms integral part of the satellite structure, it is made from the same aluminum alloy as the rest of the satellite structure. The antenna attachment point has to be electrically isolated from the ADS structure to allow antennas function properly. Also attachment point inside the ADS would mean that even with antenna deployed part of it would be inside the ADS. This would require insides of ADS to be dielectrically coated to prevent short circuiting antennas. But even with coating, part of antenna would still be inside the ADS which would lower the antenna radiation efficiency. After trying several solutions which turned to be mechanically unsatisfactory this design was abandoned also.

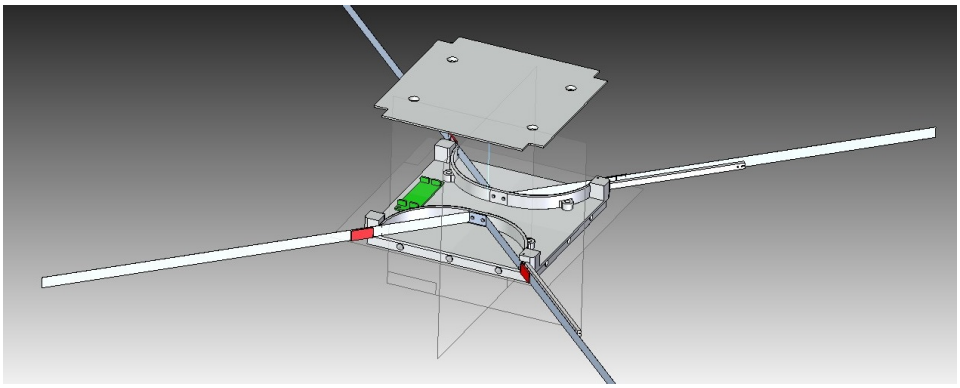

Figure 32: Simplified roll-up ADS design.

The fourth and the final prototype is a modification of the third prototype (see Figure 33). The two door design was kept but instead of a flat door an L shaped door was used. The L shaped door allowed two antennas to be attached to a single door. This modification removed antenna attachment problems assosiated with the third prototype. The fourth prototype was the starting point from which the flight model of ADS was subsequently developed.

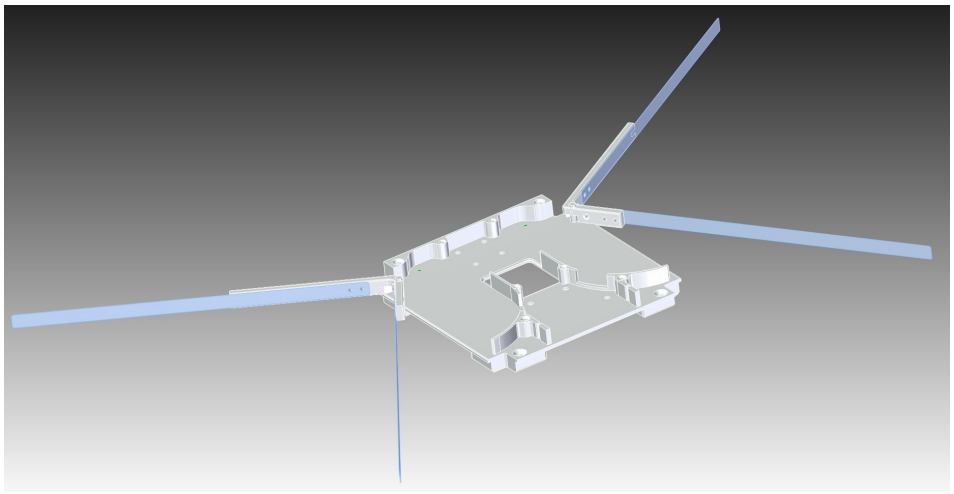

Figure 33: Modified roll-up ADS design.

4.5 RF Design

After selection of mechanical design, the next step is RF design. The first task is to decide what communication scheme is going to be used. The next task is to select what type of antennas are going to be used with choosen scheme. The selected antennas has to be simulated and optimized to achieve requirements that has been specified for ADS. Finally, a prototype is constructed, its performance measured to confirm the simulated results.

4.5.1 Communication Scheme

Most of the CubeSats operate in VHF-UHF frequency band. Some satellites use VHF (144 – 146 MHz) for downlink and UHF (435 – 438 MHz) for uplink other satellites use opposite scheme; VHF for uplink and UHF for downlink. It is possible also to use only one frequency for uplink and downlink. Before designing ADS for Aalto-1 a trade-off has been conducted to decide which communication scheme is best suitable for Aalto-1.

4.5.2 Scheme 1 – VHF downlink and UHF uplink

The most important advantage of using two different frequencies for communication is full duplex system allowing simultaneous downlink and uplink. On low Earth orbit the satellite will be visible at the ground station (GS) just about 10 minutes. In that time one has to establish a connection, receive telemetry and data and send commands. With full duplex communications establishing connection will be quicker in comparison to half duplex system where communication can be in one direction at a time. The most critical disadvantage of full duplex communication is interference from so called third harmonic frequency. This means VHF antenna can create interference for receiving UHF antenna. Choosing VHF for downlink means that free-space path loss (FSPL) for signal is lower. This is important considering that satellite radio transmitters have low transmitting power usually about 1 W. Low frequency also means that as satellite passes over the ground station the Doppler shift around the central frequency will be lower. On the other hand, VHF for downlink could be problematic because VHF band is quite congested; interference from other radio amateur transmissions could pose a problem. Also on VHF bands the sky noise is stronger than on UHF bands. Received VHF signal has to be strong enough to be above the noise floor that GS antenna will see. Another disadvantage of VHF downlink is small data rate. This disadvantage is quite minor because the amount of data required by telemetry is low and transmitting it to Earth doesn't take much time. From mechanical point of view VHF antenna is twice as long as UHF antenna and storing it in small space is more problematic.

4.5.3 Scheme 2 – UHF downlink and VHF uplink

In reverse communication scheme UHF frequency is used for downlink and VHF for uplink. Many CubeSats use this scheme because it removes many problems associated with the previous scheme. The full duplex communication advantage remains but interference from the third harmonic frequency is not that severe. However, because VHF is used now for uplink the problem appears on the ground station (GS) side. GS use typically Yagi antennas which are directive unlike omnidirectional antennas on the satellite, thus less interference is coupled from VHF to UHF antenna. Sky noise is weaker at UHF bands and thus signal-to-noise ratio at GS is better. This advantage compensates the fact that UHF signal attenuates more than VHF signal. UHF downlink also offers higher data rates than VHF. This is useful for Aalto-1 because UHF downlink could be used as a backup in case of problems with S-band.

4.5.4 Scheme 3 – UHF downlink and UHF uplink

Another, also commonly used scheme, is to use one frequency for downlink and uplink. The biggest disadvantage of this scheme is its half duplex mode of operation. Because downlink and uplink use the same frequency the satellite can't transmit and receive at the same time. Establishing communication link with the satellite will take longer reducing time available to receive telemetry and send commands. Reduced communication window means that less data can be transmitted up to the satellite or down to Earth. For Aalto-1 this doesn't pose a significant problem. Commands don't take much space and can be quickly transmitted to the satellite. For downlink, besides UHF, Aalto-1 will also have S-band transmitter. It has much higher data throughput and can transmit large ammonts of data in short time. Another advantage of communication scheme 3 is much simpler antenna design since there is only one type of antenna being used.

Majority of CubeSats use communication scheme 2. This scheme was also originally selected for Aalto-1 but during design process stowing the long VHF antennas turned to be quite problematic. Thus scheme 3 was eventually selected. While half duplex mode has obvious disadvantages, for Aalto-1 this scheme has one major advantage. Originally, Aalto-1 communication system had VHF receiver and UHF transmitter connected to their respective antennas. In the new scheme VHF antenna in ADS has been replaced with another UHF antenna. Together with replacing VHF receiver with another UHF transceiver will result in a completely redundant system. The second UHF system can be used as a backup in case the primary system fails.

Advantages and disadvantages of different communication schemes have been summarized in the Table 5.

Table 5: Communication schemes.

	Scheme 1	**Scheme 2**	**Scheme 3**
pros	full duplex decreased FSPL down more BW up less Doppler shift	full duplex more BW down sky noise problem	simpler design redundancy more BW down more BW up sky noise problem
cons	VHF band congested less BW down long VHF antennas sky noise problem 3rd harm. interference	increased FSPL down long VHF antennas less BW up less Doppler shift	half duplex more FSPL up/down less Doppler shift

4.5.5 Antenna Type Selection Trade-off

After the communication scheme has been selected the type of antenna that will be used on Aalto-1 can be decided. At UHF frequency range the most practical antenna type is a wire antenna. In CubeSats the wire antennas are typically in the form of dipole, monopole or turnstile.

From mechanical point of view the most simple antena type is a monopole antenna. It has been used on many smaller 1U CubeSats where available space is limited. From RF point of view the monopole has similar radiation patter as dipole but has lower efficiency than a dipole antenna. In theory, monopole antenna would be as efficient as a dipole antenna if it would be used with infinite and perfectly conducting ground plane. In reality, this is not the case and in the case of CubeSat the ground plane is very small. Impedance of a monopole antenna is half of a dipole. Small ground plane further reduces impedance thus a matching network is needed to connect monopole antenna to a standard 50 ohm transmission line.

Another commonly used antenna type is a dipole antenna. From mechanical point of view, the dipole is two monopole antennas and requires twice the ammount of space for storing. For a 3U CubeSat like Aalto-1 this is not a big disadvantage. From RF point of view, the dipole antenna doesn't require a ground plane. Its impedance is twice of a monopole and closer to a standard 50 ohm transmission line.

Turnstile antenna is a combination of two dipole antennas in cross configuration. The second dipole is fed with 90 degree phase shift. Turnstile has two advantages over monopole and dipole. First, cross configuration cancels nulls in the radiation pattern which exists along the axis of monopole and dipole. Second advantage of the turnstile antenna is circular polarization. Ground station antenna is circularly polarized and thus having circularly polarized antenna on the spacecraft will remove polarization mismatch unlike using monopole or dipole which are linearly polarized.

After careful consideration a dipole antenna was selected. The dipole doesn't require a ground plane like a monopole. This is an important factor when considering the Plasma Brake experiment. The Plasma Brake requires conductive surface of the satellite. In case of monopole antenna, it is not known how this will affect the performance of the antenna. Thus, dipole antenna is a safe choice. Mechanically dipole is much simplier than turnstile and not too complex when compared to monopole. Also, from RF point of view connecting dipole to transmission line like a coaxial cable is quite straightforward. Turnstile antenna while having more omnidirectional radiation pattern than dipole or monopole and having circular polarization was not choosen for several reasons. First, turnstile antenna is formed from two dipole antennas and thus redundancy factor of having two antennas is lost. Second reason is antenna placement choosen for the Aalto-1. Turnstile antenna radiates circular polarization in the direction perpendicular to the antenna plane. From ground station point of view, satellite antenna is seen from the side where turnstile radiates linear polarization and thus the advantage of circular polarizatin is lost.

4.5.6 Antenna Simulations

The ability to receive commands regardless of the satellite position is one of the most importan design requirements for satellite communication link antenna. Many CubeSats use dipole antennas and they are often described to be omnidirectional. In reality, the dipole antenna has deep nulls in the radiation pattern along the axis of the antenna (see Figure 13). After the satellite is deployed, it is in a tumbling mode before attitude control system manages to stabilize it. During that time radio contact with the satellite could be lost when null of antenna gets pointed to Earth.

The first task of simulations was to improve the standard dipole and make it more omnidirectional. Simulating antenna performance and optimization was done using CST Microwave Studio, a 3D electromagnetic simulation software [61]. Different dipole configurations were simulated and the optimal solution was found in a v-dipole, a dipole bent to 90 degree angle. Classical dipole has gain of 2.15 dB in azimuthal plane but has nulls along antenna axis that are -30 dB deep or more [27]. V-dipole gain in azimuthal plane has been reduced to 1.3 dB but nulls are just -10 dB deep. Figure 34 shows radiation patterns of classical dipole and v-dipole.

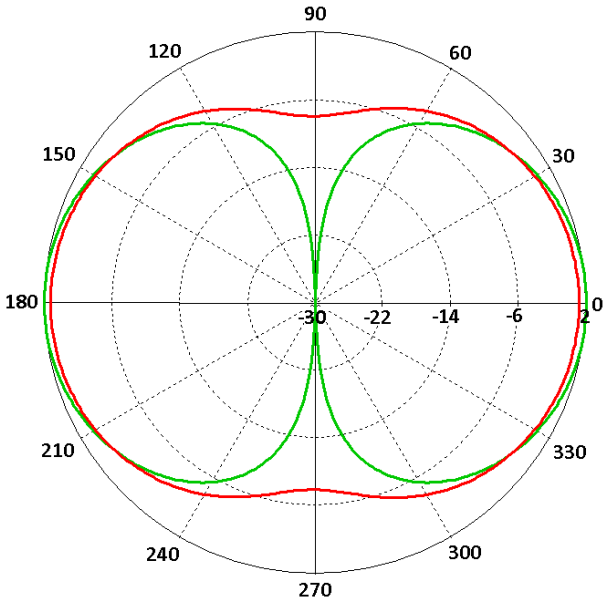

Figure 34: Classical dipole (green) and v-dipole (red) radiation patterns.

The radiation pattern of v-dipole shown in Figure 34 is the case of antennas being in free space. In reality, antennas will be attached to the satellite. The wavelength of the frequency selected is 0.686 m which is in the same order of magnitude as the length of the satellite, which is 0.34 m. The body of the satellite will thus significally affect the radiation pattern of antennas when compared to radiation pattern of antennas in free space. To take this into account, a model of the satellite was constructed in CST (Figure 35) with ADS structure defined in the mechanical design.

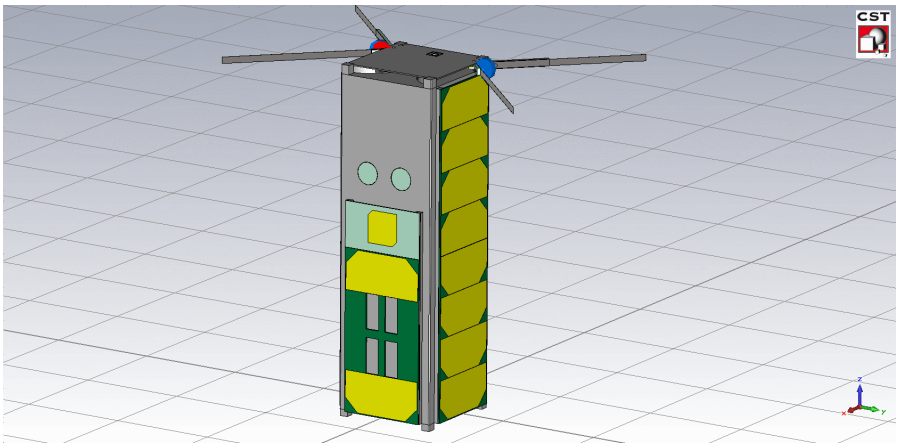

Figure 35: Aalto-1 UHF antennas simulation model.

Next task was to simulate antennas attached to the satellite. Figure 36 shows the simulated 3D radiation pattern distorted by the presence of the satellite body. Appendix B shows the same radiation pattern in three different planar cuts: from the top, +x and −y sides of the satellite.

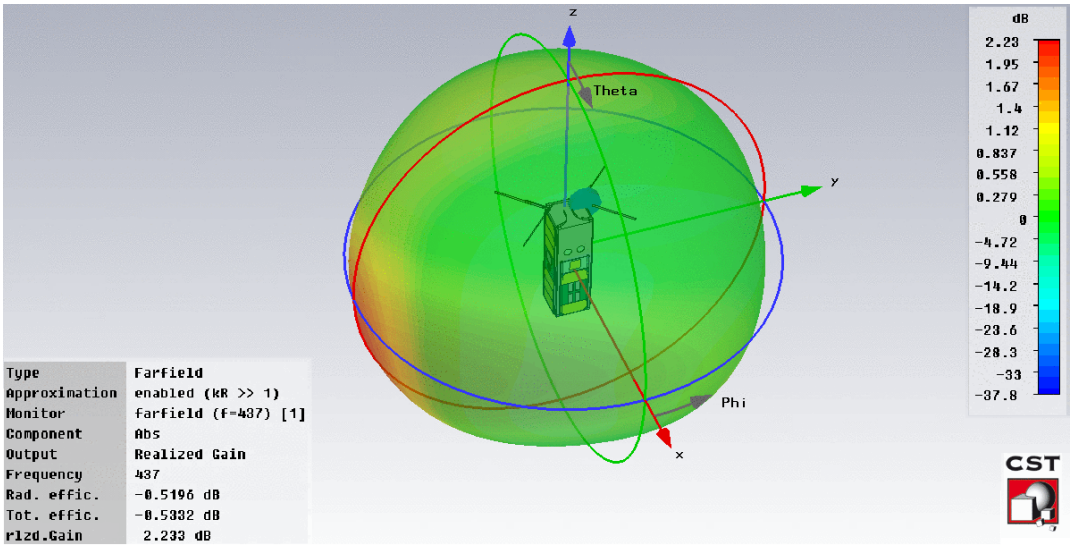

Figure 36: 3D view of the simulated radiation pattern.

The frequency bandwidth reserved for radio amateur satellite communications is only 3 MHz wide, from 435 to 438 MHz [24]. Since reserved bandwidth is quite narrow, it was unnecessary to make antennas matched over wide frequency range. Instead, the goal of optimization was to obtain excellent matching so that as much as possible power from the satellite transmitter can be delivered to the antenna. The minimum requirement for return loss (RL) was to obtain similar or better performance than ISIS ADS which has return loss less than −10 dB. Figure 37 shows the simulation results.

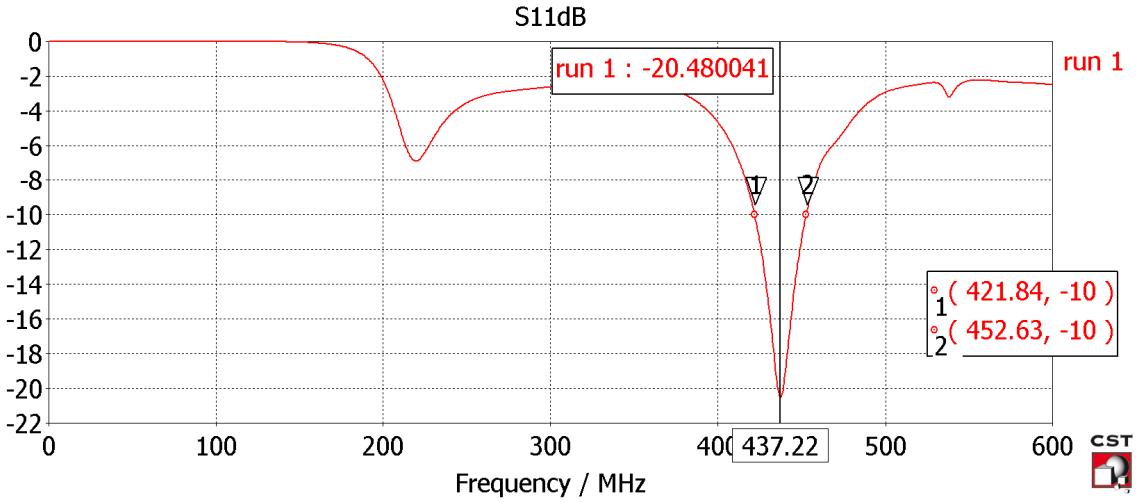

Figure 37: Simulated return loss for Aalto-1 ADS v-dipole antenna.

The antenna doors have torsion springs which open doors after satellite deployment and keep them opened at the specific angle. The door opening angle affects the input impedance of the antennas. This in turn will affect the return loss which was optimized with the ADS antenna doors opened completely. Figure 38 shows simulation results how return loss shifts from the operating frequency in case antenna doors won't open completely.

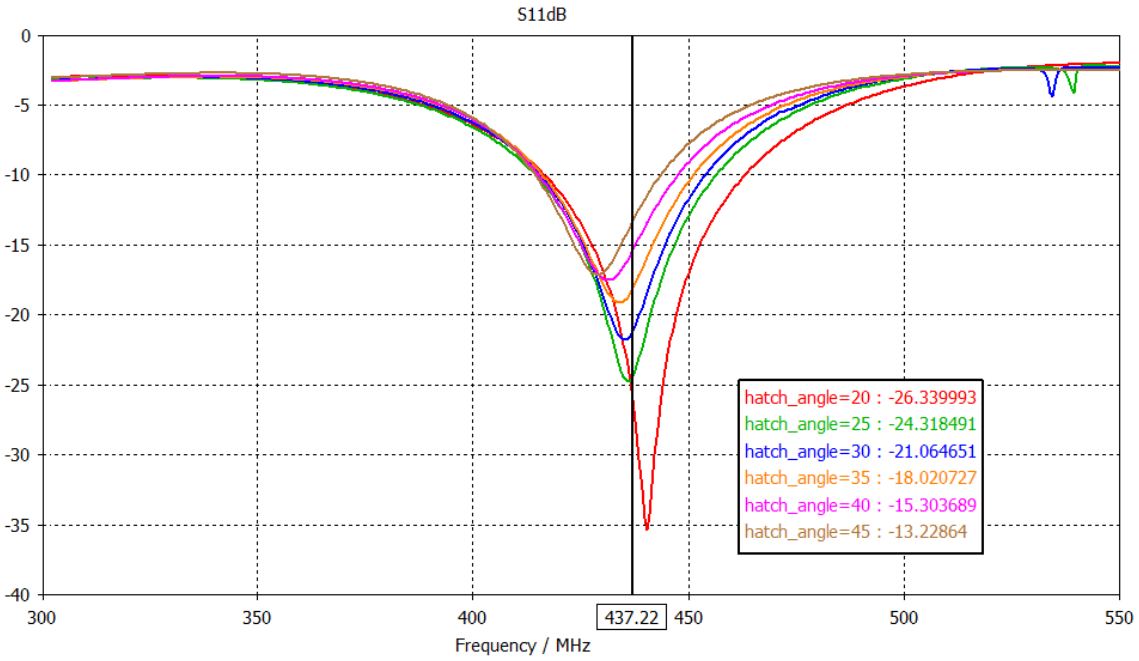

Figure 38: Antenna door opening angle influence on the return loss.

4.5.7 Spacecraft Charging

A spacecraft surface experiences charging while in orbit. The primary source of charging are plasma electrons from ionosphere. Ionosphere is a region of Earth's upper atmosphere where atmospheric gasses are ionized by solar radiation creating a plasma environment. This region extends from 86 km to 1000 km [54]. A body, e.g. a satellite, flying through this region is subjected to a flux of electrons and ions. Electrons have much higher mobility and thus the flux of electrons to uncharged surface exceeds the flux of ions in a quasi-neutral plasma where the temperature of electrons and ions are equal. As a result, the surface becomes negatively charged [47]. The electric charge accumulated on the surfaces of the satellite body and the antennas, which are electrically insulated from each other, will be different creating a static potential difference between the body and antennas. If potential difference gets high enough there is danger of electrostatic discharge. Electromagnetic energy from discharge can be coupled into satellite electronics causing upsets and damage.

To prevent static build-up, the v-dipole antenna was modified by including two DC-grounding inductors L_1 and L_2. At the antenna's operating frequency, inductors have high impedance and seen as an open circuit allowing antennas to operate normally. At DC, inductors are seen as a short circuit allowing the static potential difference between the body of the satellite and antennas to be equalized. Figures 39 and 40 shows the circuit schematic of inductors and their physical location.

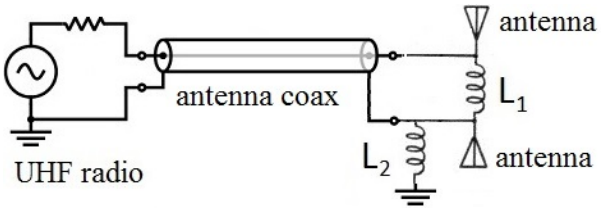

Figure 39: Circuit schematic of antenna grounding inductors.

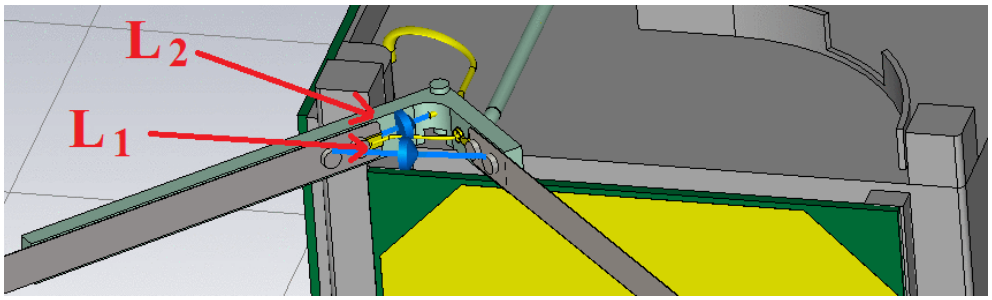

Figure 40: Location of grounding inductors in the CST simulation model.

Inductance of inductors affect the impedance of the antenna. During simulations, one task of optimizations was to find the optimal values of inductors which would not affect antenna performance negatively. Appendix C shows simulation results with different inductor values.

4.5.8 Measurements

After the antenna simulation, the final mock-up model of ADS was used to construct a functional engineering model (EM). EM along with mechanical mock-up of the satellite structure was used for measurements. The goal of measurements was to verify that actual antennas have similar performance as simulated ones. Return loss was measured with the prototype of ADS attached to the mechanical mock-up of the the satellite. Figure 41 shows comparison of simulated return loss with the measured one.

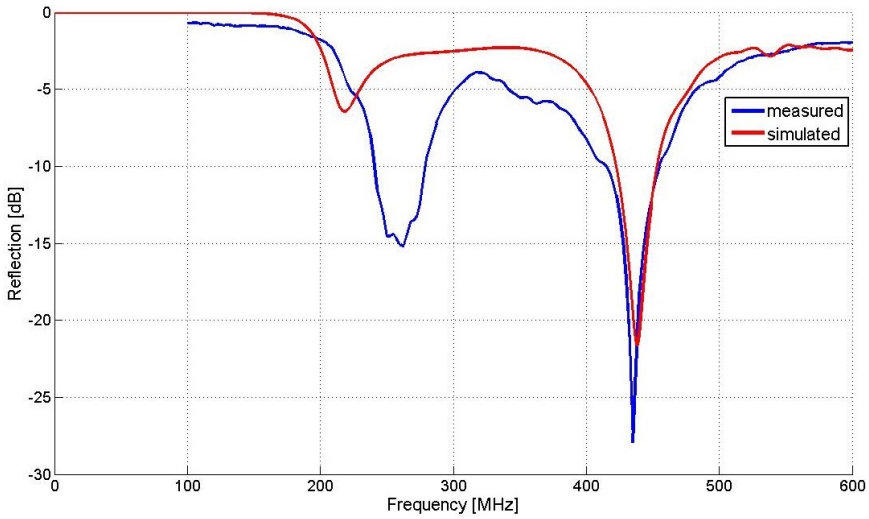

Figure 41: Measured and simulated return loss.

One of the important design requirements for ADS antennas is omnidirectional radiation pattern. To verify simulated results radiation pattern measurements were conducted in Aalto University anechoic room (Figure 42).

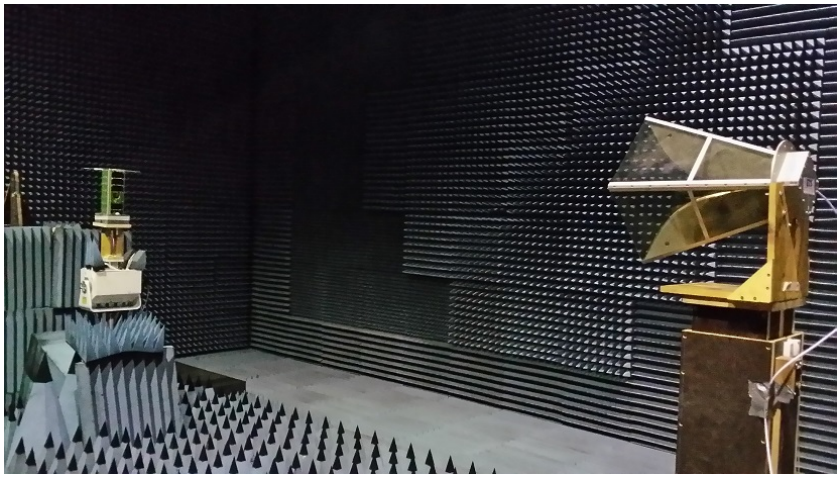

Figure 42: Radiation pattern measurement setup.

Radiation patterns were measured along three rotational axes (x, y, z) of the satellite. Measured and corresponding simulated patterns are shown in Figures 43 and 44.

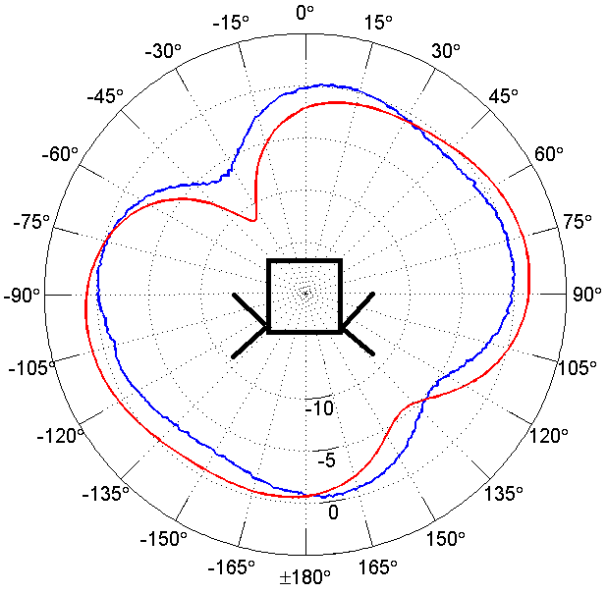

Figure 43: Measured (blue) and simulated (red) radiation patterns of Aalto-1 antenna(top view).

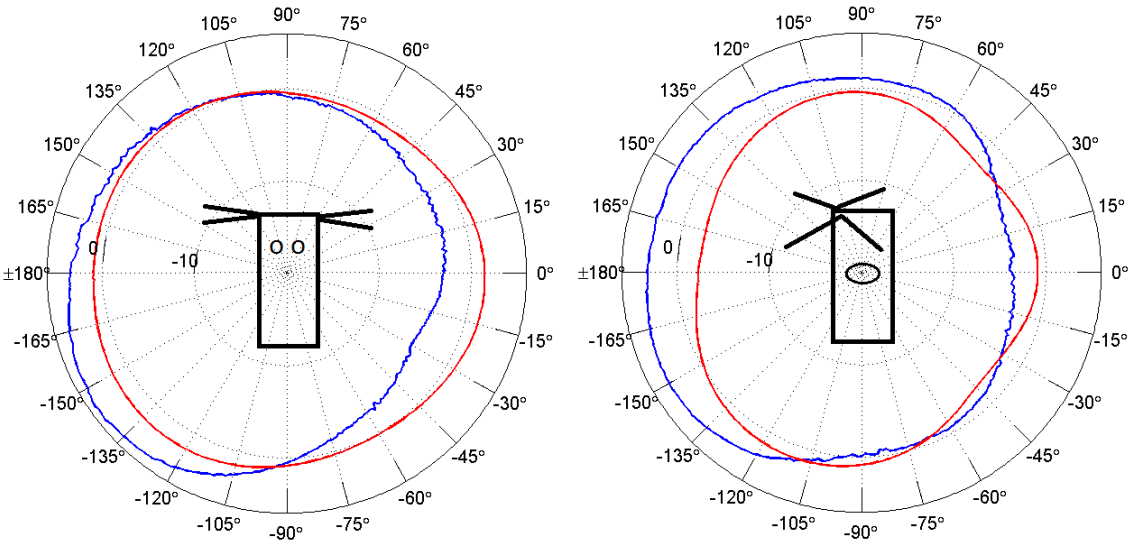

Figure 44: Measured (blue) and simulated (red) radiation pattern of Aalto-1 antenna.(front and side view).

4.5.9 Aalto-1 Link Budget for UHF Communication

Link budget is used to estimate the quality of a radio link between the satellite and the ground station, taking into account such parameters as transmitting power, antenna gain, propagation losses, impedance mismatches, etc. In it simplest form, the link budget can be described by the following equation:

$$Received\,power = Transmitted\,power + Gains - Losses. \tag{29}$$

Of all losses, the free-space path loss (FSPL) is the factor that has the greatest influence in link budget calculations. While other losses and gains are mostly static, FSPL depends on the distance between the satellite and the ground station. The distance in turn depends on the elevation angle of the satellite, as seen from the ground station. Figure 45 shows that the maximum distance between satellite and the ground station is when satellite is close to horizon.

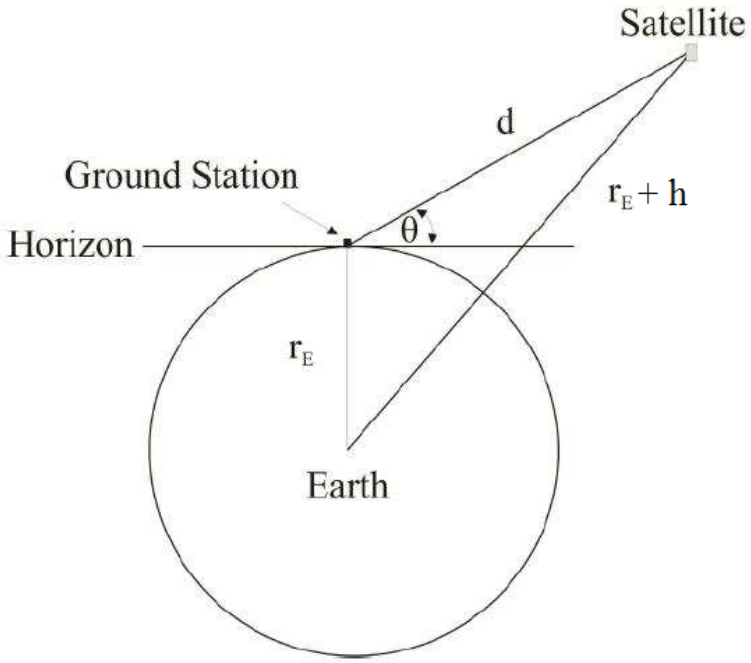

Figure 45: Distance to the satellite as a function of elevation angle [48].

Using the Equation (30) the distance d can be calculated as a function of elevation angle:

$$d = -r_E sin(\theta) + \sqrt{(r_E^2 sin^2(\theta) + (r_E + h)^2 - r_E^2)}, \tag{30}$$

where r_E is radius of the Earth, θ is elevation angle and h is the height of satellite orbit (see Figure 45). The Aalto-1 will be launched into elliptical 400 – 750 km orbit. Assuming worst case for $\theta = 10°$ and $h = 750$ km, the distance is 2260 km. Using the Equation (27), for frequency 437.22 MHz the corresponding FSPL is 152 dB.

Link budget is usually calculated separately for downlink and uplink. Antenna gains, propagation losses and impedance mismatches are reciprocal but transmitting powers and receiver sensitivities on the satellite and the ground station are different, thus resulting different link budgets for downlink and uplink. Typically, the limiting factor in nanosatellite-Earth communications is transmitting power of the satellite. CubeSats usually have radio transmitters in 1 Watt range or less [9]. Putting more powerful transmitters is difficult because power generation on CubeSats is limited by the small surface area on the satellite that is available for solar panels. Ground stations usually don't have power limitations and can transmit at much higher power levels. Table 6 summarizes parameters used to calculate link budget for downlink.

Table 6: Link budget.

Downlink			**Uplink**
Parameter	**Value**	**Parameter**	**Value**
Tx satellite	30 dBm	Tx GS	45 dBm
Rx/Tx switch losses	0.8 dB	Rx/Tx swith losses	0.8 dB
Satellite cable losses	0.4 dB	GS cable losses	5 dB
Satellite antenna gain	−6 – +4 dB	GS antenna gain	16 dB
Free-space path loss	152 dB	Atmospheric losses	0.6
Atmospheric losses	0.6 dB	Free-space path loss	152 dB
Polarization mismatch	3 dB	De-pointing loss	1 dB
De-pointing loss	1 dB	Polarization mismatch	3 dB
GS antenna gain	16 dB	Satellite antenna gain	−6 – +4 dB
GS LNA gain	21 dB	Satellite LNA gain	30 dB
GS LNA NF	1 dB	Satellite LNA NF	0.8 dB
GS cable losses	5 dB	Satellite cable losses	0.4 dB

Using the Equation (29) and parameters from the Table 6, the received signal strength at the ground station receiver is about −103 dB. In theory, to detect the signal, it has to be above the noise floor of the receiver. The noise floor of the receiver is calculated using the following equation:

$$N = 10 \cdot log_{10}(k_B T_s B), \tag{31}$$

where k_B is Boltzmann's constant ($1.38 \cdot 10^{-23} J/K$), T_s is the effective noise temperature of the receiver in Kelvins (310 K) and B is the bandwidth (50000 Hz). The calculated noise floor of the receiver is −156.7 dBm. In practice, it is not enough for signal to be just above the noise floor, it has to be above sertain level. The difference in power levels of the signal and the noise floor is known as signal to noise ratio (SNR). For ICOM IC-910H transceiver used at the ground station the SNR is 12 dB [62]. Thus the Minimum Discernable Signal (MDS) at the ground station is:

$$MDS = N + NF + SNR, \tag{32}$$

where NF is the noise figure of the receiver (3 dB for IC-910H). The resulting MDS is −141.7 dB. This means there is 38.9 dB link margin for downlink between received signal and MDS. For uplink the satellite transceiver's MDS is −123 dBm [63]. The link margin for uplink is therefore 44.4 dB.

4.6 Electrical Design of Release Mechanism and Timer

CDS requires that any deployables should deploy not earlier than 30 minutes after satellite is deployed. In many CubeSats the OBC controls the deployment of the antennas. In Aalto-1 it was decided that the radio should be as much as possible independent from the OBC. Thus, in case of its failure the satellite can transmit down at least a beacon. Independent radio also means that antenna release mechanism should be independent otherwise the benefit of independent radio is lost.

4.6.1 Antenna Release Mechanism Trade-off

Unlike big satellites, where pyrotechnical devices are the most common method to secure deployable structures, CDS defines that no pyrotechnical devices can be used [11]. Instead of pyros, three other release mechanisms have been used in CubeSat satellites, one is based on a magnet, another is based on a thin resistance wire and a third uses a COTS resistor. The magnetic release mechanism, shown in Figure 46, uses a permanent magnet to keep antennas in stowed position. After satellite is deployed an electrical magnet is switched on to counteract the attraction of the permanent magnet. The spring force of the bent antennas is then enough to set antennas free. This type of release mechanism has been tested and flown on two University of Tokyo satellites XI-IV and XI-V [64].

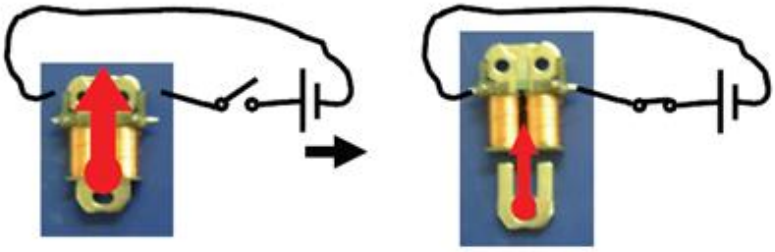

Figure 46: Magnetic release mechanism of the XI-IV satellite [64].

Another release mechanism is based on a thin resistance wire made from nichrome alloy (see Figure 47). Antennas are kept in stowed position using a thin nylon line. Nichrome wire is attached to nylon line. After satellite is deployed, a current is applied through the wire, heating it and melting the nylon line. This method is preferred by the majority of the CubeSat standard satellites.

The advantage of the magnetic release mechanism is the simplicity of resetting the system during the tests. The disadvantage is that the mechanism is heavy and mass is a major concern in CubeSat satellites. The other disadvantage is that it has been used on only two missions and while the success rate so far is 100 % but the small number of missions flown doesn't make the system reliable from the statistical point of view.

The advantages of resistance wire based release mechanism is its light weight and simple design. This system is well known and has been used to deploy antennas on majority of CubeSat satellites. The disadvantage of resistance wire is its mechanical fragility; it can't support the tension of antenna retention string by itself. A support structure has to be included in the ADS design that will keep string tensioned and close to resistance wire. The string has to be close enough that the heat from resistance wire will melt it. Although the resistance wire has been used on many successful CubeSats missions, its mechanical fragility was the reason it was not chosen.

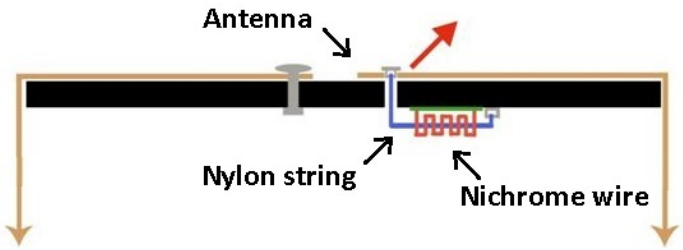

Figure 47: Nichrome wire release mechanism of the M-Cubed satellite [65].

A third option is to use a common COTS resistor instead of resistance wire as a heating element (see Figure 48). It has all advantages of resistance wire and mechanically it is very robust. A resistor soldered to a PCB can support tension of the antenna string without any additional support. This solution has been used so far on Delfi-C^3 and Xatcobeo satellites. Both satellites had their antennas successfully deployed. Although COTS resistor solution suffers from the same problem as a magnetic release mechanism i.e. not enough missions for statistical reliability, it was chosen for Aalto-1 satellite. The main reasons for this choice were: light weight and robustness. The lack of statistical reliability can be fixed by conducting numerous deployment tests.

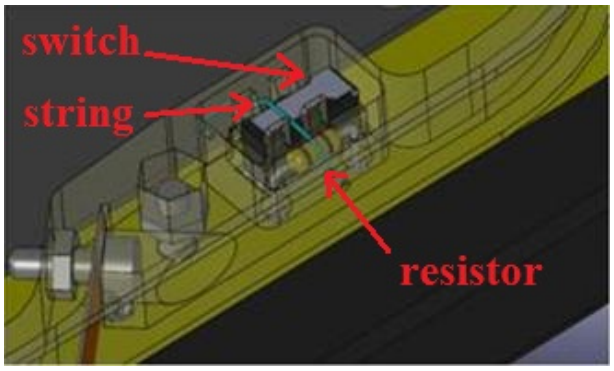

Figure 48: Resistor reliease mechanism of the Xatcobeo satellite [66].

4.6.2 Design of Timer Circuit Board

Independent deployment of antennas is implemented by designing a timer circuit that operates independently of the OBC and is integrated into ADS. This timer circuit activates after satellite is deployed from P-POD.

The required timing deley can be implemented with many different solutions. One of the solutions is to use a simple RC discharge circuit where the capasitor is discharged at a controlled rate through the resistor. The required delay can be controlled by choosing correct value for the capasitor and the resistor. This circuit would be simple to make but is impractical for long timing delays because it requires capacitors in microfarad range. Such big capacitors are available only as electrolytical capacitors which are unsuitable for space use because of the liquid electrolyte they contain.

Another option is to use a microcontroller. There are hundreds of different microcontrollers available with different packaging options and different voltage requirements. There are many available timer circuits schematics that are based on the microcontroller. Making a timer from microcontroller would require writing a program to perform such function. While a microcontroller based timer appears like a good solution it was nevertheless abandoned. Since one of the requirements for ADS was to keep design as simple as possible, the microcontroller seemed to be an overengineered solution for such a simple problem.

The final choice was to use an analog counter chip. It offered more flexibility than just RC discharge circuit and it wasn't too complex like microcontroller based timer. There are many analog counter chips available. The 555 timer chip was considered [67]. However, the final choice was a Texas Instruments' CD4060BC timer chip (see Figure 49). CD4060BC is a 14-stage ripple-carry binary counter/divider [68]. Its features include a wide operating voltage range from +3 V to +15 V and wide operating temperature range from −55 °C to +125 °C. The selected form factor is a Small Outline Integrated Circuit (SOIC) which offers small size and makes it easier to put it in confined space available on the ADS.

Figure 49: Texas Instruments' CD4060BC [69].

Logical structure of the CD4060BC is shown in Figure 50. The operating principle is based on a chain of binary counters. An external RC-circuit connected to the chip provides the clock signal for the counters which are advanced one count on the negative transition of each clock pulse. Since counters are chained, the n'th stage of the counter represents 2^n amount of counts. Figure 51 shows the corresponding pin assigments on the chip.

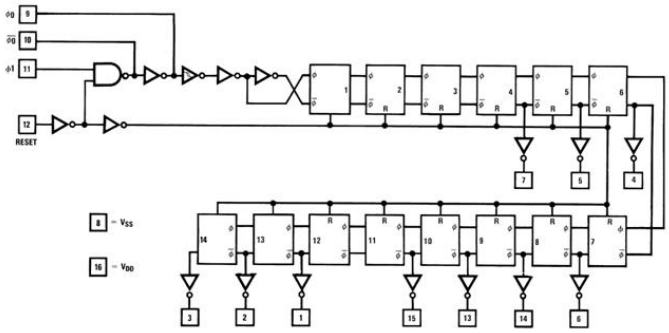

Figure 50: Logical structure of CD4060BC [70].

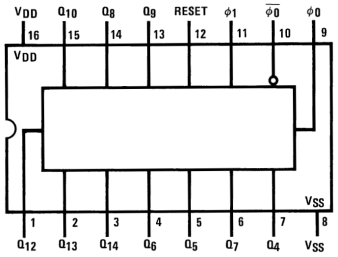

Figure 51: CD4060BC connection diagram [70].

Time delay using the CD4060BC is controlled by combination of two factors the oscillator circuit frequency and which output stage is chosen. The external oscillator circuit frequency is calculated using the following equation:

$$f = \frac{1}{2 \cdot R_t \cdot C_t}, \tag{33}$$

where R_t and C_t are resistor and capacitor values of external RC-circuit. The required time delay is calculated using the following equation:

$$t = \frac{2^{n-1}}{f}, \tag{34}$$

where n is the selected counter stage output number (Qn) and f is frequency obtained from the Equation (33). The needed delay is 30 minutes. By selecting $R_t = 1\ M\Omega$ and $C_t = 220\ nF$ the oscillator frequency is 2.27 Hz. Selecting Q13 for output pin the time delay is about 30 minutes.

The functional concept of timer circuit is shown in a block diagram in Appendix D. The schematic (Appendix E) and printed circuit board (Appendix F) of the timer were designed using CadSoft EAGLE [71]. The +12 V operating voltage is provided by UHF radio board. The output current from pin 2 (Q13) is used to open a transistor (T1) which in turn allows current to flow through heating resistors. There are four heating resistors two for each antenna. One resistor is enough to cut the string, the second is used to increase the reliability. Another feature that increases reliability is a second transistor (T2). This transistor bypasses the timer chip and allows deployment of the antennas in case timer chip fails. This transistor is connected to a separate 12 volt bypass (BP) line that EPS is programmed to turn on after 45 minutes.

The shape of printed circuit board (PCB) was defined by the space available between the antenna housings on the ADS. Figure 52 shows the main components on the timer circuit PCB: the timer chip and the required external RC circuit. Also located on the PCB are Remove Before Flight (RBF) jumper pins, heating resistors and Antenna Deployment Indicators (ADI). The task of RBF jumper pins is to disable the timer circuit during the testing of satellite systems. As the name implies the RBF jumper is removed before the satellite is put in the P-POD.

There are two ADI's located near the edges of PCB. The ADI is a microswitch that is kept pressed by antennas before deployment. The task of ADIs is to cut current to heating resistors once antennas are deployed and thus prevent unnecessary waste of power. The correct functioning of ADI is critical since ADI stuck in the closed position, after antennas have been deployed, would quickly deplete batteries and could end prematurely the whole mission. To mitigate this risk a microswitch with flight history has been selected. The selected switch is made by Omron Corporation and has been flown on Compass-1 CubeSat [72][73]. To further mitigate risk, the batch of switches was subjected to a thermal cycling test from −65 °C to +90 °C [74]. After thermal cycling, switches were tested to verify they have remained functional and these tested switches were used in assembly of all ADS models.

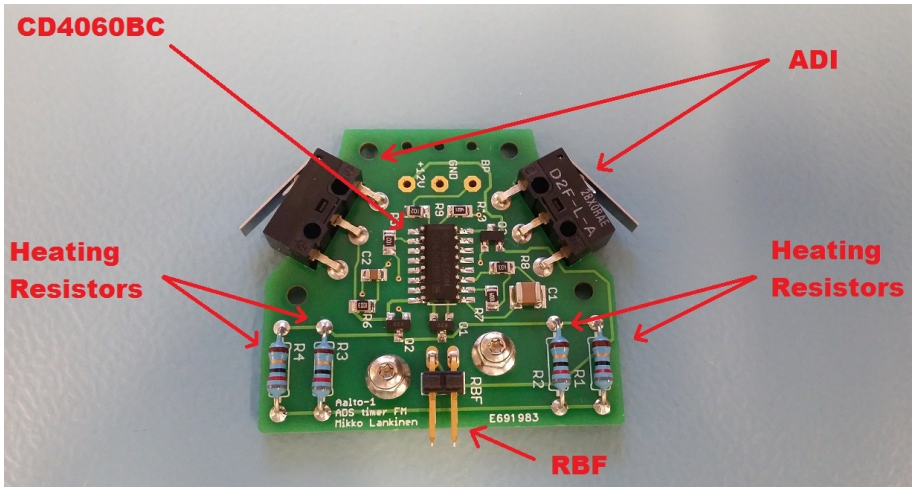

Figure 52: ADS timer circuit main components.

4.6.3 Component Selection

Electronics in CubeSats are typically made using non-space graded COTS components. While COTS components are not radiation tolerant, other properties such as temperature coefficient, value tolerance and operating temperature range vary widely. To ensure reliable function of the timer circuit it is important to select such components that are best suitable for timer circuit and space environment.

Temperature coefficient is the most important factor for two components in the timer circuit R7 and C1. These components form the external oscillator which defines operating frequency of the timer chip and thus define the needed time delay. Choosing components with small temperature coefficient ensures that 30 minutes delay doesn't change much when temperature changes. Operating temperature range is also important. The ADS will undergo cyclic temperature changes as satellite passes from day to night side of the Earth and all components has to function over the whole temperature range. Appendix G lists all electronic components used for the timer circuit.

4.7 Final Design

The final design of ADS (Figure 53) was modelled in Solid Edge a CAD modelling software [75]. The structure of ADS can be divided into four major components. The baseplate is the main structural component to which all other components are attached. The baseplate is manufactured from aluminium alloy 7075. Aluminium is a good heat conductor, ADS is for most of the time will be pointed away from the Sun and thus will be used as a radiator to radiate excess heat away from the satellite. Another important reason for choosing aluminium is because the same alloy is used in manufacturing frames and other structural components of the satellite. Since ADS will be part of satellite outer structure it is thus preferable for it to be made from the same material. The drawing of baseplate is shown in Appendix H.

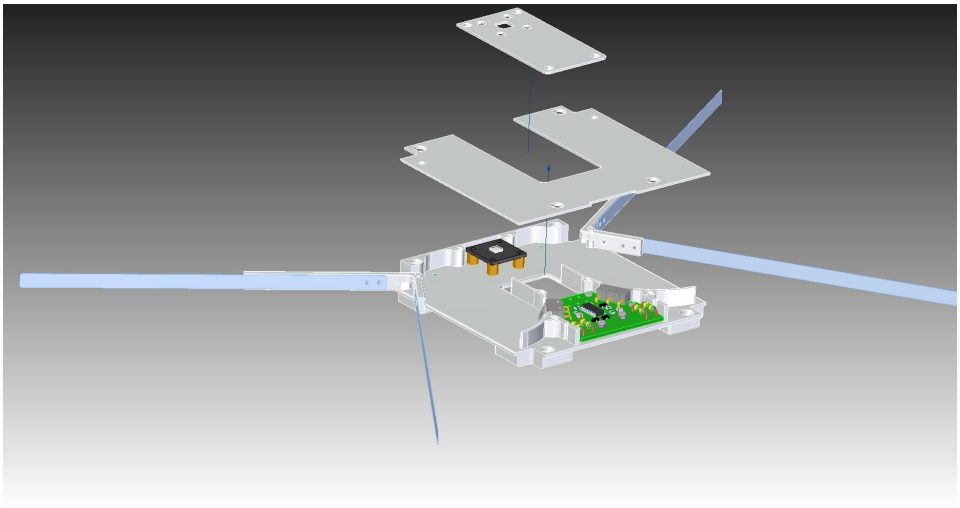

Figure 53: ADS FM CAD model.

The electronic component of ADS consists of two printed circuit boards. The timer circuit board controls the deployment of the antennas. The timer circuit board has also integrated release mechanism in the form of COTS resistors. Another board is sun sensor board which is part of ADCS that is used to control satellite orientation.

The third component is two L-shaped doors that keep antennas inside the ADS during launch. Doors are made from polyoxymethylene (POM) plastic. POM plastic has high stiffness, low friction and good dimensional stability. Its operating temperature range is from −40 °C to +175 °C. POM is widely used in CubeSats for non-conductive structures. Drawings of antenna doors are shown in Appendices I and J. Doors serve as an attachment point for antennas. Antennas are made from a conventional measuring tape a solution widely used in CubeSat design. Attached to antennas are grounding inductors, two for each antenna, that are used to equalize static potential difference between antennas and the satellite.

A dyneema string tied to one end of the door goes through the gap between ADS and satellite frame corner rail to the heating resistors. Resistors are used to cut the string. The dyneema string used is a conventional fishing line. Many CubeSat projects use nylon line but dyneema doesn't smoke while being melted which is important to prevent any residue contaminating AaSI optics.

The fourth component is a coverplate with a coverplate hatch. The coverplate and hatch is a simple 1 mm thick sheet of aluminium, the same alloy as the baseplate. The coverplate hatch can be detached separately from the coverplate. This solution allows access to antennas' coaxial connectors as well as electrical connector for sun sensor and timer circuit without removing the whole coverplate. Drawings for coverplate and coverplate hatch are shown in Appendices K and L.

Figure 54 shows the overall view of ADS FM with antennas in deployed configuration. Coverplate has been removed to show the internal structure. Figure 55 shows how antennas are positioned while being in stowed configuration during the launch. The whole ADS in anodized black to facilitate heat transfer from inside the satellite to the surface and radiate it away.

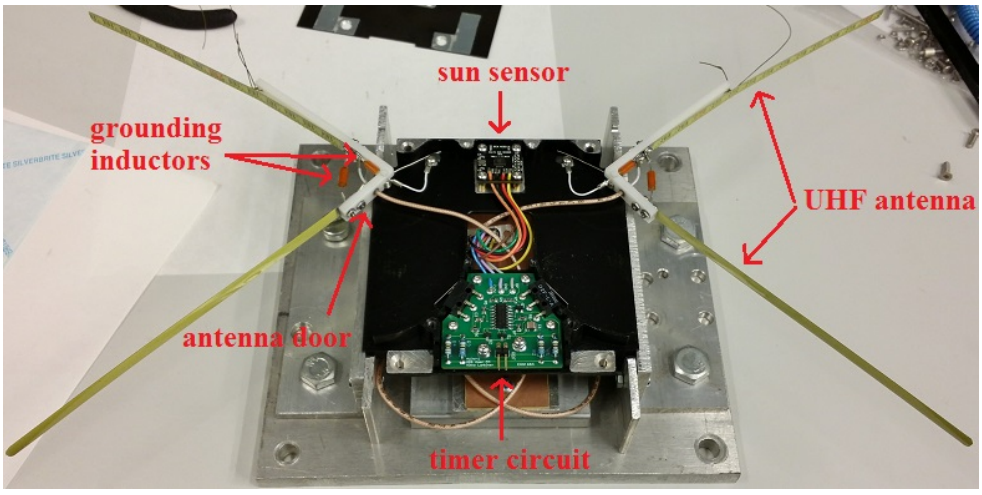

Figure 54: ADS antennas in deployed configuration.

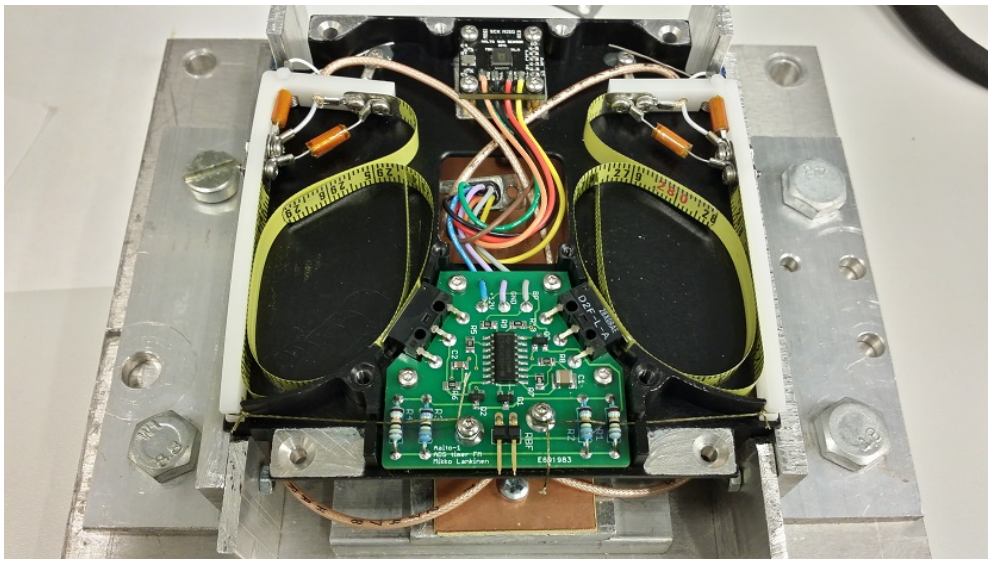

Figure 55: ADS antennas in stowed configuration.

Table 7 lists weight of ADS components. ADS requirement specifications didn't defined a certain mass limit but as with all CubeSat projects, mass is critical and the goal was to keep ADS total weight as low as possible.

Table 7: Mass budget.

Name	**Quantity**	**Weight per piece**	**Total weight**
Baseplate	1	62 g	62 g
Coverplate	1	19 g	19 g
Coverplate hatch	1	5 g	5 g
UHF antenna	2	2 g	4 g
Antenna door	2	3 g	6 g
Timer circuit	1	7 g	7 g
Sun sensor	1	1 g	1 g
Harness	1	5 g	5 g
Coaxial cable	2	4 g	8 g
Total			**117 g**

5 Testing

Testing is important part of designing space hardware. Once satellite is launched, repair is impossible if something goes wrong. For this reason it is preferable to use systems that have flight history and has proven to be reliable. Any new system that hasn't been flown before has to be subjected to extensive testing to ensure it can survive launch conditions and function properly in space.

CubeSat missions are usually university-led projects and satellites are built by the students who typically have no prior experience in building space hardware. Students operate under assumptions that if component-level assembly and testing is done then assembling the whole satellite and testing it is a quick task. As a consequence of these assumptions the majority of failed CubeSat missions have been university-led projects (see Figure 56) [12].

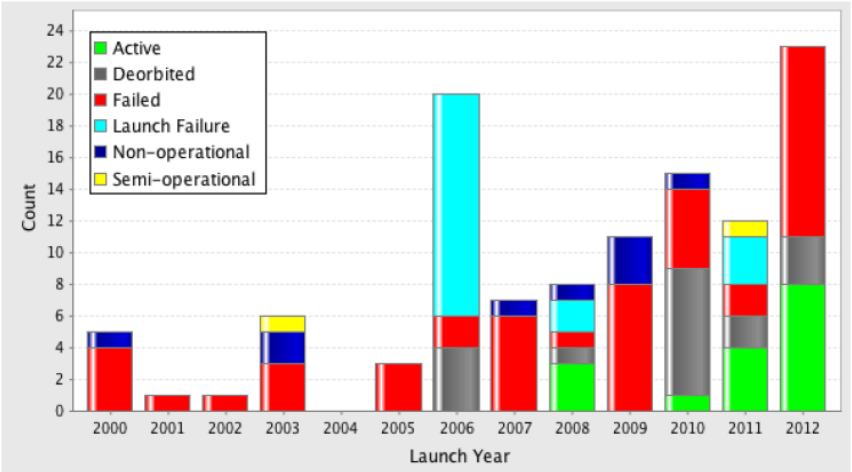

Figure 56: CubeSat missions status by launch year [12].

5.1 Test Plan

The Aalto-1 ADS is a completely new design and thus requires extensive testing to ensure it will work in space. The test plan of ADS follows the guidelines outlined in Aalto-1 Experiment Interface Document [76]. Qualification level testing will be performed on the engineering qualification model (EQM) of ADS to demonstrate that the assembled system meets specification requirements. Qualification testing is performed with much harsher operating parameters than the system will encounter normally. This ensures that tested system can operate in normal conditions and has sufficient operating margins. Acceptance level testing will be performed on the flight model (FM) of ADS to verify that the assembled system meets specification requirements and to provide quality assurance to detect any manufacturing defects. Acceptance testing is less severe than qualification testing. The detailed breakdown of various test is shown in Table 8.

Table 8: ADS test plan.

Testing level	Test type	Details
Qualification	Functional	hot, normal and cold case
	Thermal cycling	from −70 °C to +100 °C
	Vibration test	NASA GSFC-STD-7001
	Shock test	NASA GSFC-STD-7001
	Comm link test	Should match link budget
Acceptance	RL measurement	Should be similar to EM
	Functional	TVAC test with satellite FM

5.2 ADS EQM Qualification Tests

Two models were used for qualification testing EM and EQM (see Figure 57). EM was originally a mock-up model that was modified into EM and used for initial testing. Later, when EQM parts for the whole satellite were manufactured, ADS EQM was assembled. EQM resembles more closely to the actual FM and subsequently was used for the rest of the test program.

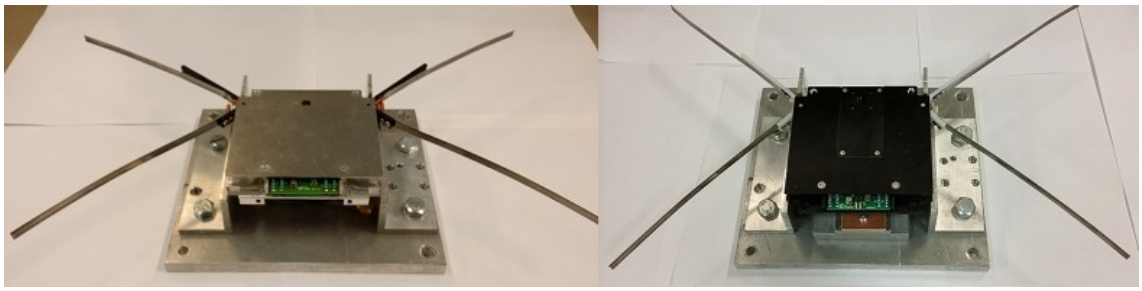

Figure 57: EM (left) and EQM (right).

5.2.1 Functional Test

Depending on the launch time, deployment of antennas could happen when satellite is in the sunlight or in the Earth's shadow. According to Thermal Analysis Report, surface temperature of the satellite will change from −21 °C to +37 °C [79]. Functional testing verifies that ADS antennas are capable of deploying in different temperatures. Because deployment of antennas is critical for success of the mission, the minimum and maximum operating temperature for qualification testing was doubled. Deployment was tested in three different cases: hot (+85 °C), normal (+20 °C) and cold (−55 °C). In addition to preliminary test runs, in total ten qualification tests for each case were performed. Table 9 shows how long it took for heating resistors to cut the strings which kept ADS doors closed.

Table 9: Functional test for ADS doors (see text for details). Times are in mm:ss.

	Antenna −Y side			**Antenna +Y side**		
Test	**Hot**	**Normal**	**Cold**	**Hot**	**Normal**	**Cold**
1	0:04	0:06	2:20	0:02	0:07	3:03
2	0:03	0:10	2:01	0:02	0:07	3:03
3	0:03	0:08	1:45	0:03	0:09	2:33
4	0:02	0:10	1:50	0:04	0:06	2:45
5	0:02	0:09	2:35	0:03	0:10	3:00
6	0:05	0:11	2:37	0:07	0:11	2:20
7	0:05	0:13	3:50	0:05	0:12	3:40
8	0:06	0:10	3:55	0:06	0:12	4:05
9	0:06	0:11	4:01	0:06	0:11	3:55
10	0:07	0:13	3:57	0:07	0:11	4:16

5.2.2 Thermal Cycling Test

As satellite orbits Earth, it will experience periodic temperature changes. The goal of temperature cycling test is to verify that ADS components will not be damaged by the constant cycling from hot to cold. Espec BTZ-175E environmental test chamber, shown in Figure 58, was used for testing [77]. The cycling test was done in normal air pressure.

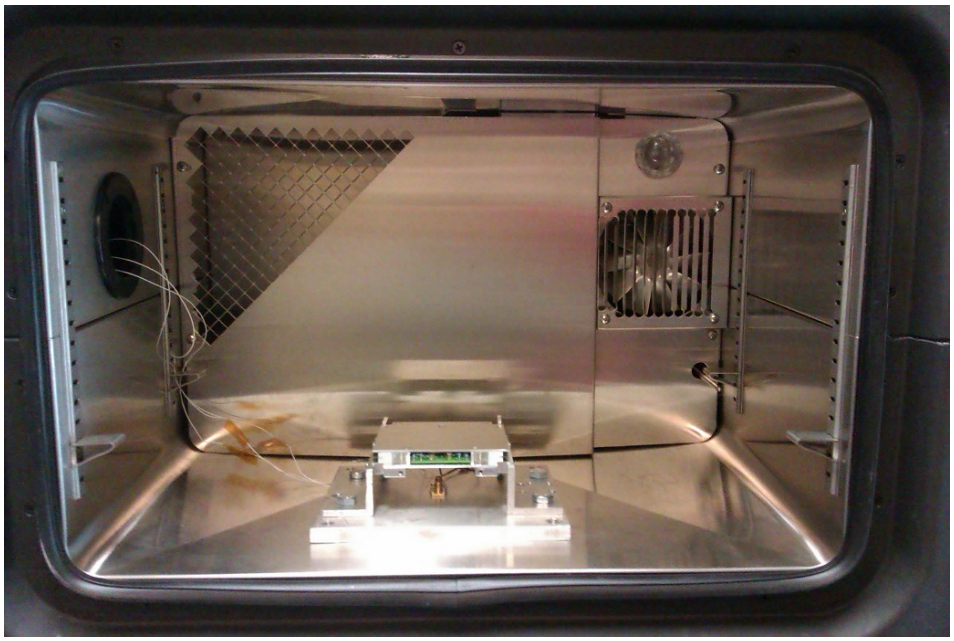

Figure 58: ADS EM with adaptor in environmental test chamber.

The chamber was programmed to perform temperature cycling according to the profile sown in Figure 59. The profile simulates temperature changes as the satellite passes from the Earth's shadow to the Sun side. The maximum temperature is (+100 °C) and the minimum temperature is (−70 °C) which are the values defined in the Aalto-1 Top-level Test Plan [78].

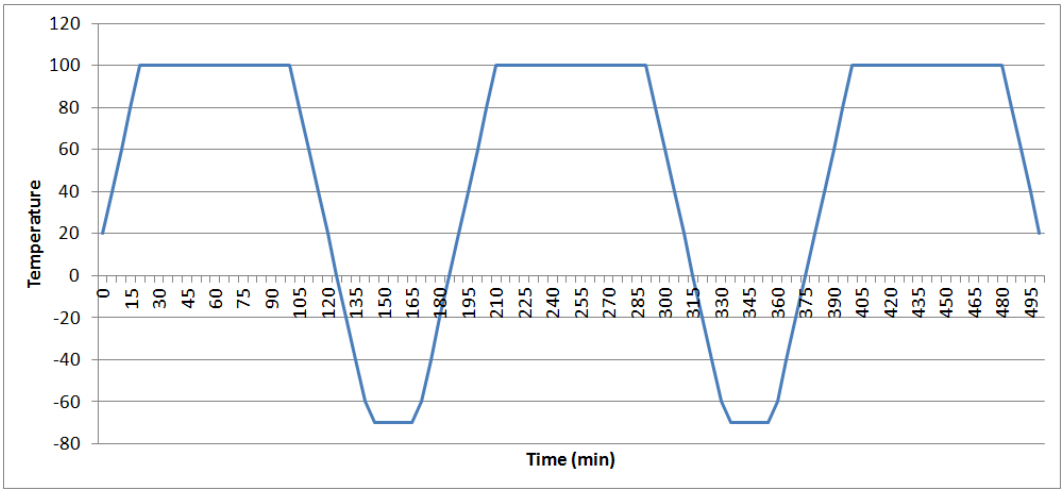

Figure 59: Temperature profile used for thermal cycling test.

In total, three tests were performed, each progressively longer than the previous one. After each test, the ADS was opened and visually inspected for any thermal damage. In addition to visual inspection, return loss of antennas was measured to verify that there was no internal damage to the antenna cables.

Table 10: Thermal cycling test.

Test	**Duration**
1	5 cycles
2	13 cycles
3	40 cycles

5.2.3 Vibration Test

Launch event creates the most stressful load levels that satellite will encounter during its mission. In addition to vibrations from working rocket engines, rocket stage separations cause shocks which add additional loads to satellite structure and systems. Vibration test verifies that the system will be in working condition once satellite reaches the orbit. Vibration testing was conducted at VTT Expert Services test laboratory in Otaniemi. Two models were tested, the EM and the EQM. The EM was tested as a stand-alone system without the satellite (see Figure 60) and the EQM was tested later as a part of the whole satellite vibration testing.

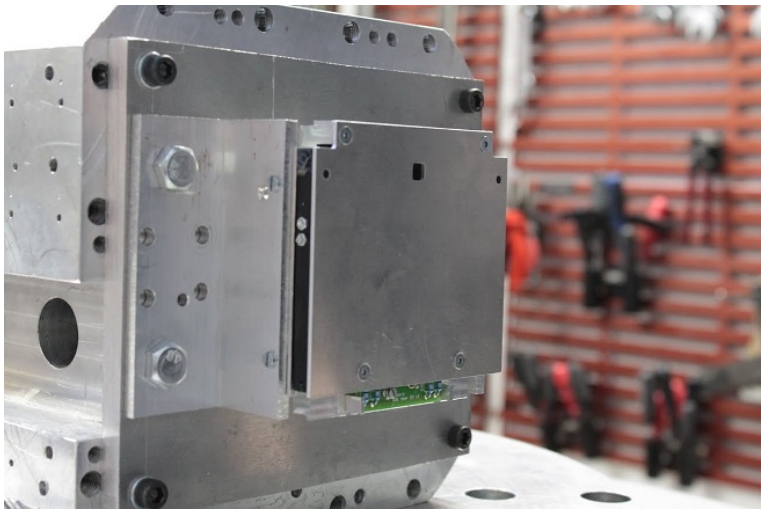

Figure 60: ADS EM on a vibration bench.(Picture by Bérenger Villat)

The type of test EM was subjected is random vibration test. The test is used to identify latent defects and manufacturing flaws which could cause fractures in the structure and system components breaking loose e.g. electrical connectors, nuts, bolts, etc. Testing was done according to NASA GSFC-STD-7000 standard qualification level testing with frequency sweep range from 20 Hz to 2000 Hz. The profile of the sweep is shown in Figure 61.

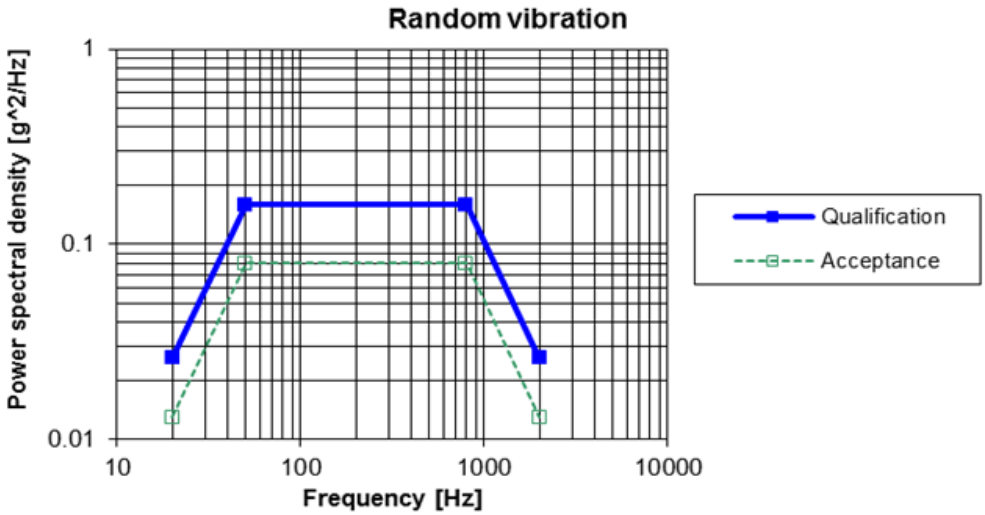

Figure 61: Generalized random vibration test levels [81].

In the second test, the EQM version of ADS was used. ADS EQM was integrated into satellite EQM and was tested as a part of the whole satellite EQM vibration test. The satellite EQM was placed into ISIPOD testpod, shown in Figure 62, a deployment pod similar to P-POD [80].

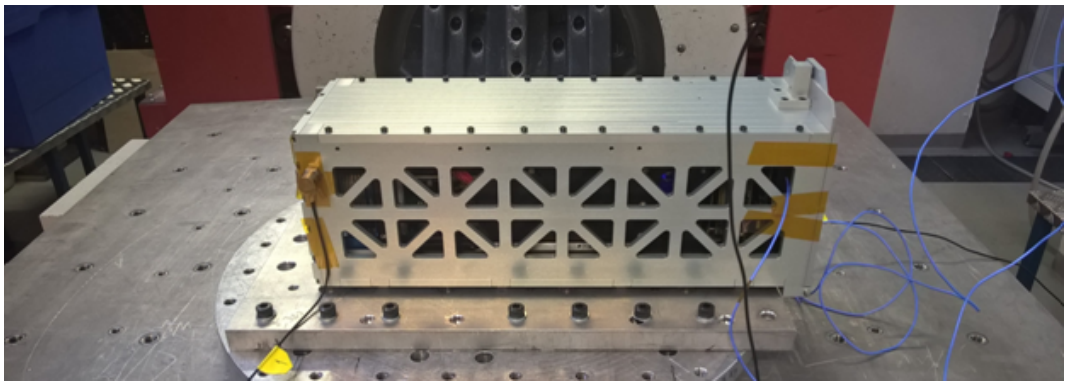

Figure 62: ISIPOD testpod [81].

The second test was more comprehensive and included three different types of vibration tests shown in Table 11. Modal survey is done first to find out the resonance frequency of the structure. After other tests are done modal survey is repeated and resulting resonance frequencies are compared. The change in frequency indicates a possible defect in the structure that wouldn't be possible to detect visually. Sine and random vibration tests simulate rocket launch by creating similar vibration environment.

Table 11: Satellite EQM vibration tests [81].

Test	**Notes**
Modal survey (before and after)	amplitude 0.4 g frequency 5 – 20000 Hz sweep rate 2 octave/min
Acceleration by sine wave	amplitude: 18.75 g frequency 20 Hz duration 15 sec
Random vibration	frequency range 20 – 2000 Hz

5.2.4 Shock Test

Shock testing simulates launch vehicle (LV) stage separation. LV stages are usually connected using explosive bolts. Explosion cuts the bolts and separates stages. The shock from separation reaches the satellite through LV structure. The test verifies that the system will be functional once satellite reaches the orbit.

Shock tests were also conducted at VTT Expert Services test laboratory. As with vibration tests, shock tests were done to the ADS EM and the EQM. Adapter with the ADS EM was attached to a large aluminum plate. The plate was struct with the horizontal and vertical hammer to simulate the shock in different directions (Figure 63). Shock tests were done along all three axis of the ADS. Results from the shock tests can be seen in Appendix M.

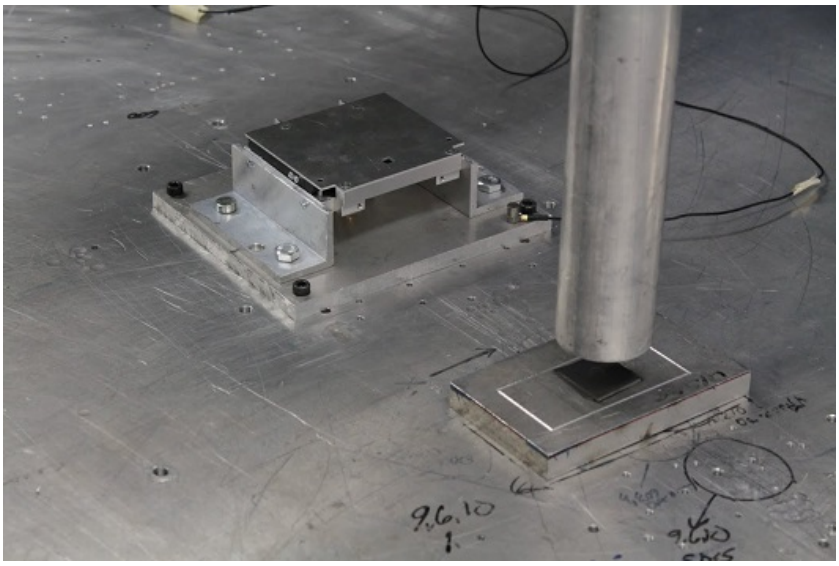

Figure 63: Test setup for ADS EM shock testing with vertical hammer.(Picture by Bérenger Villat)

The test of ADS EQM was again done as a part of the whole satellite EQM shock testing. The same test setup was used for the satellite EQM shock testing. The satellite was placed inside the ISIPOD testpod. The ISIPOD was attached to adapter and adapter attached to the shock table (see Figure 64). Shock tests were done along all three axis of the satellite. More detailed results for the satellite EQM vibration and shock testing are presented in "A1-MEC-PL-01-v3 Vibration & Shock Qualification Test Plan, Procedures and Results" document [81].

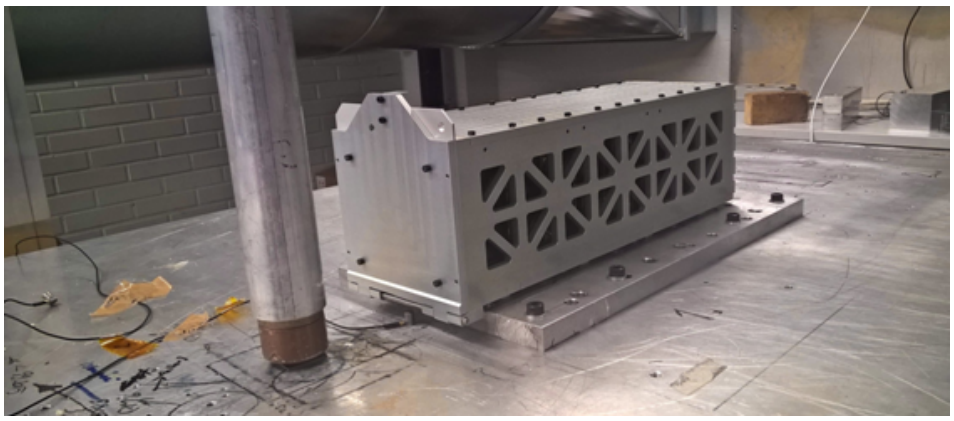

Figure 64: Test setup for satellite EQM shock testing with vertical hammer [81].

5.2.5 Communication Link Test

The purpose of communication link test is to verify that the calculated link budget is correct and communication link with the satellite can be established. The link test was conducted in Aalto University using roof of School of Electrical Engineering building as a test site (see Figure 65). The ADS EM was attached to satellite mock-up and mock-up was secured to a rotating stand. The stand was placed in the furthest corner of the building. The ground station antenna, located in the other corner, was turned towards the satellite. The resulting line-of-sight distance was 129 m. Using the Equation (27) the free-space path loss from 129 m is 67.5 dB. In real situation, as has been shown in Link Budget chapter, the maximum distance between satellite and the ground station is 2260 km. This correspond to FSPL of 152 dB. The difference, 84.5 dB, was added to measured results to simulate the actual 2260 km distance.

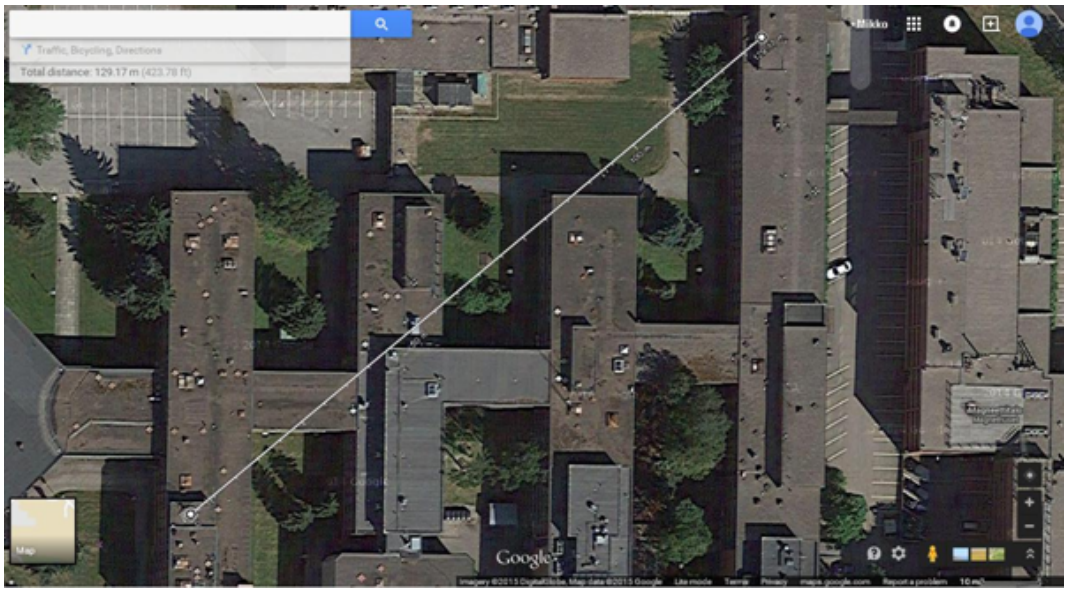

Figure 65: Test setup for communication link test.

The test was done by rotating the stand while satellite UHF radio was in transmitting mode and measuring received signal strength with spectrum analyser at the ground station. Rotation axis of the satellite was changed and test repeted until all three axes were measured. Measured results can be seen in Appendix N.

5.3 ADS FM Acceptance Tests

The ADS FM is an exact copy of EQM. The EQM has been extensively tested, thus the FM should perform the same way in test conditions as the EQM did. However, to mitigate the risk of damaging components, the FM is subjected only to acceptance level tests wich are less severe than qualification tests.

5.3.1 Return Loss Measurement Test

The return loss measurement was done to verify that parameters of ADS FM antennas, return loss and operating frequency, are the same as EQM. For testing the ADS FM was attached to the mock-up of the satellite and measured. Results can be seen in Appendix O.

5.3.2 Functional Test

The ADS FM functional testing includes two deployment tests. The first test was done in normal (+20 °C) temperature. The FM was attached to a mock-up of satellite and timer circuit was powered by external power source. This test served as preliminary test to verify timer circuit performance and that there are no mechanical problems that would prevent antenna doors from opening. Another deployment test was done as a part of the whole satellite thermal vacuum (TVAC) testing. This final test allows functionality of ADS to be tested in the environment most closely matched to a real space environment.

6 Conclusion

This thesis presented the design, construction and testing of Aalto-1 Antenna Deployment System (ADS). The Aalto-1 ADS was designed to consist of two redundant v-shaped dipoles that provide omnidirectional radiation pattern which in turn allows communication with the satellite regardles of the orientation. Only one antenna is needed for communication, the other antenna is a backup that can be switched on if necessary.

Integrated into ADS is timer circuit with deployment mechanism based on the COTS resistors. The timer circuit is powered immediately after the satellite is deployed from the P-POD and provides required 30 minutes delay before opening the antennas. As a redundancy timer circuit includes a "bypass" feature allowing another timer on the EPS board to serve as a backup if ADS own timer fails. Also integrated into ADS is a sun sensor for the satellite's ADCS.

Since the Aalto-1 ADS is a new design that has no flight history, an extensive qualification test program has been conducted on the engineering model of the ADS. The test program included functional, thermal, vibration, shock and communication link tests. Finally, a flight model of ADS was constructed and subjected to acceptance tests. The end result of these tests is a simple and robust ADS that is capable of surviving launch conditions and fulfills mission requirements for Aalto-1 satellite.

References

[1] *NSSDC Master Catalog Search*, NASA, [Online] 2014, Available: http://nssdc.gsfc.nasa.gov/nmc/spacecraftDisplay.do?id=1957-001B (Accessed Oct. 20, 2014).

[2] D.J. Brain, A.W. Rudge, "Efficient satellite antennas", *Electronics and Power*, vol. 30, no. 1, pp. 51-56, January 1984.

[3] *UCS Satellite Database*, [Online] 2014, Available: http://www.ucsusa.org/nuclear_weapons_and_global_security/solutions/space-weapons/ucs-satellite-database.html (Accessed Feb. 18, 2015).

[4] *Spacecraft Encyclopedia*, [Online] 2014, Available: http://claudelafleur.qc.ca/Spacecrafts-index.html (Accessed Feb. 18, 2015).

[5] *Satellites to be built & launched by 2022 world market survey*, [Online] 2014, Available: https://web.archive.org/web/20131121044956/http://www.euroconsult-ec.com/report/download?rep=brochure&name=satellites-built-launched-by-2022-brochure.50.pdf (Accessed Feb. 18, 2015).

[6] *NSSDC Master Catalog Search*, NASA, [Online] 2014, Available: http://nssdc.gsfc.nasa.gov/nmc/spacecraftDisplay.do?id=1961-034B (Accessed Feb. 18, 2015).

[7] *History of Amateur Radio Satellite Launches*, [Online] 2014, Available: http://archive.is/H7W0W (Accessed Feb. 18, 2015).

[8] B. Klofas, K. Leveque, "The Future of CubeSat Communications: Transitioning Away from Amateur Radio Frequencies for High-speed Downlinks", *Proceedings of the AMSAT-NA Space Symposium*, Orlando, Florida, 2012.

[9] B. Klofas, "Survey of CubeSat Communication Systems: 2009-2012", *10th Annual CubeSat Developers' Workshop*, USA, 2013.

[10] *Nano/Microsatellite Market Assesment*, [Online] 2015, Available: http://www.sei.aero/eng/papers/uploads/archive/SpaceWorks_Nano_Microsatellite_Market_Assessment_January_2014.pdf (Accessed Feb. 19, 2015).

[11] *CubeSat Design Specification, Rev. 13*, [Online] 2015, Available: http://www.cubesat.org/images/developers/cds_rev13_final.pdf (Accessed Feb. 19, 2015).

[12] M. Swartwout, "The First One Hundred CubeSats: A Statistical Look", *Journal of Small Satellites*, Vol. 2, No. 2, pp. 213 - 233, 2013.

[13] R. Nugent, R. Munakata, A. Chin, R. Coelho, and Dr. Jordi Puig-Suari, "The CubeSat: The Picosatellite Standard for Research and Education", *AIAA SPACE 2008 Conf.& Expo.*, San Diego, Calif., 2008.

[14] J. Puig-Suari, C. Turner, R. Twiggs, "CubeSat: The Development and Launch Support Infrastructure for Eighteen Different Satellite Customers on One Launch", *Proceedings of the 15th Annual AIAA/USU Conference on Small Satellites*, SSC01-VIIIb-5, USA, 2001.

[15] *P-Pod orbital Deployer*, [Online] 2015, Available: `http://amsat-uk.org/?attachment_id=11771` (Accessed Feb. 20, 2015).

[16] CubeSat Kit, *Pumpkin Inc.*, [Online] 2015, Available: `http://www.cubesatkit.com` (Accessed Feb. 20, 2015).

[17] *PC/104*, [Online] 2015, Available: `http://pc104.org/hardware-specifications/pc104/` (Accessed Feb. 20, 2015).

[18] *SUBCHAPTER M - INTERNATIONAL TRAFFIC IN ARMS REGULATIONS*, [Online] 2015, Available: `http://www.gpo.gov/fdsys/pkg/CFR-1999-title22-vol1/pdf/CFR-1999-title22-vol1-chap-id2-subchapM.pdf` (Accessed Feb. 21, 2015).

[19] S. Bhowmik, R. Benedictus, "Performance of space durable polymeric nano composite under electromagnetic radiation at Low Earth Orbit", *Applied Electromagnetics Conference*, Kolkata, 2007.

[20] A. Kestilä, T. Tikka, P. Peitso, J. Rantanen, A. Näsilä, K. Nordling, H. Saari, R. Vainio, P. Janhunen, J. Praks, and M. Hallikainen, "Aalto-1 nanosatellite - technical description and mission objectives", *Geoscientific Instrumentation, Methods and Data Systems Discussions*, Vol. 2, No. 1, pp. 121 - 130, 2013.

[21] A. Näsilä, "Validation of Aalto-1 Spectral Imager Technology to Space Environment", Master's Thesis, 2013.

[22] A1-RAD-PL-02-v1, "Development Plan for RADMON", Aalto-1 satellite design documentation, 2011.

[23] A1-EPB-PL-03-v1, "Science Mission of Electrostatic Plasma Brake", Aalto-1 satellite design documentation, 2011.

[24] ITU-R, "Radio Regulations", 2012.

[25] *Amateur Satellite Frequency Coordination Request*, [Online] 2015, Available: `http://www.iaru.org/uploads/1/3/0/7/13073366/iarucoordinationrequestversion28.pdf` (Accessed Feb. 21, 2015).

[26] B. Klofas, *CubeSat Communications System Table*, [Online] 2015, Available: `http://www.klofas.com/comm-table/table.pdf` (Accessed Feb. 21, 2015).

[27] C. Balanis, *Antenna Theory - Analysis and Design*, 3rd ed., NJ, USA, : Wiley, 2005.

[28] J. Costantine, Y. Tawk, S. Moth, C.G. Christodoulou, S.E. Barbin, "A modified helical shaped deployable antenna for cubesats", *IEEE-APS Topical Conference on Antennas and Propagation in Wireless Communications*, pp. 1114 - 1116, Cape Town, 2012.

[29] J. Costantine, D. Tran, M. Shiva, Y. Tawk, C.G. Christodoulou, S.E. Barbin, "A deployable quadrifilar helix antenna for CubeSat", *IEEE Antennas and Propagation Society International Symposium*, pp. 1 - 2, Chicago, 2012.

[30] M. Aherne, J. Barrett, L. Hoag, E. Teegarden, R. Ramadas, "Aeneas - Colony I Meets Three-Axis Pointing", *Proceedings of the 25th Annual AIAA/USU Conference on Small Satellites*, CubeSat Missions, SSC11-XII-7, USA, 2011.

[31] C. MacGillivray, "Miniature Deployable High Gain Antenna for CubeSats", *8th CubeSat Developers' Workshop*, USA, 2011.

[32] Inflatable antennae could give CubeSats greater reach, *MIT News*, [Online] 2015, Available: `http://newsoffice.mit.edu/2013/inflatable-antennae-could-give-cubesats-greater-reach-0906` (Accessed Feb. 22, 2015).

[33] *Innovative Solutions in Space*, [Online] 2015, Available: `http://www.isispace.nl/cms/` (Accessed Feb. 21, 2015).

[34] *Deployable Antenna System for CubeSats*, [Online] 2015, Available: `http://cubesatshop.com/index.php?page=shop.product_details&flypage=flypage.tpl&product_id=66&category_id=6&option=com_virtuemart&Itemid=70` (Accessed Feb. 21, 2015).

[35] *UHF Turnstile Antenna*, [Online] 2015, Available: `http://gomspace.com/index.php?p=products-ant430` (Accessed Feb. 21, 2015).

[36] *The Twelveth Anniversary of XI-IV on Orbit Operation*, [Online] 2015, Available: `http://www.space.t.u-tokyo.ac.jp/cubesat/index-e.html` (Accessed Feb. 22, 2015).

[37] *M-Cubed/COVE*, [Online] 2015, Available: `http://space.skyrocket.de/doc_sdat/m-cubed.htm` (Accessed Feb. 22, 2015).

[38] *Delfi-n3Xt Communication Subsystem*, [Online] 2015, Available: `http://www.delfispace.nl/delfi-n3xt/comms` (Accessed Feb. 22, 2015).

[39] Å.G. Riise et al., nCube: The First Norwegian Student Satellite", *Proceedings of the 17th Annual AIAA/USU Conference on Small Satellites*, CubeSat Missions, SSC03-VII-4, USA, 2003.

[40] *Nature of Radiation*, [Online] 2015, Available: https://www.nde-ed.org/EducationResources/CommunityCollege/RadiationSafety/theory/nature.htm (Accessed Feb. 22, 2015).

[41] J. Kraus, *Antennas*, 2nd ed., New Delhi, India, : Tata McGraw-Hill, 1997.

[42] "521-2002 - IEEE Standard Letter Designations for Radar-Frequency Bands", *IEEE*, ISBN 0-7381-3356-6, 2003.

[43] "145-1993 - IEEE Standard Definitions of Terms for Antennas", *IEEE Transactions on Antennas and Propagation*, IEEE Std 145-1983, 1983.

[44] H. J. Visser, *Antenna Theory and Applications*, USA, : Wiley, 2012.

[45] W. L. Stutzman, G. A. Thiele, *Antenna Theory and Design*, 3rd ed., USA, : Wiley, 2012.

[46] A.R. Harish, M. Sachidananda, *Antennas and Wave Propagation*, UK, : Oxford University Press, 2007.

[47] W. A. Imbriale, S. Gao, L. Boccia, *Space Antenna Handbook*, USA, : Wiley, 2012.

[48] C. Capela, "Protocol of Communications for VORSat Satellite", Master's Thesis, 2012.

[49] L. J. Ippolito, *Propagation Effects Handbook for Satellite Systems Design*, USA, : NASA, 1998.

[50] C. Levis, J. T. Johnson, F. L. Teixeira, *Radiowave Propagation: Physics and Applications*, USA, : Wiley, 2010.

[51] J. Jussila, "S-band transmitter for Aalto-1 nanosatellite", Master′s Thesis, 2013.

[52] G. Maral, M. Bousquet, S. Zhili, *Satellite Communications Systems - Systems, Techniques and Technology*, 5th ed., USA, : Wiley, 2009.

[53] *Falcon 1 Launch Vehicle Payload User's Guide*, [Online] 2015, Available: https://foiaelibrary.gsfc.nasa.gov/_assets/doclibBidder/tech_docs/3.%20Falcon1UsersGuide.pdf (Accessed Oct. 21, 2015).

[54] P. Fortescue, J. Stark, G. Swinerd, *Spacecraft Systems Engineering*, 3rd ed., West Sussex, UK, : Wiley, 2003, pp. 13 - 14, 24, 27 - 30.

[55] "Assessment of Cold Welding between Separable Contact Surfaces due to Impact and Fretting under Vacuum", *ESA Publications*, ESA Communication Production Office, 2009.

[56] Outgassing Data for Selecting Spacecraft Materials, *NASA*, [Online] 2015, Available: http://outgassing.nasa.gov/ (Accessed Mar. 20, 2015).

[57] J. Friedel, S. McKibbon, *Thermal Analysis of the CubeSat CP3 Satellite*, [Online] 2015, Available: http://digitalcommons.calpoly.edu/cgi/viewcontent.cgi?article=1054&context=aerosp (Accessed Mar. 20, 2015).

[58] A1-Q-PL-01-v3, "Product Assurance Plan", Aalto-1 satellite design documentation, 2013.

[59] J. Springmann, B. Kempke, J. Cutler, H. Bahcivan, "Initial Flight Results of the RAX-2 Satellite", *Proceedings of the 26th Annual AIAA/USU Conference on Small Satellites*, Mission Lessons II, SSC12-XI-5, USA, 2012.

[60] *Vermont Technical College CubeSat Laboratory*, [Online] 2015, Available: http://www.cubesatlab.org/BasicLEO-Hardware.jsp (Accessed Sep. 30, 2015).

[61] *CST - Computer Simulation Technology*, [Online] 2015, Available: https://www.cst.com (Accessed Aug. 18, 2015).

[62] *IC-910H VHF/UHF All Mode Transceiver*, [Online] 2015, Available: http://www.icomamerica.com/en/products/amateur/satellite/910h/specifications.aspx (Accessed Sep. 10, 2015).

[63] *Ultra-High Performance RF Narrowband Transceiver*, [Online] 2015, Available: http://www.ti.com/lit/ds/symlink/cc1125.pdf (Accessed Sep. 10, 2015).

[64] *University of Tokyo CubeSat Technical CDR*, [Online] 2015, Available: http://www.space.t.u-tokyo.ac.jp/cubesat/publication/cdr.ppt (Accessed Mar. 20, 2015).

[65] K. A. Dontchev, K. Ghorakavi, C. E. Haag, T. M. Liu, R. Ramos, "M-Cubed: University of Michigan Multipurpose MiniSatellite with Optical Imager Payload", *Proceedings of the AIAA Space 2010 Conference & Exhibition*, 2010.

[66] J. Plaza, J. Vilán, F. Agelet, J. Mancheño, M. Estévez, C. Fernández, F. Ares, "Xatcobeo: Small Mechanisms for CubeSat Satellites - Antenna and Solar Array Deployment", *Proceedings of the 40th Aerospace Mechanisms Symposium*, 2010.

[67] M. S. Prakash Rao, *Pulse and Digital Circuits*, 1st ed., New Delhi, India, : Tata McGraw-Hill, 2006.

[68] *CD4060B CMOS 14-Stage Ripple-Carry Binary Counter/Divider and Oscillator*, [Online] 2015, Available: http://www.ti.com/product/cd4060b (Accessed Oct. 6, 2015).

[69] *SMD CD4060 - Circuito Integrado*, [Online] 2015, Available: http://proesi.com.br/smd-cd4060-circuito-integrado.html (Accessed Aug. 20, 2015).

[70] *CD4060BC, 14-Stage Ripple Carry Binary Counters*, [Online] 2015, Available: http://www.fairchildsemi.com/ds/CD/CD4060BC.pdf (Accessed Aug. 20, 2015).

[71] *CadSoft EAGLE PCB Design Software*, [Online] 2015, Available: http://www.cadsoftusa.com/ (Accessed Aug. 20, 2015).

[72] *Ultra Subminiature Basic Switch*, [Online] 2015, Available: https://www.components.omron.com/components/web/pdflib.nsf/0/5673FC48B47CDC9C85257201007DD56F/$file/D2F_1113.pdf (Accessed Aug. 20, 2015).

[73] *COMPASS-1 PICOSATELLITE: STRUCTURES & MECHANISMS*, [Online] 2015, Available: http://www.raumfahrt.fh-aachen.de/compass-1/download/Structure%20of%20the%20COMPASS-1%20Cubesat.pdf (Accessed Aug. 20, 2015).

[74] A1-MEC-TR-02-v1, "Preliminary Tests and Temperature Cycling of Microswitches for ADS", Aalto-1 satellite design documentation, 2012.

[75] *Solid Edge: Siemens PLM Software*, [Online] 2015, Available: http://www.plm.automation.siemens.com/en_us/products/solid-edge/ (Accessed Sep. 20, 2015).

[76] A1-SYS-EID-01-v7, "Experiment Interface Document", Aalto-1 satellite design documentation, 2013.

[77] *Environmental Test Chambers*, [Online] 2015, Available: http://www.espec.com/ (Accessed Sep. 1, 2015).

[78] "Aalto-1 Top-level Test Plan", Aalto-1 satellite design documentation, 2014.

[79] A1-THE-RP-01-v1, "Thermal Analysis Report", Aalto-1 satellite design documentation, 2015.

[80] *ISIPOD CubeSat Deployer*, [Online] 2015, Available: http://www.isispace.nl/brochures/ISIS_ISIPOD_Brochure_v.7.11.pdf (Accessed Sep. 2, 2015).

[81] A1-MEC-PL-01-v3, "Vibration & Shock Qualification Test Plan, Procedures and Results", Aalto-1 satellite design documentation, 2015.

A CubeSat Communications System

Version 9; Page 1 of 2. This chart shows the 256 total CubeSats deployed in orbit so far, for a total of 499 Units. March 10, 2015.
Bryan Klofas, bklofas@gmail.com. Green are University CubeSats; Red are Commercial or Private; Blue are US Government.

Launch	Satellite	Size	Radio	Downlink	Satellite Service	Power	TNC	Protocol	Data Rate/Modulation	Downloaded	Lifetime	Antenna	Status
NLS-1/Rocket 30 June 2003	AAU1 CubeSat	1U	Wood & Douglas SX450	437.475 MHz	amateur	500 mW	MX909	AX.25, Mobitex	9600 baud GMSK	1 kB	3 months	dipole	Dead
	DTUsat-1	1U	RFM/D RF2905	437.475 MHz	amateur	400 mW		AX.25	2400 baud FSK	0[1]	0 days	caned turnstile	DOA
	CanX-1	1U	Motorola	437.880 MHz	amateur	500 mW		Custom	1200 baud MSK	0[1]	0 days	crossed dipoles	DOA
	Cute-1	1U	Alinco DJ-C4 (data)	437.470 MHz	amateur	350 mW	MX614	AX.25	1200 baud AFSK	>10 MB[2]	118+ months	monopole	Alive
	(CO-55)		Maki Denki (beacon)	436.8375 MHz	amateur	100 mW	PIC16LC73A	CW	50 WPM	N/A		monopole	
	QuakeSat-1	3U	Tiku KS-960	436.675 MHz	amateur	2 W	BeyFac BF-96A	AX.25[3]	9600 baud FSK	423 MB	7 months	turnstile	Dead
	XI-IV	1U	Nishi RF Lab (data)	437.490 MHz	amateur	1 W	PIC16C622	AX.25	1200 baud AFSK	>11 MB[2]	118+ months	dipole	Alive
	(CO-57)		Nishi RF Lab (beacon)	436.8475 MHz	amateur	80 mW	PIC16C716	CW	50 WPM	N/A		dipole	
SSETI Express 27 Oct 2005	XI-V	1U	Nishi RF Lab (data)	437.345 MHz	amateur	1 W	PIC16C622	AX.25	1200 baud AFSK	N/A	90+ months	dipole	Alive
	(CO-58)		Nishi RF Lab (beacon)	437.465 MHz	amateur	80 mW	PIC16C716	CW	50 WPM			dipole	
	NCube-2	1U		437.505 MHz	amateur			AX.25	1200 baud AFSK	0[1]	0 days	monopole	DOA
	UWE-1	1U	PR430	437.505 MHz	amateur	1 W	HSS/2674B[5]	AX.25	1200/9600 baud AFSK		3 weeks	end-fed dipole	Dead
MVP-8 22 Feb 2006	Cute-1.7+APD (CO-56)	2U	Alinco DJ-C5 Telemetry (beacon)	437.505 MHz 437.385 MHz	amateur	300 mW 100 mW	CMX589A HSS/2328[5]	AX.25/SHLL CW	1200 AFSK/9600 GMSK 50 WPM	<1 MB N/A	2.5 months	dipole dipole	Deorbited
Minotaur-1 11 Dec 2006	GeneSat-1	3U+	Microhard MHX-2400	2.4 GHz	experimental	1 W	Integrated[6]	Proprietary		500 kB	3 months	patch	Deorbited
			Stensat (beacon)[7]	437.067 MHz	amateur	500 mW	PIC12C617	AX.25	1200 baud AFSK	N/A		monopole	
Dnepr 2 17 Apr 2007	CSTB1	1U	Yaesu VX-2R	400.18375 MHz	experimental	300 mW	PIC	Proprietary	1200 baud AFSK	6.77 MB	18 months	dipole	Dead
	AeroCube-2	1U	FreeWave FGRM	915 MHz	experimental	2 W	Integrated[6]	Proprietary	38.4 kbaud	500 kB	1 week	patch	Dead
	CP4	1U	TI CC1000/RF2117	437.325 MHz	amateur	1 W	PIC18LF6720	AX.25	1200 baud FSK	487 kB	2 months	dipole	Dead
	Libertad-1	1U	Stensat	437.405 MHz	amateur	400 mW		AX.25	1200 baud AFSK	0[8]	1 month	monopole	Dead
	CAPE1	1U	TI CC1020	435.245 MHz	amateur	1 W	PIC16LF452	AX.25	9600 baud FSK	0[8]	4 months	dipole	Dead
	CP3	1U	TI CC1000/RF2117	436.845 MHz	experimental	1 W	PIC18LF6720	AX.25	1200 baud FSK	2.0 MB[2]	19+ months	dipole	Dead
	MAST[10]	3U	Microhard MHX-2400	2.4 GHz	experimental	1 W	Integrated[6]	Proprietary	15 kbps	>2 MB	0.75 months	monopole	Dead
NLS-4/PSLV-C9 28 Apr 2008	Delfi-C3	3U	Custom (transponder)	145.9-435.55 MHz	amateur	200 mW	N/A	Linear	40 kHz wide	N/A	60+ months	turnstile	Alive
	(DO-64)		Custom (beacon)	145.870 MHz	amateur	400 mW	PIC18LF4680	AX.25	1200 baud BPSK	60 MB[11]		turnstile	
	Seeds-2	1U	Musashino Electric (data)	437.485 MHz	amateur	450 mW		AX.25	1200 baud AFSK	500 kB[2]	60+ months	monopole	Alive
	(CO-66)		Musashino Electric (beacon)	437.485 MHz	amateur	90 mW		CW	N/A	N/A		monopole	
	CanX-2	3U	Custom S-Band	2.2 GHz	space research	500 mW	Integrated	NSP	16-256kbps BPSK	250 MB	60+ months	patch	Active
	AAUSAT-II	1U	Holger Eckhardt (DF2FQ)	437.425 MHz	amateur	610 mW	PIC18LF6680	AX.25	1200 baud NSK	8 MB[2]	60+ months	dipole	Alive
	Compass-1	1U	Holger Eckhardt (data)	437.405 MHz	amateur	300 mW	C8051F123, FX614	AX.25	1200 baud AFSK/MSK	<1 MB[2]	60+ months	dipole	Alive
			BG549 (beacon)	437.275 MHz	amateur	200 mW	PIC12F629	CW	15 WPM	N/A		dipole	
Minotaur I 19 May 2009	AeroCube-3	1U	FreeWave FGRM	915 MHz	experimental	2 W	Integrated	Proprietary	77 kbaud GFSK	52 MB	7 months	patch	Deorbited
	CP6	1U	CC1000/RF2117	437.365 MHz	amateur	1 W	PIC18LF6720	AX.25	1200 baud FSK		4 months	dipole	Deorbited
	HawkSat-1	1U	Microhard MHX-425	437.345 MHz	amateur	1 W	Integrated	Proprietary		0 kB	0 days	monopole	DOA
	PharmaSat	3U+	Microhard MHX-2400	2.4 GHz	experimental	1 W	Integrated	Proprietary	10 kbps	650 kB	10 days	patch	Deorbited
			Stensat (beacon)[7]	437.465 MHz	amateur	500 mW	Integrated	AX.25	1200 baud AFSK	N/A	1 month	monopole	
H-IIA F17 20 May 2010 ISHLaunch 01/ PSLV-C14 23 Sep 2009	BEESAT-1	1U	STE BK-778	436.000 MHz	amateur[13]	500 mW	CMX909B	Mobitex	4800/9600 baud GMSK		43+ months	monopole	Alive
	UWE-2	1U	Custom	437.385 MHz	amateur			AX.25	1200 baud AFSK		1 week	dipole	Dead
	ITUpSAT-1	1U	Microhard MHX-425	437.325 MHz	amateur	1 W	Integrated	Proprietary	19200 baud	0 kB[8]	43+ months	dipole	Alive
			BeeLine/CC1050	437.325 MHz	amateur	350 mW		CW		N/A		monopole	
	SwissCube	1U	Butler oscillator/RF5110G	437.505 MHz	amateur	1 W	MSP430F1611	AX.25	1200 baud FSK	6 MB	43+ months	monopole	Active
			RF2516 (beacon)	437.505 MHz	amateur	100 mW	Integrated	CW	10 WPM	N/A		monopole	
	Hayato	1U	Custom	13.975 GHz	Earth exploration	100 mW	Integrated		10 Kbps/1 Mbps BPSK	0 kB[8]	18 days	patch	Deorbited
	Waseda-SAT2	1U	TXE430-301A	437.485 MHz	amateur	150 mW	H8/3052F[5]	AX.25	9600 baud FSK	0 kB	0 days	monopole	DOA
			TXE430-301A (beacon)	437.485 MHz	amateur	100 mW	H8/3052F[5]	CW		N/A		dipole	Deorbited
	Negai-Star	1U	Data	437.305 MHz	amateur	150 mW		AX.25	1200 baud FSK		1 month	dipole	Deorbited
			Beacon Radio	437.305 MHz	amateur	100 mW		CW	50 WPM	N/A		dipole	
NLS-6/ PSLV-C15 12 July 2010	Tisat-1	1U	Alinco DJ-C6	437.305 MHz	amateur	500 mW	MSP430F169	AX.25	1200 baud AFSK		33+ months	monopole	Active
			CC1010 (beacon)	437.305 MHz	amateur	400 mW	MSP430F169	CW	15-110 WPM	N/A		monopole	
	StudSat	1U	CC1020	437.505 MHz	amateur	500 mW	UC3A0512[9]	Custom AX.25	4800 baud FSK	0 kB[8]	5 days	monopole	Dead
			MAX1472 (beacon)	437.860 MHz	amateur	10 mW	UC3A0512[9]	CW	22 WPM	N/A		monopole	
STP-S26 19 Nov 2010	RAX-1	3U	Lithium-1	437.505 MHz	amateur	750 mW	Integrated	AX.25	9600 baud GMSK	4.8 MB	2 months	turnstile	Dead
	O/OREOS	3U+	Microhard MHX-2400	2.4 GHz	experimental	1 W	Integrated	Proprietary	Variable	8 MB	29+ months	patch	Alive
			Stensat (beacon)[7]	437.305 MHz	amateur	500 mW	Integrated	AX.25	1200 baud AFSK	N/A		monopole	
	NanoSail-D2	3U+	Microhard MHX-2400	2.4 GHz	experimental	1 W	Integrated	Proprietary	Variable	N/A	5 days[14]	patch	Deorbited
			Stensat (beacon)[7]	437.270 MHz	amateur	500 mW	Integrated	AX.25	1200 baud AFSK			monopole	

Figure A1: Deployed CubeSats 30 June 2003 – 19 November 2010.

Falcon 9-002 8 Dec 2010	Perseus (4)	1.5U			government	1 W			9600 baud GMSK		1 month	dipole	Deorbited
	QbX (2)	3U	TTC	450 MHz	government						1 month	quadrafillar helix	Deorbited
	SMDC-ONE	3U	Periclе	UHF	government						1 month	turnstile	Deorbited
	Mayflower	3U	Microhard MHX-425 Stensat (beacon)[7]	437.000 MHz 437.600 MHz	unlicensed unlicensed	1 W 1 W	Integrated Integrated	Proprietary AX.25	Variable 1200 baud AFSK	0 kB[8] N/A	2 days	dipole	Deorbited
PSLV-C18 12 Oct 2011	Jugnu	3U	CC1070/RF5110G MAX1472 (beacon)	437.505 MHz 437.505 MHz	amateur amateur	1 W 10 mW		AX.25 CW	2400 baud FSK 20 WPM	N/A	18+ months	monopole monopole	Alive
ELaNa-3/ NPP 28 Oct 2011	AubieSat-1	1U	Melexis TH72011	437.475 MHz	amateur	800 mW	ATmega128L[5]	CW	20 WPM	0 kB	22+ months	dipole	Alive
	DICE (2)	1.5U	L3 Cadet	465 MHz	meteorological	1 W	Integrated	Proprietary	2.6 Mbps OQPSK	8.4 GB	20 months	dipole	Dead
	HRBE	1U	CC1000	437.505 MHz	amateur	850 mW		AX.25	1200 baud FSK	[11]	22+ months	monopole	Active
	M-Cubed	1U	Lithium-1	437.485 MHz	amateur	1 W	Integrated	AX.25	1200 baud FSK	0 kB[8]	22+ months	monopole	Alive
	RAX-2	3U	Lithium-1	437.345 MHz	amateur	1 W	Integrated	AX.25	9600 baud GMSK	242 MB	18 months	turnstile	Dead
Vega VV01 13 Feb 2012	Xatcobeo	1U	GomSpace U482C	437.365 MHz	amateur	500 mW	Integrated	AX.25/CW	1200 baud MSK/20 WPM		18+ months	turnstile	Active
	ROBUSTA	1U	MC12181/MAX2608	437.325 MHz	amateur	800 mW	PIC18F4580[5]	AX.25	1200 baud AFSK	0 kB[15]	2 days	dipole	Dead
	e-st@r	1U	BHX2-437-5	437.445 MHz	amateur	500 mW	PIC16	AX.25	1200 baud AFSK	0 kB[8]	3 days	dipole	Dead
	Goliat	1U	Alinco DJ-C7 Microhard MHX-2420	437.485 MHz 2.4 GHz	amateur	500 mW 1 W	FX614/MSP430 Integrated	AX.25/CW Proprietary	1200 baud AFSK/20 WPM Variable	0 kB[15]	1 week	monopole patch	Dead
	PW-Sat	1U	ISIS TRXUV	145.900 MHz	amateur	200 mW	Integrated	AX.25/CW	1200 baud BPSK/12 WPM		10 months	dipole	Dead
	Mesat-1	1U	Si4432	437.345 MHz	amateur	100/400 mW	dsPIC33F[8]	Custom/CW	GFSK/120 CPM	305 MB	18+ months	monopole	Active
	UniCubeSat-GG	1U	AstroDev Custom	437.305 MHz	amateur	500 mW	Integrated	AX.25/CW	9600 baud GFSK	0 kB[8]	2 days	dipole	Dead
ELaNa-6/NROL-36 13 Sep 2012	SMDC-ONE (2)	3U	Periclе	UHF	government							turnstile	Alive
	AeroCube-4 (3)	1U	FreeWave MM2 CC1101	915 MHz 915 MHz	experimental experimental	2 W 1.3 W	Integrated Integrated	Proprietary Proprietary	38.4 kbaud 500 kbps FSK		8+ months	patch patch	Active
	Aeneas	3U	MHX-425 Stensat (beacon)[7]	437.000 MHz 437.600 MHz	experimental amateur	1 W 1 W	Integrated Integrated	Proprietary AX.25	Variable 1200 baud FSK	N/A	8+ months 8+ months	monopole monopole	Alive
	CSSWE	3U	Lithium-1	437.345 MHz	experimental	1 W	Integrated	AX.25	9600 baud GFSK	60 MB	12+ months	monopole	Active
	CP5	1U	CC1000/RF2117	437.405 MHz	amateur	500 mW	PIC18LF6720	AX.25	1200 baud FSK	500 kB	4 months	dipole	Dead
	CXBN	2U	Lithium-1	437.525 MHz	amateur	1 W	Integrated	AX.25	9600 baud GFSK		8+ months	turnstile	Active
	CINEMA	3U	Emhiser	2260 MHz	space research	1 W	FPGA	Proprietary	1 Mbps FSK		8+ months	patch	Active
	Re	3U	Helium-100	915 MHz	government	1 W	Integrated	AX.25	57.6 kbps FSK	0 kB	0 days	dipole	DOA
HTV-3/ISS 4 Oct 2012	FITSat-1	1U	High-speed Custom Custom (data) Custom (beacon)	5.84 GHz 437.445 MHz 437.250 MHz	amateur amateur amateur	2 W 10 mW	PIC16F886 PIC16F1519 PIC16F1519	AX.25 CW	115.2 kbps FSK 1200 baud AFSK	N/A	9 months	patch monopole monopole	Deorbited
	TechEdSat[16]	1U	Stensat (beacon)[7]	437.465 MHz	amateur	1 W	Integrated	AX.25	1200 baud AFSK	N/A	7 months		Deorbited
	F-1	1U	VX-3R VX-3R	145.980 MHz 437.485 MHz	amateur amateur	1 W 200 mW	PIC18F PIC16F	AX.25 FM PWM CW	1200 baud AFSK 20 WPM	0 kB N/A	0 days	dipole dipole	Deorbited
	WE-WISH	1U	(data) (beacon)	437.505 MHz 437.505 MHz	amateur amateur	100 mW		SSTV CW	30 kbps SSTV		5 months	monopole monopole	Deorbited
	RAIKO	2U	Custom	13 GHz							10 months	patch	Deorbited
PSLV-C20 25 Feb 2013	STRaND-1	3U	Custom SSC/SSTL	437.575 MHz	amateur	1.6 W	PIC24	HDLC	9600 baud FSK		6+ months	monopole	Active
	AAUSAT3	1U	ADF7021/AWT6388	437.425 MHz	amateur	900 mW	ATmega32U4	CCSDS/CW	2400 bps/30 WPM		6+ months	turnstile	Active
ISSLaunch-02/Soyuz 19 April 2013	OSSI-1	1U	ADF7021	437.525 MHz	amateur	2 W		AX.25	9600 baud FSK	0 kB	0 days	dipole	DOA
	SOMP	1U	ADF7021 (beacon) Si4420	145.980 MHz 437.485 MHz	amateur amateur	80 mW 500 mW		CW Custom	12 WPM 23 kbps BPSK	N/A	2 months	monopole turnstile	Dead
				437.485 MHz	amateur	500 mW		CW/AX.25	12 WPM/1200 baud FSK			turnstile	
	BEESAT-2	1U	STE BK-77B	435.950 MHz	amateur	500 mW	CMX909B	Mobitex	4800 bps GMSK		2+ weeks	monopole	Alive
	BEESAT-3	1U	STE BK-77B	435.950 MHz	amateur	500 mW	CMX909B	Mobitex	4800 bps GMSK		2+ weeks	monopole	Alive
	Dove-2	3U	Custom UHF MHX-2420	401.3 MHz 2.4 GHz	experimental experimental	1.6 W 1 W	Integrated	Proprietary	2.4 kbps FSK variable		4+ months	monopole patch	Alive
Antares Demo 21 April 2013	Phonesat 1.0 (Graham)[16]	1U	Stensat (beacon)[7]	437.425 MHz	amateur	1 W	Integrated	AX.25	1200 baud FSK		1 week	monopole	Deorbited
	Phonesat 1.0 (Bell)	1U+	Stensat (beacon)[7] Iridium Q9602	437.425 MHz 1616 MHz	amateur experimental	1 W 1.6 W	Integrated Integrated	AX.25 Proprietary	1200 baud FSK 340 byte packet		1 week	monopole Patch	Deorbited
	Phonesat 2.0b (Alexander)[16]	1U	Stensat (beacon)[7]	437.425 MHz	amateur	1 W	Integrated	AX.25	1200 baud FSK		1 week	monopole	Deorbited
	Dove-1	3U	Custom UHF D3-8925	401.3 MHz 8.925 GHz	experimental experimental	1.6 W 3 W		IP over DVB-S2	2.4 kbps FSK 4 Mbps QPSK		1 week	monopole patch	Deorbited
Long March-2D/ Gaofen 1 26 April 2013	TurkSat-3USat	3U	Custom Transponder BeeLine/Astrodev?	435.225 MHz 437.225 MHz	amateur amateur	1 W	N/A Integrated	N/A CW/AX.25	50 kHz 9600 baud FSK	N/A	1 week	monopole monopole	Dead
	CubeBug-1	2U	Lithium-1	437.445 MHz	amateur	1 W	Integrated	AX.25	1200 baud AFSK		4+ months	turnstile	Alive
	NEE-01 Pegasus	1U	Custom	910 MHz		1.9 W	Integrated	SSTV/Audio			1 month		Dead
Vega VV02 7 May 2013	ESTCube-1	1U	Data Beacon	437.505 MHz 437.250 MHz	amateur amateur	500 mW 100 mW		AX.25 CW	9600 baud FSK 18 WPM		3+ months	monopole monopole	Alive

Figure A2: Deployed CubeSats 8 December 2010 – 7 May 2013.

Launch	Satellite	Size	Radio	Downlink	Satellite Service	Power	TNC	Protocol	Data Rate/Modulation	Downloaded	Lifetime	Antenna	Status
HTV-4/ISS 19 Nov 2013	ArduSat-1	1U	NanoCom U482C	437.000 MHz	Experimental	1 W	NanoMind A712D[1]	CSP	9600 baud FM-MSK/20 WPM CW		2+ months	turnstile	Alive
	ArduSat-X	1U	NanoCom U482C	437.000 MHz	Experimental	1 W	NanoMind A712D[1]	CSP	9600 baud FM-MSK/20 WPM CW		2+ months	turnstile	Alive
	Pico Dragon	1U	(data) (beacon)	437.365 MHz 437.250 MHz	Amateur Amateur	800 mW 100 mW		AX.25 CW	1200 baud AFSK		1 month	monopole monopole	Alive
	TechEdSat-3P	3U	Stensat (beacon) Iridium Q9602	437.465 MHz 1616 MHz	Experimental Experimental	1 W 1 W	Integrated Integrated	AX.25 Proprietary	1200 baud AFSK	N/A	1 month	monopole patch	
ORS-3/ELaNa-4 20 Nov 2013	COPPER	1U	AstroDev He-100	437.290 MHz	Experimental	1 W	Integrated	AX.25	9600 baud FSK			dipole	DOA
	TJ3Sat	1U	Stensat	437.320 MHz	Experimental	1 W	Integrated	AX.25, CW	1200 baud AFSK				
	Vermont Lunar Cube	1U	Helium-100	437.305 MHz	Experimental	1.5 W	Integrated	AX.25	9600 baud FSK		1+ month	Crossed Dipoles	Alive
	SwampSat	1U		437.385 MHz	Experimental	1 W		AX.25	9600 baud FSK				
	CAPE-2 (LO-75)	1U	CC1101 RadioMetrix Parrot repeater	437.325 MHz 145.825 MHz	Experimental Experimental	1 W 1 W	Integrated	TI Parrot repeater	9600 baud FSK FM	N/A	1+ month		Alive
	Ho'oponopono-2	3U	Microhard MHX-2420 AstroDev Ne-1 (beacon)	2.4 GHz 437.220 MHz	Experimental Experimental	1 W	Integrated dsPIC33F	Proprietary	57.6 kbps			patch monopole	DOA
	PhoneSat-v2.4	1U	StenSat	437.425 MHz	Experimental	1 W	Integrated	AX.25	1200 baud AFSK			monopole	Alive
	Trailblazer	1U	AstroDev He-100	437.425 MHz	Experimental	1 W	Integrated	AX.25	9600 baud FSK			turnstile	DOA
	DragonSat-1	1U	AstroDev He-100	145.870 MHz	Experimental	500 mW	Integrated	AX.25	9600 baud FSK			monopole	DOA
	KySat-2	1U	AstroDev Li-1	437.405 MHz	Experimental	1.5 W	Integrated	AX.25	9600 baud FSK		1+ month	turnstile	Alive
	ChargerSat-1	1U	CC1100	437.405 MHz	Experimental	1 W			9600 baud FSK			dipole	DOA
	NPS-SCAT	1U	Microhard MHX-2400 CC1000 (beacon)[2]	2.4 GHz 437.525 MHz	Experimental Experimental	1 W 1 W	Integrated Integrated	Proprietary AX.25	1200 baud FSK	N/A		patch dipole	Alive
	Black Knight 1	1U	MHX-425	437.345 MHz	Experimental	1 W	Integrated	Proprietary					
	OHS A	3U			Government								
	OHS B (2)	3U			Government								
	Prometheus (8)	1.5U			Government								
	SENSE (2)	3U	Innoflight SCR-100	2.2 GHz	Government							patch	Alive
	FireFly	3U	L-3 Cadet	425 MHz	Government	1 W	Integrated	Proprietary	QPSK			dipole	Alive
	Horus	3U	AstroDev	915 MHz	Government							patch	DOA
ISIL aunch-03/Dnepr 21 Nov 2013	FUNcube-1	1U	AMSAT	145.936 MHz	Amateur	300 mW	N/A		1200 baud BPSK	70 MB+	2+ months	dipole	Active
	ZACube-1	1U	Custom	437.345 MHz	Amateur			AX.25	1200 baud AFSK/9600 baud FSK		2+ months	dipole	Alive
	HiNcube	1U		437.305 MHz	Amateur			AX.25	9600 baud GMSK				DOA
	First-MOVE	1U	ISIS TRXUV	145.970 MHz	Amateur	230 mW	Integrated	AX.25	1200 baud BPSK		2+ months	dipole	Alive
	UWE-3	1U		437.385 MHz	Amateur			AX.25	9600 baud FSK		2+ months		Alive
	Velox-PII	1U	ISIS?	145.980 MHz	Amateur	230 mW	Integrated	AX.25	1200 baud BPSK		2+ months		Alive
	NEE-02 KRYSAOR	1U		980 MHz									
	CubeBug-2	2U	AstroDev Li-1	437.445 MHz	Amateur	1 W	Integrated	AX.25	1200/9600 baud AFSK/GFSK		2+ months	turnstile	Alive
	KHUSAT (2)	3U	Emhiser	2.2 GHz	Space Research	1 W	FPGA	Proprietary	1 Mbps FSK		2+ months	patch	Alive
	TRITON-1	3U	ISIS TRXUV	145.815 MHz	Amateur	230 mW	Integrated	AX.25	9600 baud BPSK		2+ months	dipole	Alive
	Delfi-n3xt	3U	ISIS TRXUV ISIS Custom	145.900 MHz 2.405 GHz	Amateur Amateur	230 mW 125 mW	Integrated	AX.25	9600 baud BPSK 20-500 kbps MSK		2+ months	dipole patch	Alive
	OPTOS	3U		402 MHz	Earth-exploration								
	Dove-3	3U+	D3-400-T D3-8200-T	401.3 MHz 8.1 GHz	Experimental Experimental	1.6 W 3 W		IP over DVB-S2				monopole patch	Active
	PUCP-SAT-1[3]	1U	Telemetry Beacon	145.840 MHz 437.200 MHz	Amateur Amateur	1.5 W 10 mW		AX.25 CW	1200 baud AFSK 12 WPM	N/A		dipole dipole	
	ICUBE-1[3]	1U	ISIS TRXUV	145.947 MHz	Amateur	230 mW	Integrated	AX.25	1200 baud BPSK				
	HumSAT-D[3]	1U	NanoCom U482C	437.325 MHz	Amateur	500 mW		CSP/CW	1200 baud MSK		2+ months	turnstile	Active
	Dove-4[3]	3U+	D3-400-T D3-8200-T	401.3 MHz 8.1 GHz	Experimental Experimental	1.6 W 3 W		IP over DVB-S2				monopole patch	
NROL-39/ELaNa-2 5 Dec 2013	IPEX	1U		437.270 MHz	Experimental	1 W		AX.25	9600 baud FSK		2+ months	dipole	Active
	MCubed-2	1U	AstroDev Li-1	437.485 MHz	Experimental	1 W		AX.25	9600 baud GMSK		2+ months	monopole	Active
	CUNYSAT-1	1U		437.505 MHz	Experimental	1.2 W							
	FIREBIRD (2)	1.5U		437.405 MHz	Experimental	1 W				27+ MB	2+ months	dipole	Active/DOA
	Alice	3U			Government								
	AeroCube-5 (2)	1.5U	Freewave FGRM CC1101	915 MHz 915 MHz	Experimental experimental	1.3 W	Integrated	Proprietary	500 kbps FSK			patch	
	SMDC-ONE (2)	3U			Government								
	TacSat-6	3U			Government								
	SNAP	3U			Government								

Figure A3: Deployed CubeSats 19 November 2013 – 5 December 2013.

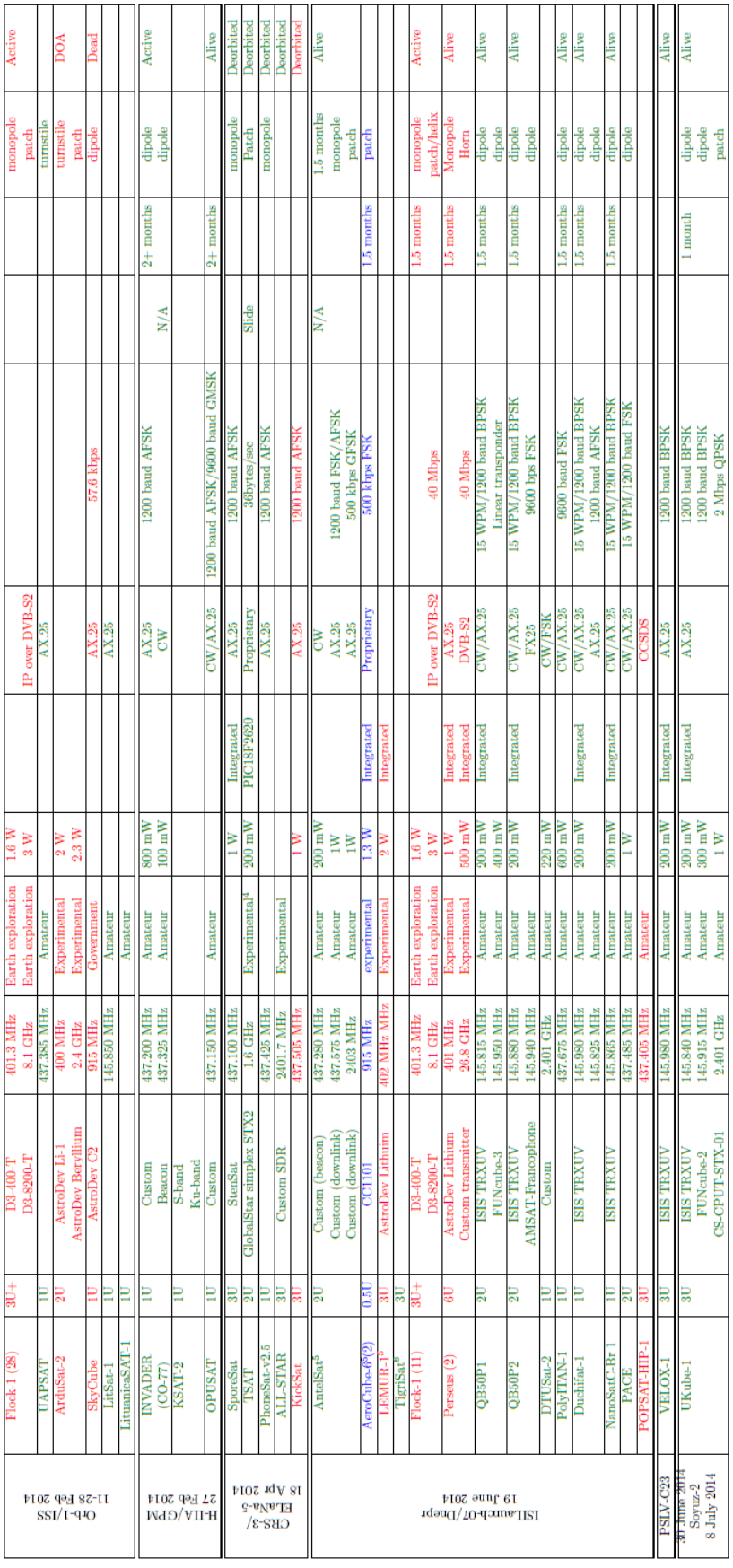

Figure A4: Deployed CubeSats 11-28 February 2014 – 8 July 2014.

B Simulated Radiation Pattern

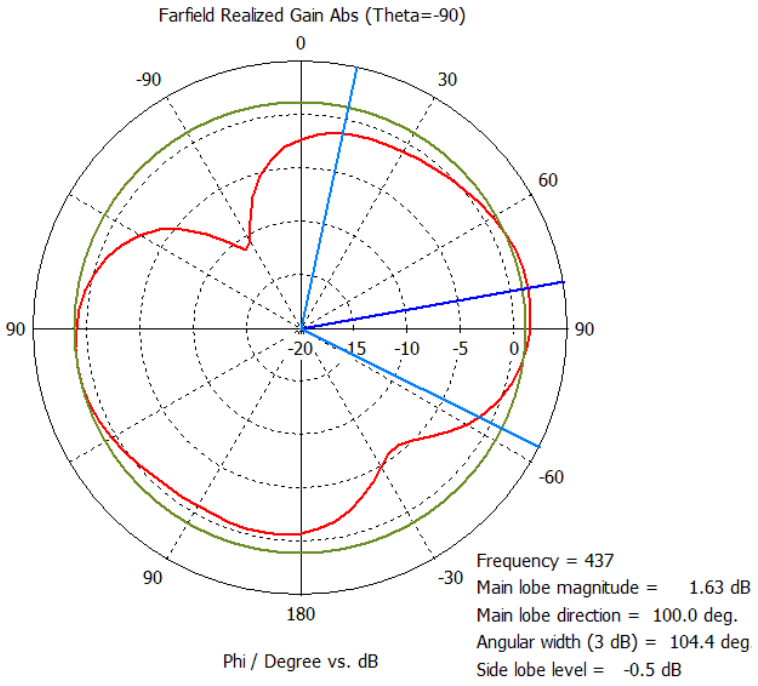

Figure B1: Top (+Z) view.

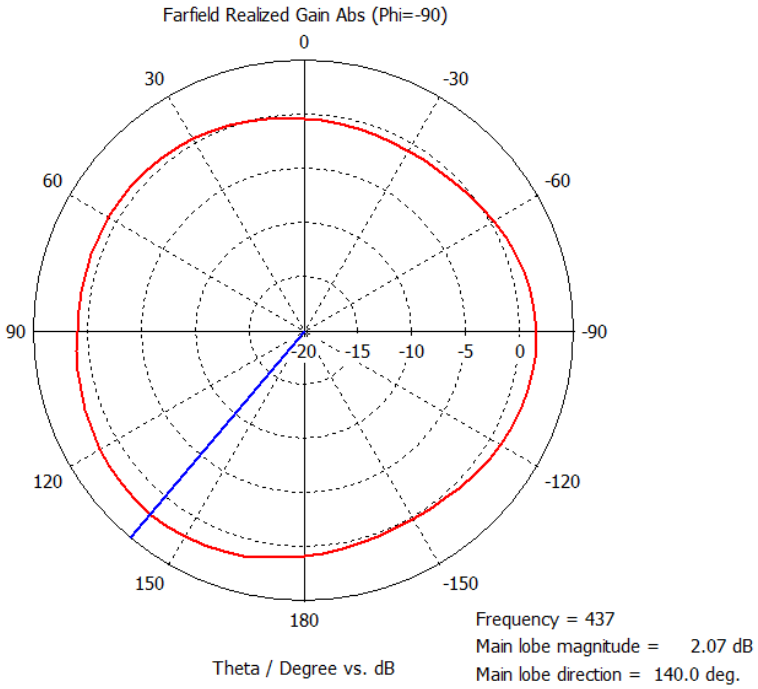

Figure B2: Side (+X) view.

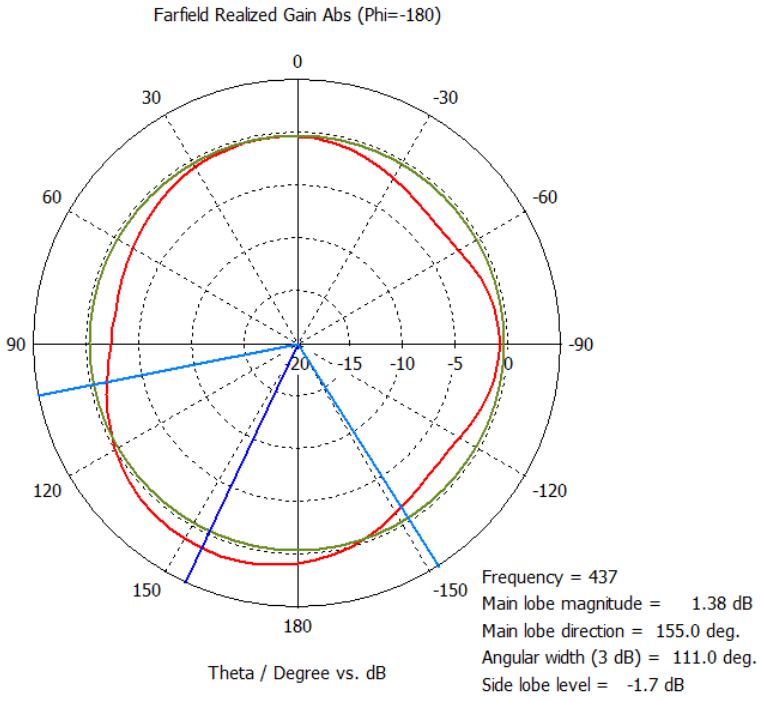

Figure B3: Side (−Y) view.

C Simulated Grounding Inductors

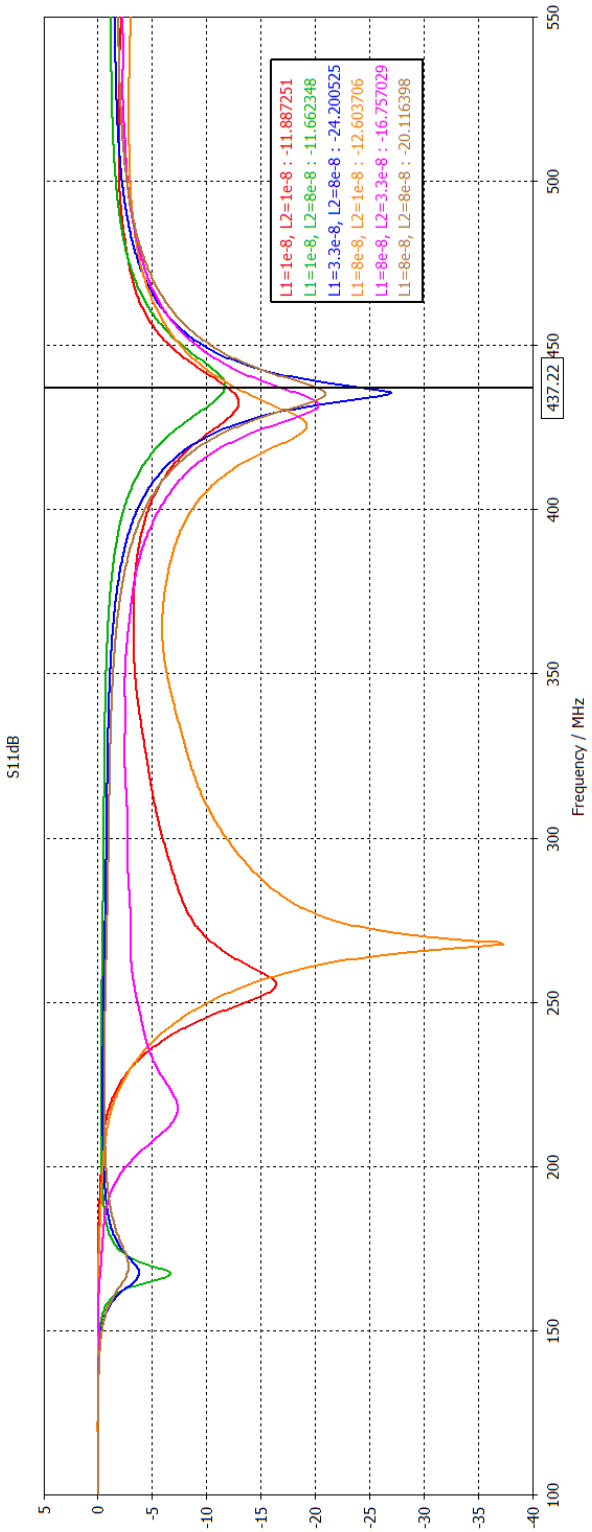

Figure C1: Grounding inductors influence on the return loss.

D ADS Block Diagram

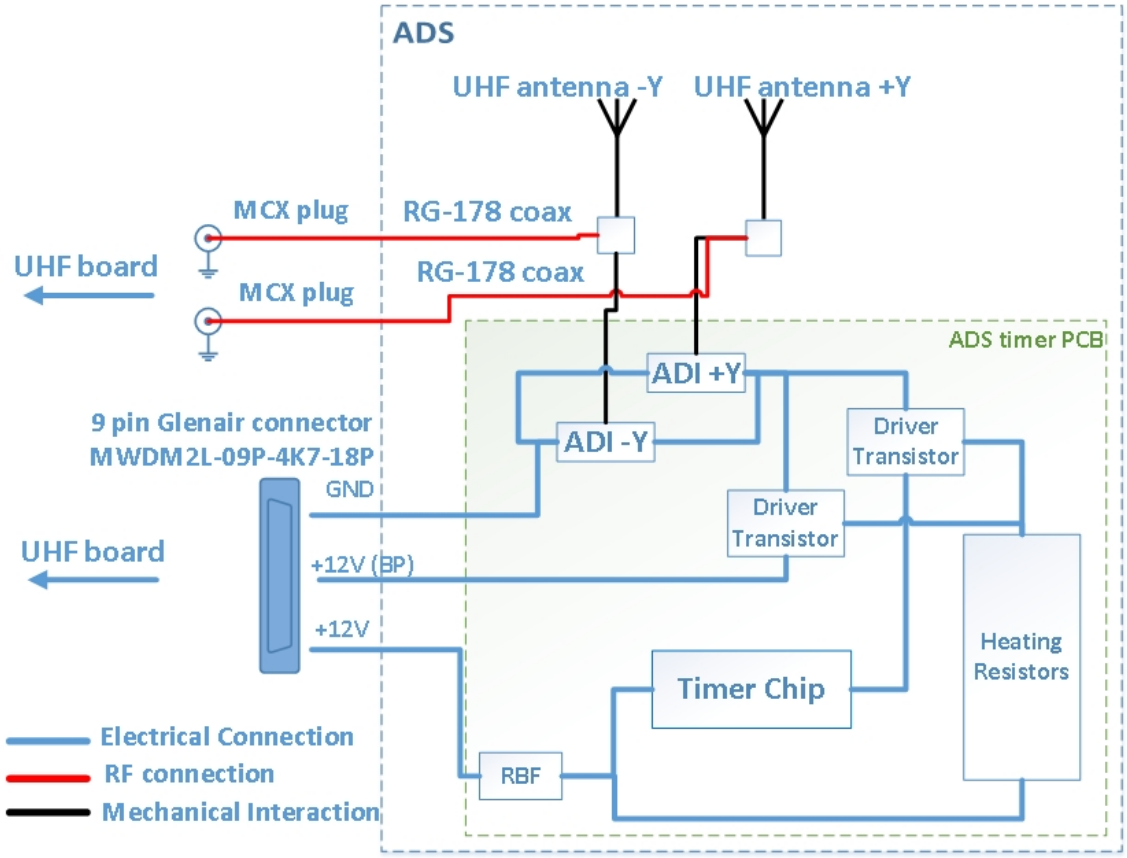

Figure D1: ADS block diagram.

E Timer Circuit Schematic

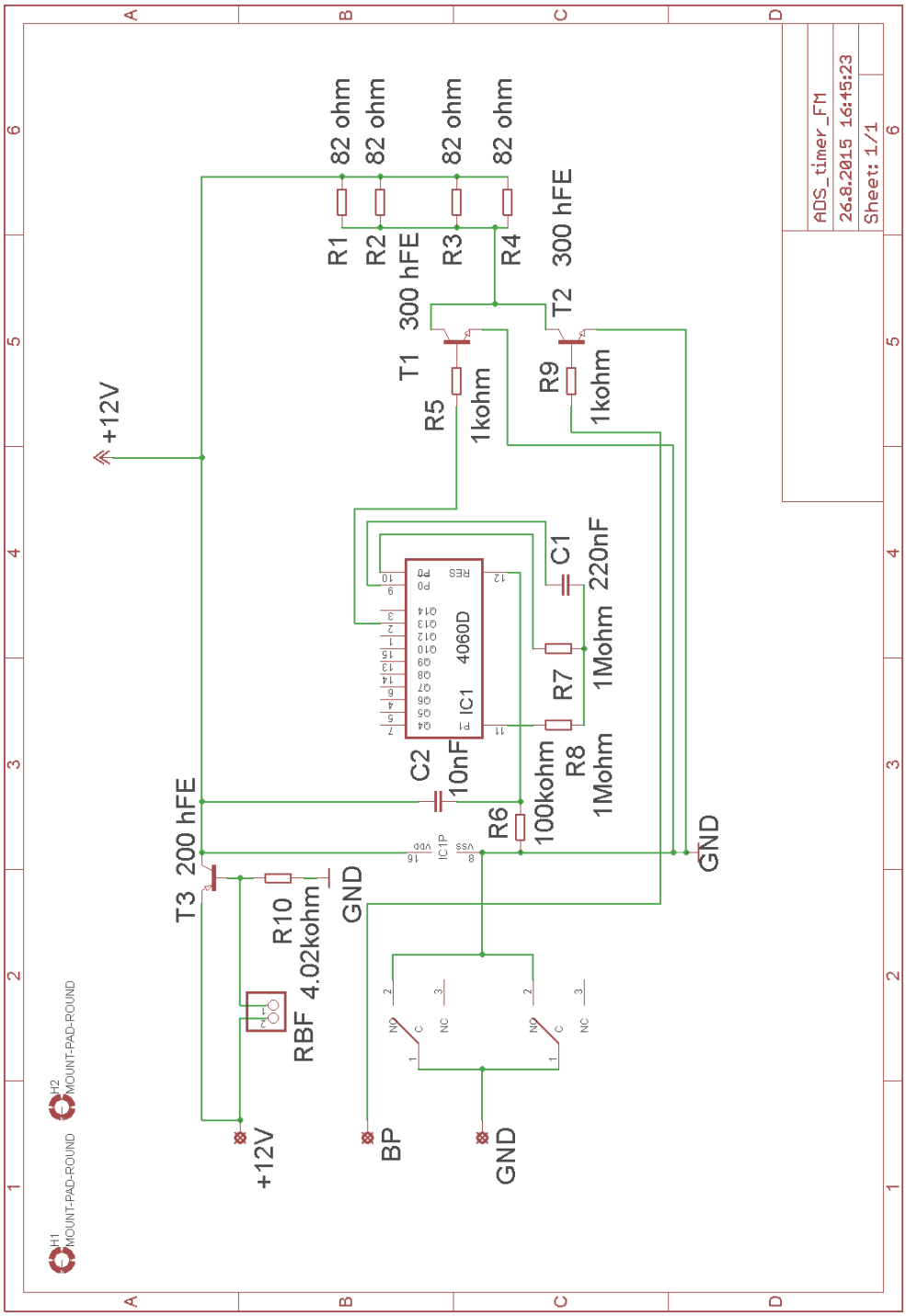

Figure E1: Timer circuit schematic.

F Timer Circuit PCB

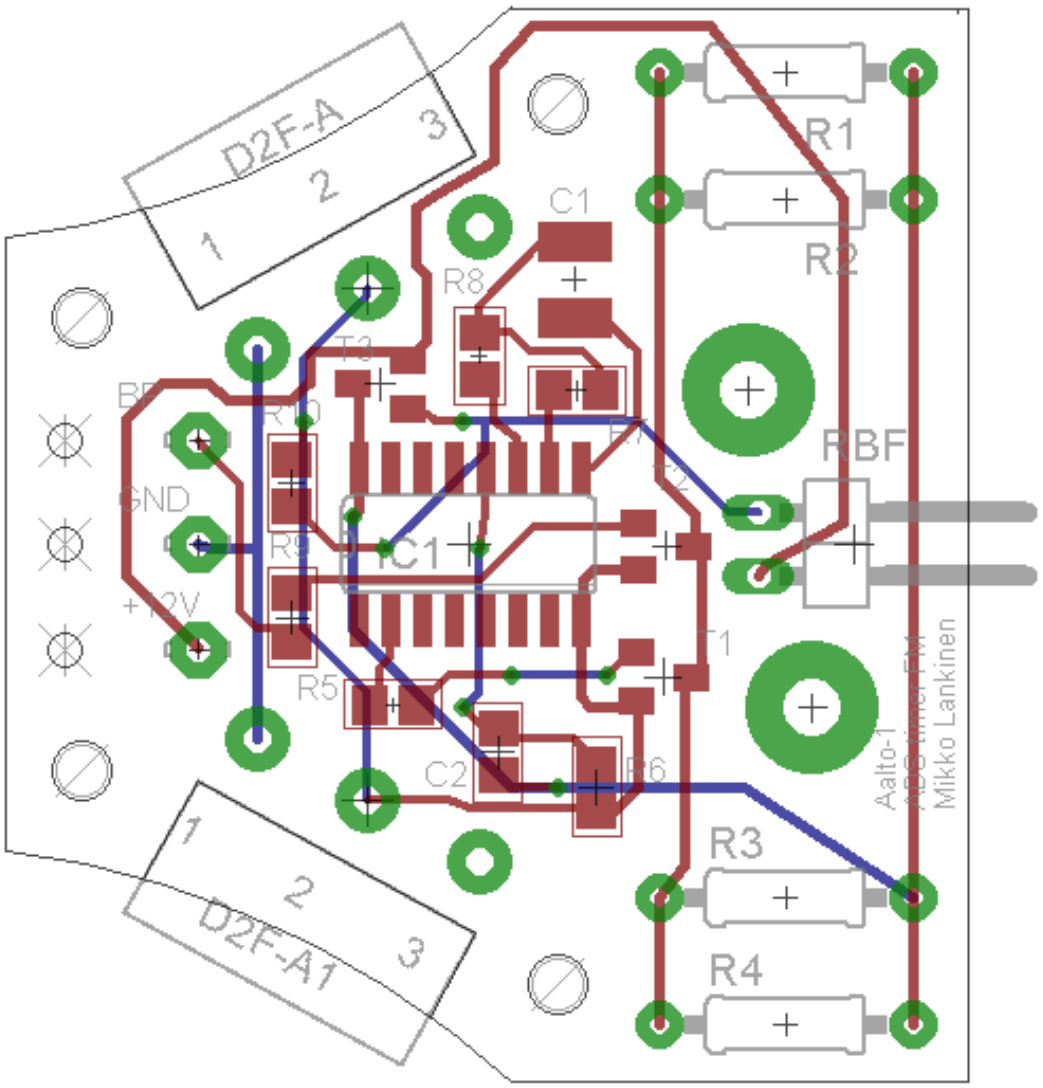

Figure F1: Timer circuit PCB layout.

G Timer Circuit Bill of Materials

Table G1: Timer circuit Bill of Materials.

Qty	Item description	Ref	Manufacturer	Part number
1	LOGIC, BIN COUNTER, 16SOIC	IC1	Texas Instruments	CD4060BM
2	BJT Transistor, NPN, 80 V, 160 MHz, 625 mW, 1.5 A, 300	T1, T2	Diodes Inc	FMMT620TA
1	BJT Transistor, PNP, 60 V, 250 MHz, 1.25 W, 3 A, 200	T3	Diodes Inc	ZXTP25060BFH
1	SMD Multilayer Ceramic Capacitor, C Series, 0.22 μF, ± 5%, C0G / NP0, 25 V, 1210	C1	Kemet	C1210C224J3GACTU
1	SMD Multilayer Ceramic Capacitor, C Series, 0.01 μF, ± 10%, X8R, 50 V, 0805	C2	Kemet	C0805C103K5HACTU
1	SMD Resistor, Thick Film, CRG Series, 1 Mohm, 330 mW, ± 1%, 150 V	R7, R8	TE CONNECTIVITY	CRGH0805F1M0
1	SMD Resistor, Thick Film, CRG Series, 100 kohm, 330 mW, ± 1%, 150 V	R6	Kemet	CRGH0805F100K
1	SMD Resistor, Thick Film, AEC-Q200 ERJ Series, 4.02 kohm, 500 mW, ± 1%, 400 V	R10	PANASONIC	ERJP06F4021V
2	SMD Resistor, Thick Film, MC Series, 1 kohm, 100 mW, ± 5%, 150 V	R5, R9	MULTICOMP	MC01W080551K
4	Resistor, MF25 Series, 82 ohm, 250 mW, ± 1%, 250 V	R1, R2, R3, R4	MULTICOMP	MF25 82R

H ADS Baseplate Drawing

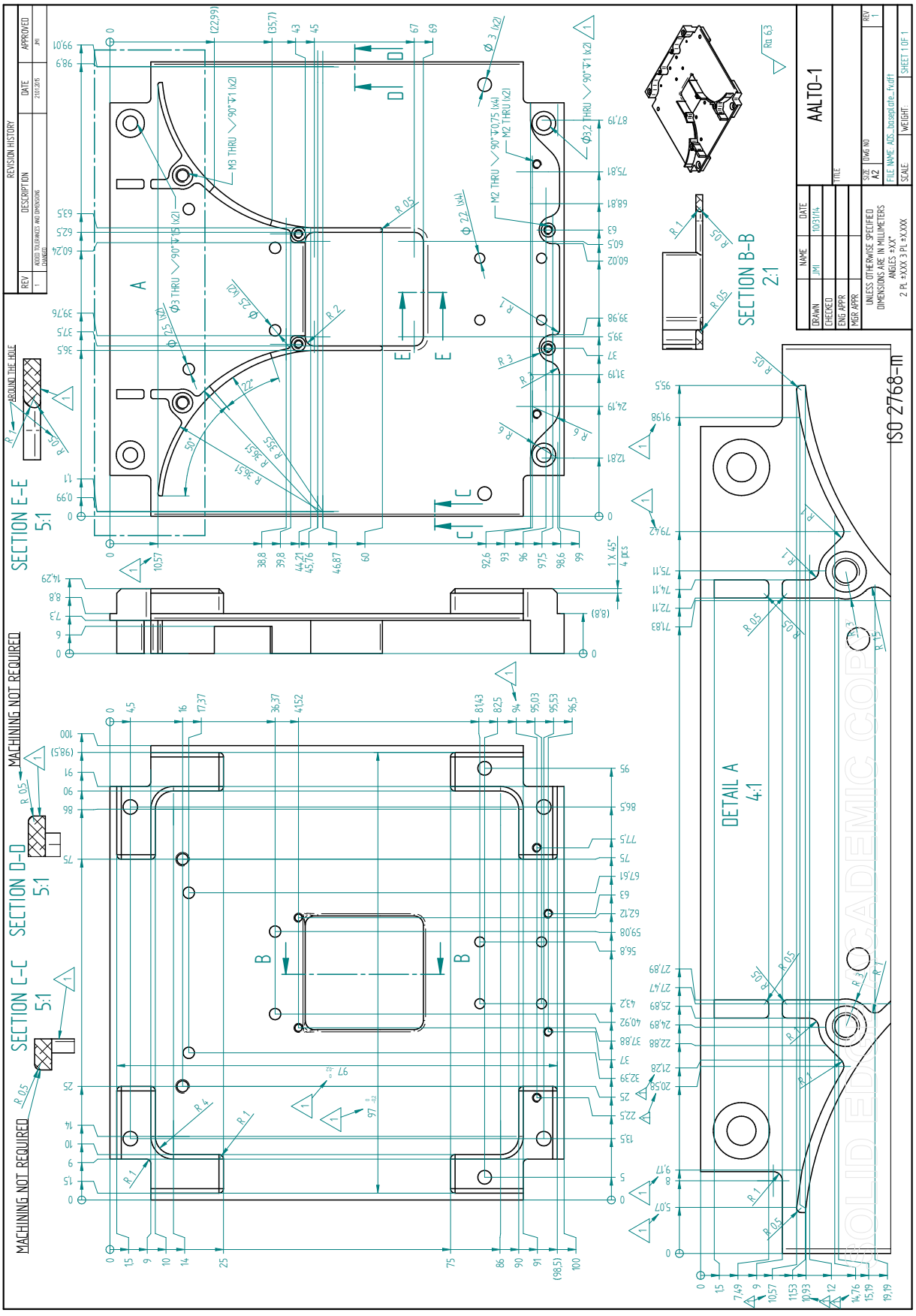

I ADS Door –Y Drawing

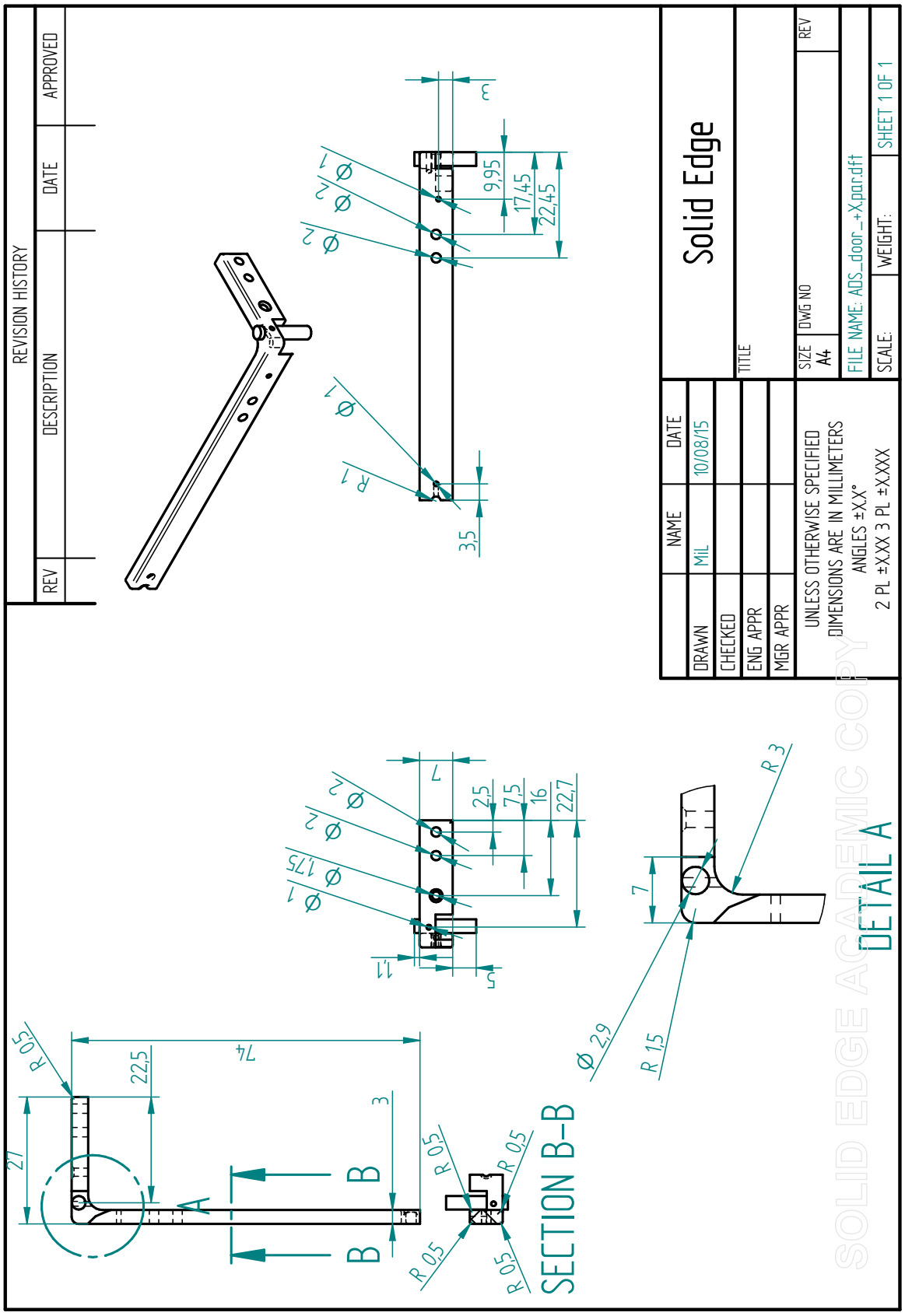

J ADS Door +Y Drawing

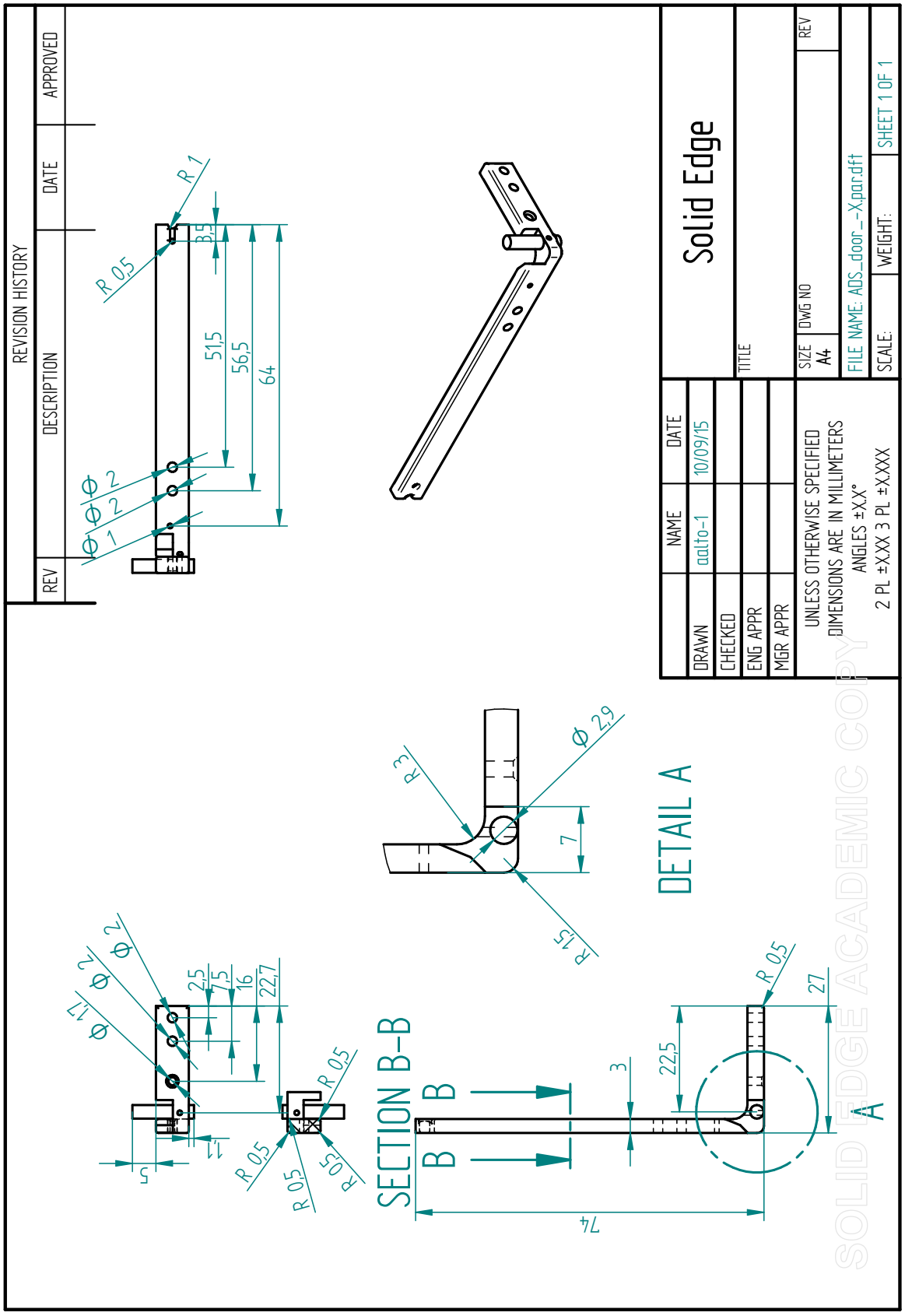

K ADS Coverplate Drawing

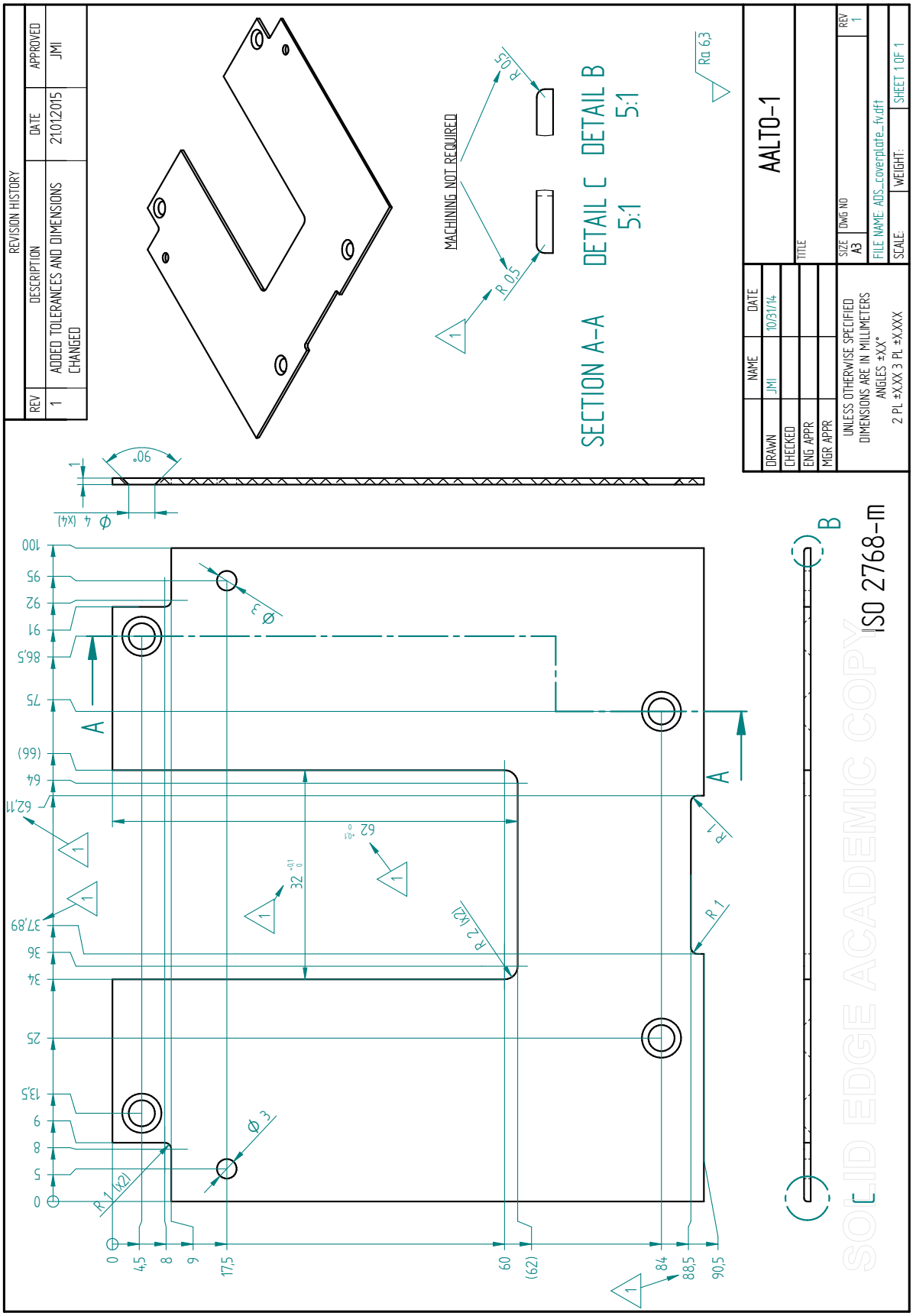

L ADS Coverplate Hatch Drawing

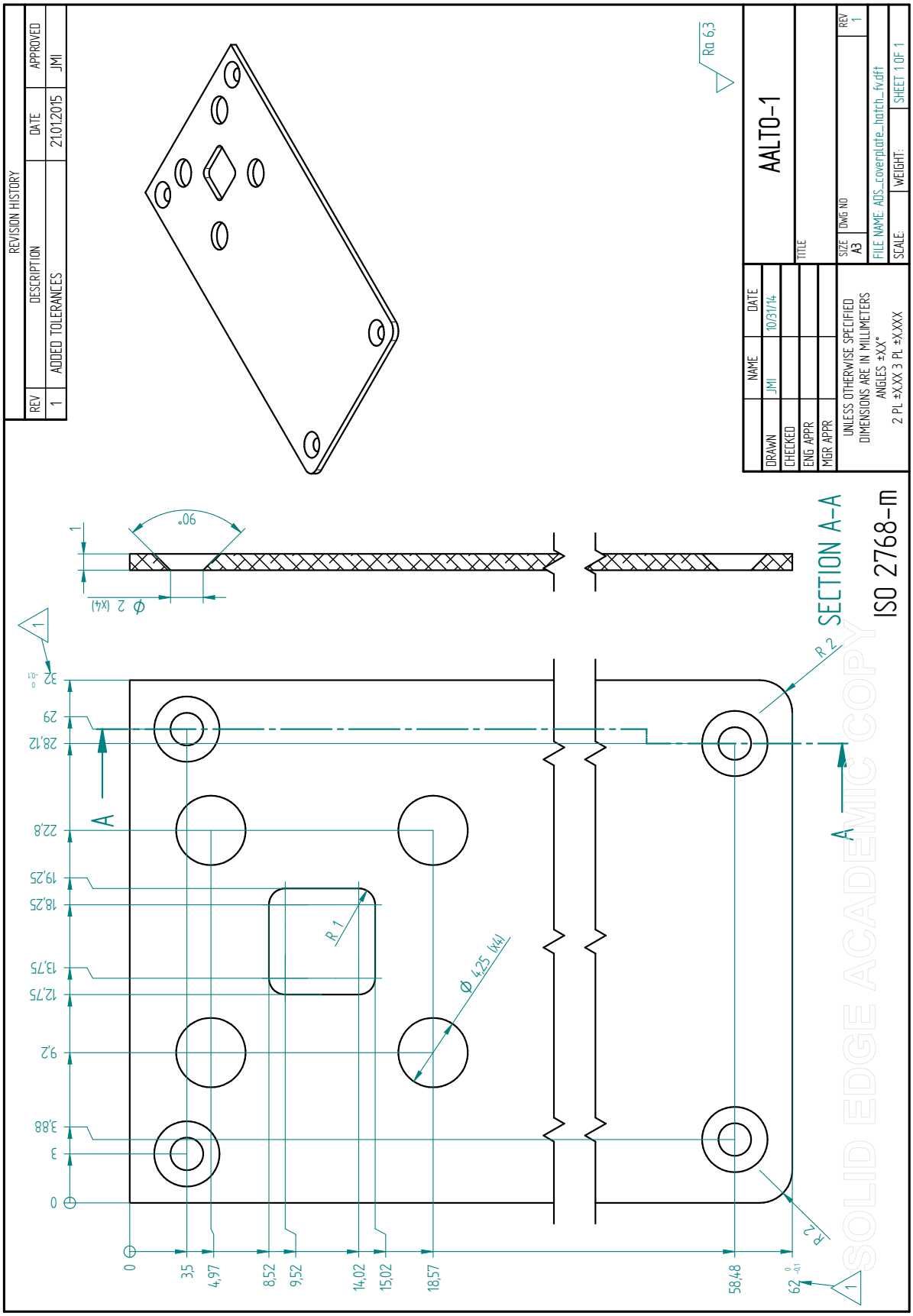

M ADS EM Shock Test Results

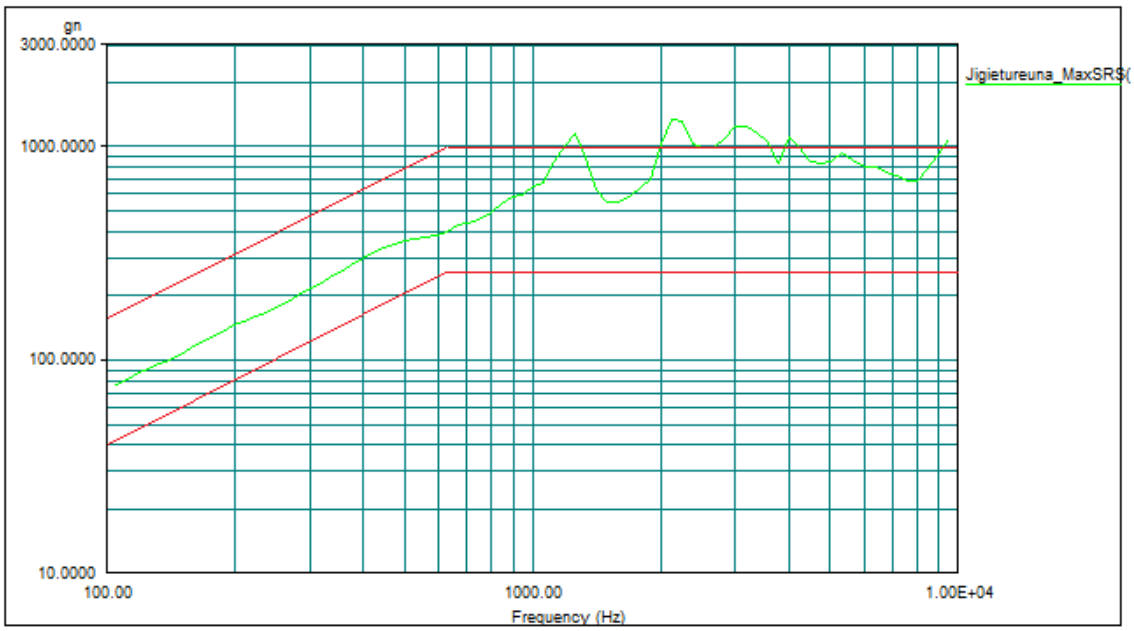

Figure M1: Frequency response to acceleration loads in +x-axis direction.

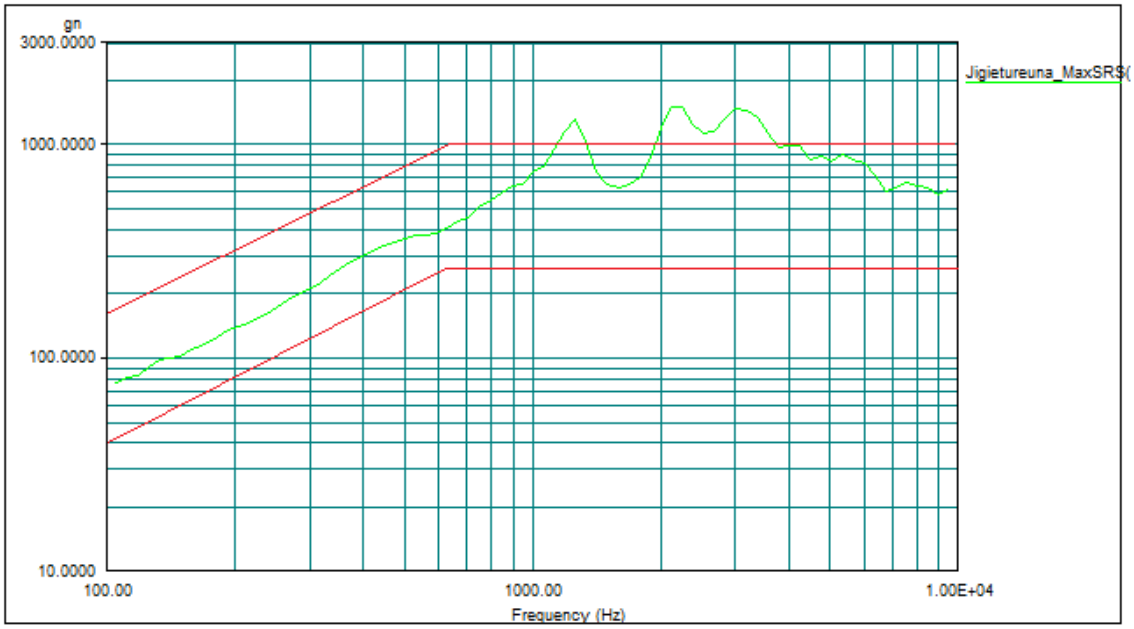

Figure M2: Frequency response to acceleration loads in −x-axis direction.

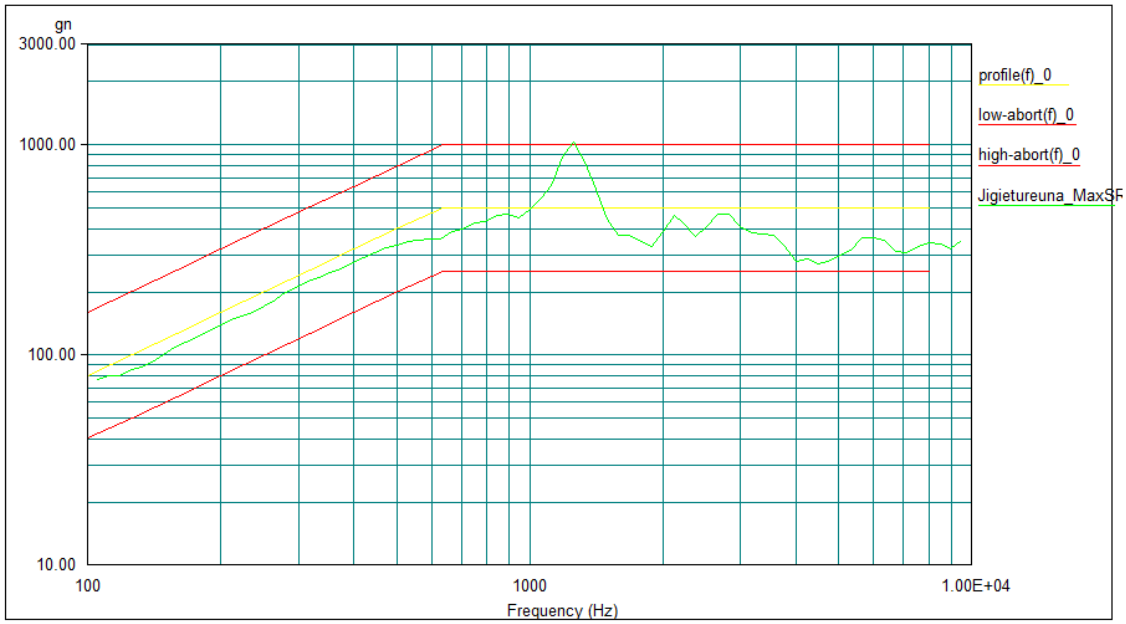

Figure M3: Frequency response to acceleration loads in +y-axis direction.

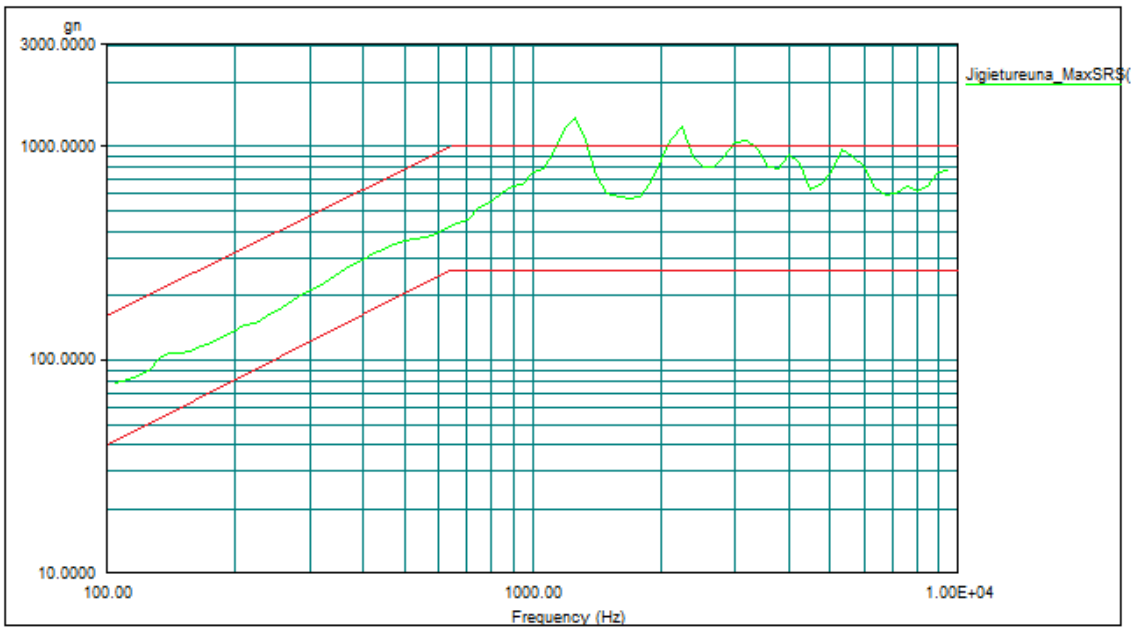

Figure M4: Frequency response to acceleration loads in −y-axis direction.

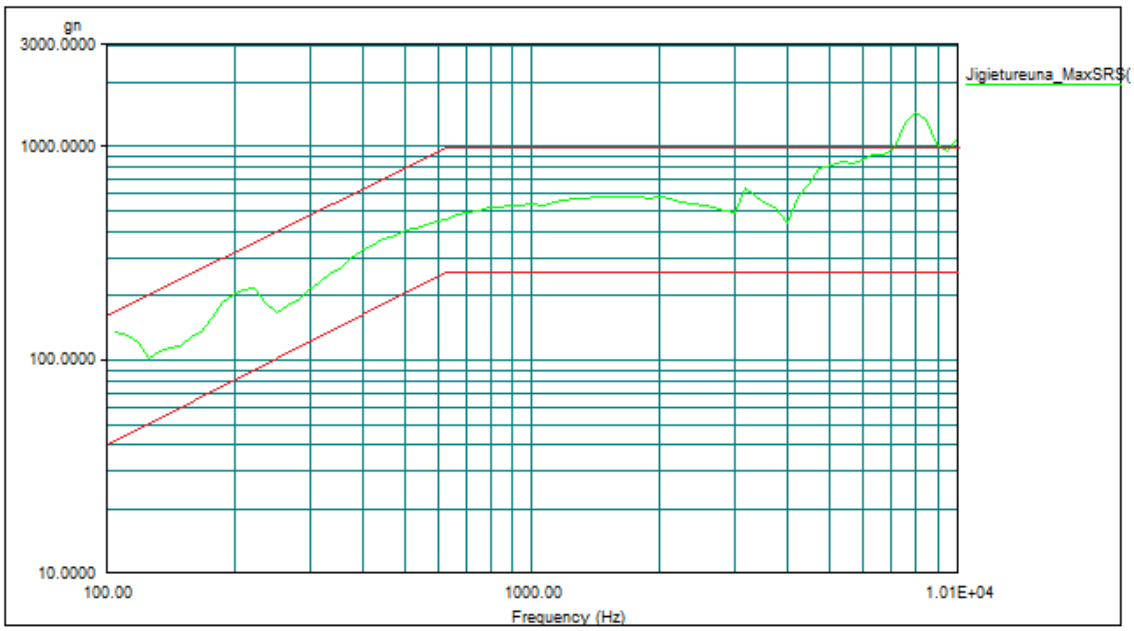

Figure M5: Frequency response to acceleration loads in −z-axis direction.

N Communication Link Test Results

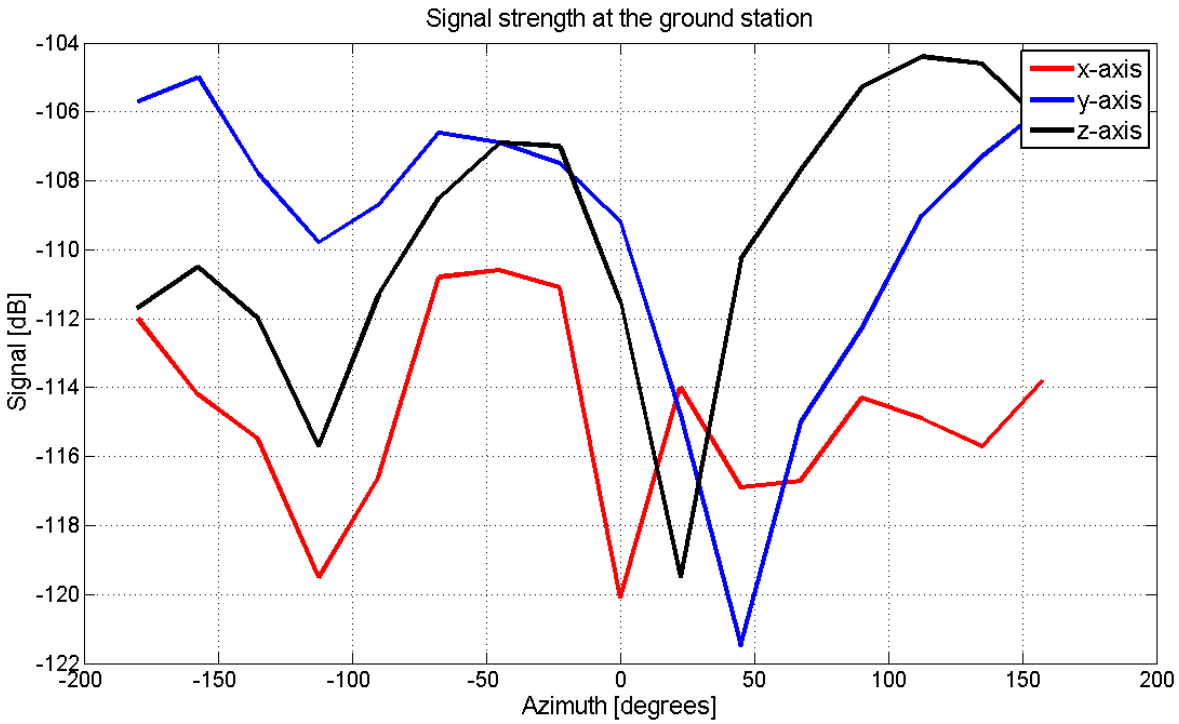

Figure N1: Communication link test results.

O ADS FM Return Loss Measurement

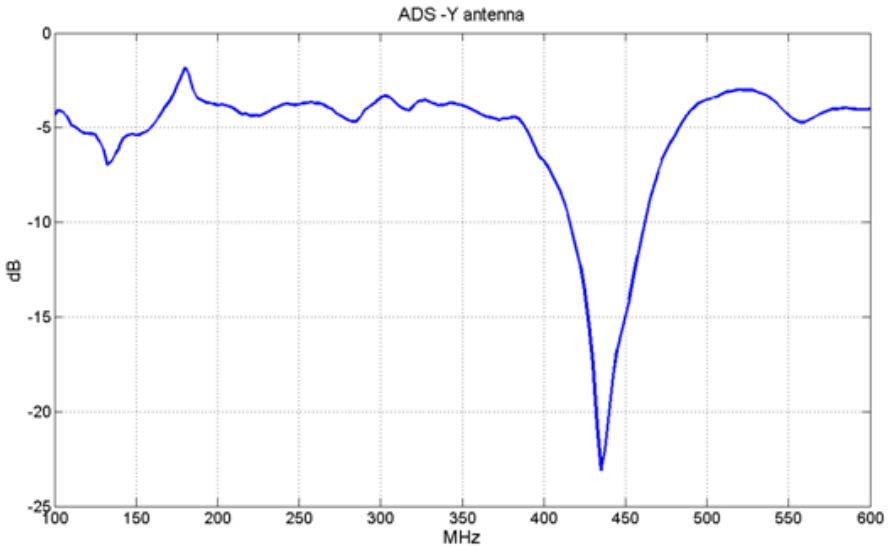

Figure O1: Return loss for −Y side antenna.

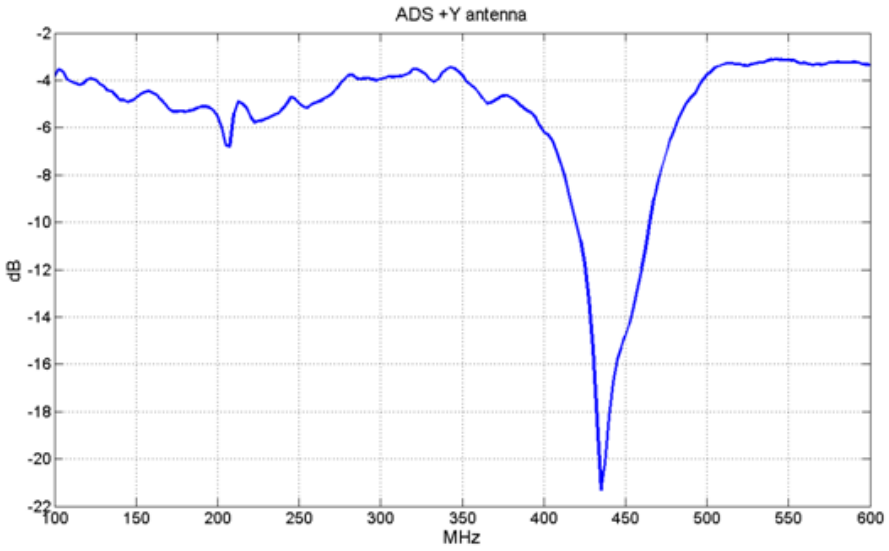

Figure O2: Return loss for +Y side antenna.